Geodiversity of Hydrothermal Processes Along the Mid-Atlantic Ridge and Ultramafic-Hosted Mineralization: A New Type of Oceanic Cu-Zn-Co-Au Volcanogenic Massive Sulfide Deposit

Yves Fouquet,[1] Pierre Cambon,[1] Joël Etoubleau,[1] Jean Luc Charlou,[1] Hélène Ondréas,[1] Fernando J. A. S. Barriga,[2] Georgy Cherkashov,[3] Tatiana Semkova,[3] Irina Poroshina,[3] M. Bohn,[4] Jean Pierre Donval,[1] Katell Henry,[1] Pamela Murphy,[1] and Olivier Rouxel[1]

Several hydrothermal deposits associated with ultramafic rocks have recently been found along slow spreading ridges with a low magmatic budget. Three preferential settings are identified: (1) rift valley walls near the amagmatic ends of ridge segments; (2) nontransform offsets; and (3) ultramafic domes at inside corners of ridge transform-fault intersections. The exposed mantle at these sites is often interpreted to be a detachment fault. Hydrothermal cells in ultramafic rocks may be driven by regional heat flow, cooling gabbroic intrusions, and exothermic heat produced during serpentinization. Along the Mid-Atlantic Ridge (MAR), hydrothermal deposits in ultramafic rocks include the following: (1) sulfide mounds related to high-temperature low-pH fluids (Logatchev, Rainbow, and Ashadze); (2) carbonate chimneys related to low-temperature, high-pH fluids (Lost City); (3) low-temperature diffuse venting and high-methane discharge associated with silica, minor sulfides, manganese oxides, and pervasive alteration (Saldanha); and (4) stockwork quartz veins with sulfides at the base of detachment faults (15°05′N). These settings are closely linked to preferential circulation of fluid along permeable detachment faults. Compared to mineralization in basaltic environments, sulfide deposits associated with ultramafic rocks are enriched in Cu, Zn, Co, Au, and Ni. Gold has a bimodal distribution in low-temperature Zn-rich and in high-temperature Cu-rich mineral assemblages. The Cu-Zn-Co-Au deposits along the MAR seem to be more abundant than in ophiolites on land. This may be because ultramafic-hosted volcanogenic massive sulfide deposits on slow spreading ridges are usually not accreted to continental margins during obduction and may constitute a specific marine type of mineralization.

[1]IFREMER, Centre de Brest, Plouzané, France.
[2]GeoFCUL/Creminer, Faculdade de Ciencias, Universidade Lisboa, Lisbon, Portugal.
[3]Institute for Geology and Mineral Resources of the Ocean, St. Petersburg, Russia.
[4]CNRS-IFREMER, Centre de Brest, Plouzané, France.

Diversity of Hydrothermal Systems on Slow Spreading Ocean Ridges
Geophysical Monograph Series 188

10.1029/2008GM000746

1. INTRODUCTION

The first sulfide mineralization on the seafloor was discovered in 1978 at 21°N on the East Pacific Rise (EPR) [*Cyamex*, 1978; *Francheteau et al.*, 1979; *Spiess et al.*, 1980] and the Galápagos ridge [*Corliss*, 1979]. These discoveries were the proof that hydrothermal activity was a major process associated with the formation of young oceanic crust. Research conducted over the past 30 years has shown a wide variety of hydrothermal mineralization in the modern oceans [*Fouquet*,

1997; *Herzig and Hannington*, 1995; *Rona*, 1988; *Rona and Scott*, 1993]. More than 100 hydrothermal fields with sulfide deposits are now known at water depths ranging from a few hundred to 4100 m. Based on the different geodynamic settings and on the composition of basement rocks, several types of deposits are identified. Hydrothermal deposits occur at fast and slow spreading ridges, on sedimented ridges, in back-arc and arc environments, and in intracontinental back-arc rifts. Major deposits are also found on axial and off-axis volcanoes. Basement rocks which are sources for metals are dominantly mafic volcanic rocks (Normal-Mid-Ocean Ridge Basalt (N-MORB)) along fast, intermediate, and slow spreading ridges. Enriched-MORB (E-MORB) type compositions are typical of hotspot domains [*Dosso et al.*, 1999]. Felsic volcanic rocks occur in immature young back-arcs close to active arcs [*Allen et al.*, 2002; *Lentz*, 1998]. Sediments interact with the hydrothermal fluids in the upper part of the hydrothermal system in sedimented rifts and at some back-arc spreading centers close to the continental margins. Thus, depending on the source rocks and the geological setting, the compositions of the sulfide deposits can vary considerably. Mid-ocean ridge deposits associated with N-MORB are typically enriched in Cu and Zn [*Bogdanov et al.*, 1995; *Fouquet et al.*, 1993c, 1996, 1998b; *Hannington et al.*, 1991, 1995, 1999; *Herzig and Hannington*, 1995; *Humphris et al.*, 1995; *Krasnov et al.*, 1995; *Mozgova et al.*, 1999]. Back-arc and arc systems associated with felsic rocks are enriched in Zn, Pb, Cu, As, Sb, Ag, Au, Hg, and Ba [*Binns and Scott*, 1993; *Binns et al.*, 1993; *de Ronde et al.*, 2005; *Dekov et al.*, 1999; *Fouquet et al.*, 1993b; *Herzig et al.*, 1993; *Petersen et al.*, 2003, 2004; *Tanahashi et al.*, 2006; *Tufar*, 1989]. Sediment-hosted mid-ocean ridge sulfide deposits have generally lower concentrations of base metals than deposits on sediment-starved ridges [*Ames et al.*, 1993; *Goodfellow and Franklin*, 1993; *Houghton et al.*, 2004; *Koski et al.*, 1985, 1988; *Peter and Scott*, 1988; *Zierenberg et al.*, 1993, 1998]. Immature back-arc systems related to intracontinental rifting are highly enriched in Pb, As, Ag, and Hg [*Halbach et al.*, 1989, 1993]. Precious metals such as gold and silver are typically enriched in immature back-arc systems. The largest black smoker deposits contain between 3 and 15 million tons (e.g., TAG hydrothermal field [*Humphris et al.*, 1995] and Krasnov field on the Mid-Atlantic Ridge (MAR) [*Cherkashov et al.*, 2008], Galapagos Rift, Southern Explorer Ridge, and 13°N on the EPR [*Fouquet*, 1997]), although two sediment-hosted deposits, Middle Valley (10–20 million tons) on the Juan de Fuca Ridge [*Zierenberg et al.*, 1998] and the Atlantis II Deep (90 million tons) in the Red Sea [*Diehl*, 1987] are known to be much larger.

Until 1984, it was predicted that the heat flow on slow spreading ridges would be insufficient to support high-temperature venting [*Macdonald*, 1984]. Following the discovery of high Mn concentration in the water column along the MAR in 1984 [*Klinkhammer et al.*, 1985], water column and camera surveys identified the first high-temperature vent field on a slow spreading ridge, the TAG hydrothermal field at 26°N [*Rona et al.*, 1986]. Subsequent studies have now identified about 33 active or inactive hydrothermal deposits (Plate 1) (Table 1) and a number of other sites with sulfide veins and chemical anomalies in the water column [*Aballea et al.*, 1998; *Bougault et al.*, 1993, 1998; *Charlou et al.*, 1997, 1998, 2000; *German and Parson*, 1998; *Klinkhammer et al.*, 1985]. In 1995, a new field (Logatchev) of sulfide mineralization [*Krasnov et al.*, 1995] was discovered at 14°45′N the MAR at a place of extremely low magmatic budget and where serpentinized ultramafic rocks are outcropping.

In addition to the MAR, ultramafic-hosted hydrothermal deposits are reported from a few other places along slow and ultraslow spreading ridges with low magma budget. On the Southwest Indian Ridge, a hydrothermal deposit occurs on partially serpentinized peridotite associated with basalt. The deposits consist of opal, basalt breccias cemented by smectite and Mn oxides (birnessite) and partially oxidized massive sulfide [*Bach et al.*, 2002]. Sulfide and hydrothermal plumes also occur on ultraslow spreading ridges in the northern Atlantic at Gakkel ridge [*Baker et al.*, 2004; *Edmonds et al.*, 2003; *Michael et al.*, 2003], Lena Trough [*Snow et al.*, 2001] and Mohns ridge [*Pedersen et al.*, 2001]. A hydrothermal field associated with ultramafics was also recently found on the Indian ridge [*Gallant and Von Damm*, 2006; *Nakamura et al.*, 2008]. Ultramafic rocks are very common along these ridges.

In this chapter, we review the diverse array of hydrothermal deposits along the MAR with emphasis on sulfides associated with ultramafic rocks. We examine the geological control on the mineralization, basement rock composition, mineralogical and chemical compositions of sulfides, and compositions of hydrothermal fluids. Specific characteristics of ultramafic-hosted deposits are identified and compared to other hydrothermal fields related to N-MORB and E-MORB type basement rocks, in order to develop a model for ultramafic-rock-hosted mineralization.

2. OCCURRENCES OF ULTRAMAFIC ROCKS ALONG SLOW SPREADING RIDGES

Outcrops of serpentinized peridotite are a general characteristic of slow and ultraslow spreading ridges [*Cannat*, 1993; *Cannat and Casey*, 1995; *Dick*, 1989; *Dick et al.*, 2003]. A negative residual gravity anomaly at the central part of the segments suggests relatively thick mafic crust and hot mantle at depth, whereas the ends of the segments have a

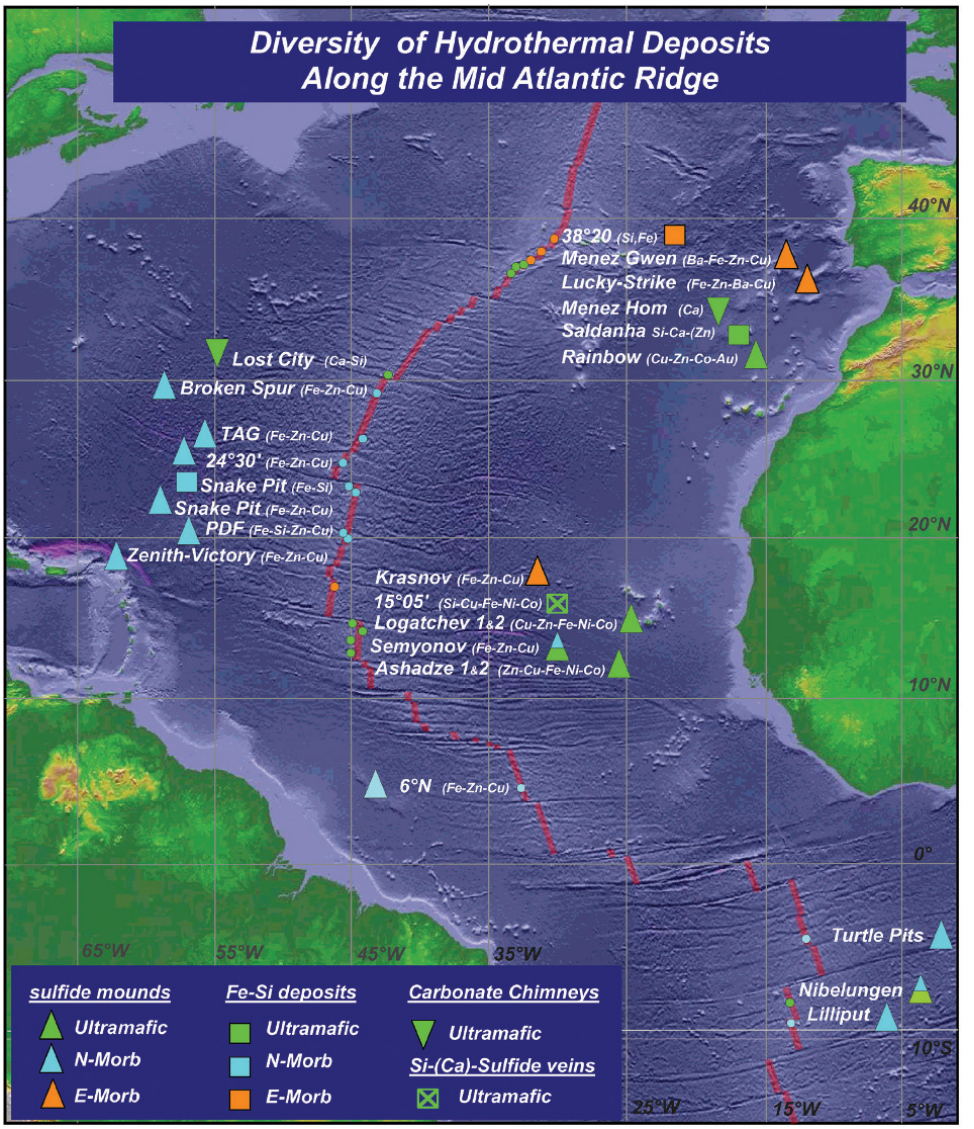

Plate 1. Location and types of hydrothermal deposits along the Mid-Atlantic Ridge (MAR) between 15°S and 50°N. Additional mineralization occurring as veins in basaltic environments is only shown in Figure 1.

positive residual gravity anomaly suggesting a thin mafic or serpentinite crust and a relatively starved magmatic environment [*Cannat and Casey*, 1995; *Escartín and Lin*, 1998; *Escartín and Cannat*, 1999]. Ultramafic rocks are commonly observed along the rift valley walls near and within axial discontinuities [*Gracia et al.*, 1997] and at the inner corner of large fracture zones. In some portions of ultraslow spreading ridges (Southwest Indian and Gakkel ridges), peridotites are common on the rift valley floor [*Dick et al.*, 2003; *Michael et al.*, 2003; *Sauter et al.*, 2004]. Peridotites have the composition of residual mantle rocks, more or less modified by interaction with basaltic magma [*Cannat and Casey*, 1995; *Dick*, 1989; *Hellebrand et al.*, 2000; *Johnson and Dick*, 1992; *Seyler et al.*, 2003].

Because of the low rate of magmatism on the MAR, extension of the ocean floor is accommodated mainly by tectonic stretching [*Bougault et al.*, 1993; *Cannat et al.*, 1997; *Lagabrielle et al.*, 1998; *Rona et al.*, 1987]. This leads to the formation of a basement composed of mantle-derived ultramafic rocks and associated gabbroic intrusions. These Oceanic Core Complexes are the result of long-lived (millions of years), large-displacement, low-angle detachment

Table 1. Main Characteristics of Hydrothermal Fields Along the Mid-Atlantic Ridge

Name	Latitude	Longitude	Depth (m)	Basement Rocks	Geological Control	Distance From Axis
Gallionella Garden	71°18′N	05°47′W	550	MORB	Rift graben faults	0
Kolbeinsey	67°05′N	18°42′W	100	MORB	Seamount, axial zone	0
Grimsey field	66°36′N	17°39′W	400	MORB	Volcanic ridge,	0
Steinaholl field	63°06′N	24°32′W	300	MORB	Axial zone, volcanic ridge	0
38°20′N	38°20′N	30°40′W	600	MORB	Layered volcaniclastic	0
Menez Gwen	37°50′N	31°31′W	820	E-MORB	Top central volcano, axial graben, volcaniclastic	0
Lucky Strike	37°17′N	32°16′W	1650	E-MORB	Top central volcano, lava lake (300 m), caldera	0
Menez Hom	37°07N	32°26W	1830	Harzburgite	Intersection dome, nontransform offset	8
Famous	36°50′N	33°10′W	2300	MORB	South wall fracture zone	1
Saldanha	36°33′N	33°26W	2325	Harzburgite	Intersection dome massif, non transform offset	11
Rainbow	36°14′N	33°54W	2400	Harzburgite	Center of nontransform offset, ultramafic dome	6
Lost City	30°10′N	42°10′W	700	Harzburgite	Top of an intersection massif, detachment fault	15
Broken Spur	29°10′N	43°10′W	3050	MORB	Top of neovolcanic ridge, axial summit fissure	0
TAG	26°08′N	44°49′W	3670	MORB	Rift wall, central part of segment, volcanic centers	7
TAG (*Alvin*)	26°09′N	44°49′W	3500	MORB	Rift wall, central part of segment, volcanic centers	8
TAG (Mir)	26°08′N	44°49′W	3600	MORB	Rift valley wall, 2.5 km east of axis	8
25°48′N	25°48′N	44°59′W	3295	MORB	Rift valley wall	?
24°30′N	24°30′N	46°10′W	4000	MORB	East rift valley wall	4
24°21′N	24°21′N	46°12′W	3200	MORB	Rift valley wall	?
Kane	23°35′N	45°00′W	3500	Gabbro	Nodal basin	2
23°30′N	23°30′N	45°00′W	2500	MORB	Top of rift valley wall	8
Snake Pit	23°22′N	44°57′W	3500	MORB	Topographic high, neovolcanic ridge	0

Type of Mineralization	Size (m)	Maximum Temperature	Activity	Major Minerals[a]	References
Chimneys	500	260°C	A	An, Ba, Sp, Py	*Pedersen et al.* [2005]
Breccia	-	-	A	Ba, Gy, Op, Sp, Cb, Cv, Bn	*Stefansson* [1983], *Olafsson et al.* [1990]
Anhydrite chimneys	-	-	A	An	*Hannington et al.* [2001]
Anhydrite deposits	-	-	A	An, Mn	*German et al.* [1994], *Palmer et al.* [1995]
Si-Fe as cement in volcaniclastic	-	-	I	Op, Hm	*Fouquet et al.* [1994]
Two small fields of chimneys	100 × 50	281°C	A	An, Ba, Op, Py, Sp, Cpy	*Fouquet et al.* [1993a, 1993b], Fouquet et al. (this study), *Charlou et al.* [2000]
Tectonized mature deposits	1000 × 1000	324°C	A	Py, Ba, Op, An, Sp, Cpy	*Langmuir et al.* [1997], Fouquet et al. (this study), *Charlou et al.* [2000]
Carbonate chimneys, CH4 discharge	-	-	I	Ar	Fouquet et al. (this study), *Iris Diving Cruise* 2001
Iron silica mound	-	-	I	Fe, Op	*Hoffert et al.* [1978]
Silicified serpentinite and basalt	-	9°C	A	Fe, Op, Sp	*Fouquet et al.* [1997], *Barriga et al.* [1998], *Costa et al.* [2002], *Dias et al.* [2002]
Field of chimneys + massive sulfides	400 × 100	365°C	A	Is, Cpy, Sp, Po, Pn, Au	*Fouquet et al.* [1997, 1998a, 1998b], *Charlou et al.* [2002], *German et al.* [1999]
Large field of chimneys (60 m high)	400	90°C	A	Ca, Ar, Br	*Kelley et al.* [2001], *Fruh-Green et al.* [2003]
4 Small groups chimneys	-	360°C	A	Py, Cpy, Sp, Is	*Murton et al.* [1994, 1995], *Elderfield et al.* [1993], *Duckworth et al.* [1995], *James et al.* [1995]
Mound	250 × 250 × 45	363°C	A	Py, An, Cpy (Sp)	*Rona* [1984], *Rona et al.* [1993], *Thompson et al.* [1988], *Hannington et al.* [1988], *Humphris et al.* [1995], *Lalou et al.* [1986]
Inactive mounds	-	-	I	Py, Cpy, Sp	*Rona et al.* [1993]
Several mounds	1000 × 900	-	I	Py, Cpy (Sp)	*Rona et al.* [1993], *Krasnov et al.* [1995], *Lisitsyn et al.* [1989], *Zonenshain et al.* [1989]
Veins	-	-	I	Op, Py, Chl	*Rona et al.* [1982], *Rona* [1984]
Massive sulfides	-	-	I	-	*Krasnov et al.* [1995]
Veins	-	-	I	Op, Py, Cpy, Chl	*Rona* [1984]
Veins	-	-	I	Op, Py, Cpy, Chl	*Delaney et al.* [1987], *Kelley and Delaney* [1987]
Si-Fe-Mn mound	-	-	I	Op, Hm	Fouquet et al. (this study)
3 Coalescent mounds	300 × 150	350°C	A	Po, Is, Py, Sp, Cpy, Ma	*Thompson et al.* [1988], *Honnorez et al.* [1990], *Fouquet et al.* [1993c], *Krasnov et al.* [1995], *Karson and Brown* [1989]

Table 1. (continued)

Name	Latitude	Longitude	Depth (m)	Basement Rocks	Geological Control	Distance From Axis
22°30′N	22°30′N	45°00′W	2820	MORB	Rift valley wall	?
Tamar (PDF)	20°30′N	45°39′W	1960	MORB	Top of axial volcano	0
Zenith Victory	20°00′N	45°38′W	2400	MORB	Top of rift valley wall, central part of segment	9
Krasnov	16°38′N	46°28′W	3700	MORB	Top of rift valley wall - lateral volcano	7
15°51′N	15°51′N	46°23′W	(3000)	MORB	Abyssal hills	?
15°05′N	15°05′N	44°56 W	2600	Harzburgite	West rift alley wall, shear zone, detachment fault	2
14°55′N	14°55′N	44°54′W	3500	Harzburgite	East rift valley wall	?
Logatchev 1	14°45′N	44°58′W	3000	Harzburgite	Top of east valley wall; no recent lava	8
Logatchev 2	14°43′N	44°56′W	2700	Harzburgite	Top of east valley wall; no recent lava	12
14°43′N	14°43′N	44°52′W	(3000)	MORB	Top of rift valley wall	?
Semyenov	13°31′N	44°55′W	3700	Harzburgite	W. rift valley wall, base of detachment fault	2?
Ashadze 2	12°59′N	44°54′W	3250	Harzburgite	W. rift valley wall, spreading offset, detachment fault	9
Ashadze 1	12°58′N	44°52′W	4040	Harzburgite	W. rift valley wall, spreading offset, detachment fault	4
12°48′N	12°48′N	44°47′W	2440	MORB	East rift valley wall	?
11°N	11°N	-	3100	MORB	Transform, Vema	?
6°N	6°N	-	?	MORB	Rift zone	?
0°N	0°N	-	3100	MORB	Transform, Romanche	?
Turtle Pits	4°48′S	12°22′W	2990	MORB	Rift valley, fresh Lava	0
Nibelungen	8°18′S	13°30′W	2915	Harzburgite	Nontransform offset	9
Lilliput	9°33′S	12°12W	1500	MORB	Rift valley, lava lake	0

[a]Abbreviations are Ba, barite; Gy, gypsum; Op, opal; Sp, sphalerite; Cv, covellite; Bn, bornite; An, anhydrite; Mn, manganese oxydes; Hm, hematite; Py, pyrite; Cpy, chalcopyrite; Ga, galena; Tn, tennantite; Ar, aragonite; Fe, iron oxyhydroxide; Is, isocubanite; Po, pyrrhotite; Pn, pentlandite; Au, native gold; Ca, calcite; Chl, chlorite; Ma, marcasite; Cb, cubanite; Br, brucite; Mt, magnetite; Wu, wurtzite. Activity : A, active; I, inactive.

Type of Mineralization	Size (m)	Maximum Temperature	Activity	Major Minerals[a]	References
Veins	-	-	I	Py, Op, Chl	*Rona et al.* [1982], *Rona* [1984]
Several mounds	-	-	I	Py, Ma, Cpy, Op	Fouquet et al. (this study), P. Gente (personal communication, 1998)
Mound	1000 × 600	-	?	Py (Cpy, Sp)	*Cherkashov* [2008]
Mound	700 × 400 × 70	-	?	Py (Cpy, Sp)	*Bel'tenev et al.* [2004], *Cherkashov* [2008], *Fouquet et al.* [2008]
Veins	-	-	I	He, Py, CPy	*Akimtsev et al.* [1991]
Quartz veins + silicified harzburgite	-	-	I	Op, Py, Cpy, Cb, Ga	*Fouquet et al.* [1993a, 1993b, 1993c], *Charlou et al.* [1991], *Rona et al.* [1992], *Akimtsev et al.* [1991]
Chimneys	-	-	A	?	*Rona* [1987], *Rona et al.* [1992], *Eberhart et al.* [1989]
Mound and chimneys	400 × 150	353°C	A	Cpy, Is, Sp, Py, Pn	*Krasnov et al.* [1995], *Murphy and Meyer* [1998], *Mozgova et al.* [1999], *Lein et al.* [2003], *Fouquet et al.* [2007]
Small mound and chimneys	100 × 200	320°C	A	Cpy, Is, Sp, Py, Po	*Torokhov et al.* [2002], *Fouquet et al.* [2008]
Veins	-	-	I	Sulfides	*Akimtsev et al.* [1991]
Several mound and chimneys	-		?	Fe and Cu sulfides, Op	*Cherkashov* [2008], *Murton et al.* [2007], *Searle et al.* [2007], *Beltenev et al.* [2009]
Massive sulfides, carbonates	200	296°C	A	-	*Bel'tenev et al.* [2003], *Cherkashov* [2008], *Fouquet et al.* [2008]
Massive sulfides	200	372°C	A	-	*Bel'tenev et al.* [2003], *Cherkashov* [2008], *Fouquet et al.* [2008]
Disseminated	-	-	I	Py, Chl	*Rona et al.* [1982], *Rona* [1984]
Stockwork	-	-	I	Cpy, Py, Po, Chl	*Bonatti et al.* [1976a], *Kirst* [1976]
Massive sulfides + veins	-	-	?	Py, Cpy	*Pushcharovsky* [2003]
Stockwork	-	-	I	Cpy, Py, Po, Ga, Chl	*Bonatti et al.* [1976b], *Kirst* [1976]
Mound + chimneys	-	407°C	A	Cpy, Is, Po, Sp, Py, An, Hm, Mt	*Devey et al.* [2005], *Koschinsky et al.* [2006, 2008], *Haase et al.* [2007]
Chimneys		>153°C	A	Mt, Py, Sp, Wu, Hm	*Koschinsky et al.* [2006], *Melchert et al.* [2008]
Mound of Fe-rich sediments	-	-	I	Fe	*Koschinsky et al.* [2006]

faults [*Cannat et al.*, 1997; *Karson and Rona*, 1990; *Tucholke et al.*, 1998] that expose lower crust and mantle rocks at slow spreading mid-ocean ridges. The discovery of "corrugated" structures on the rift valley flanks [*Cann et al.*, 1997; *Tucholke et al.*, 1998] is a strong argument for this hypothesis. Sampling of these surfaces and their modeling [*Lavier et al.*, 1999] demonstrate that they are normal faults paleo-plans with a large throw. The MAR is characterized by many core complexes exposing ultramafic and gabbroic rocks along detachment faults [*Cann et al.*, 1997; *Escartín et al.*, 2008; *Searle et al.*, 2007; *Smith et al.*, 2006]. These mantle domains are associated with an asymmetry of the ridge [*Escartín et al.*, 2008]. Detachment faults are the main process for bringing peridotites and ultramafic rocks to the seafloor [*Escartín et al.*, 2008]. They are also specific locations where, due to tectonic activity and active serpentinization processes, low and high temperature water circulation may be favored [*Cannat et al.*, this volume; *McCaig et al.*, 2007]. However not all of the ultramafic outcrops are associated with corrugated surfaces, and some may have a more complicated tectonic story [*Cannat et al.*, 1997].

3. HYDROTHERMAL MINERALIZATION ASSOCIATED WITH ULTRAMAFIC ROCKS ALONG THE MAR

Categorized by rock composition (N-MORB, E-MORB, and ultramafic), three major types of vent deposits are identified along the MAR (Plate 1 and Figure 1). Four subtypes associated with specific ultramafic rocks are identified: (1) high temperature sulfide deposits; (2) low temperature carbonate chimneys; (3) pervasive alteration and silicification of ultramafic rocks and Mn oxide precipitates; and (4) deep seated quartz-sulfide veins. Numerous examples of stockwork mineralization also occur within fracture zones along the ridge [*Bonatti et al.*, 1976b] (Figure 1). Recent investigations demonstrate that the Azores triple junction and the 15°N areas are hydrothermally more active than the rest of the ridge. These sites are both associated with E-MORB. Major characteristics of significant hydrothermal sites along the MAR are summarized in Table 1.

Basaltic hosted deposits are at, or near, the volcanic center of the ridge segment and the base and top of the rift valley walls [*Fouquet et al.*, 1995] (Figure 2). The first type includes the Snake Pit [*Fouquet et al.*, 1993c; *Thompson et al.*, 1988], Lucky Strike and Menez Gwen fields [*Fouquet et al.*, 1994, 1995; *Langmuir et al.*, 1997; *Ondréas et al.*, 2009]. A specific case for this type is the Puy des folles field at the top of a very well defined central circular volcano near 20°30′N. At Krasnov, the sulfide deposit is located at the top of the eastern rift wall, where a large circular volcano, rising from the rift valley floor to the top of the rift valley walls, coalesces with the rift wall [*Cherkashov et al.*, 2008; *Fouquet et al.*, 2008]. Some major basaltic hydrothermal fields, such as TAG [*Rona et al.*, 1993; *Thompson et al.*, 1985], are also controlled by deep rooted detachment fault [*deMartin et al.*, 2007] and are at the same latitude as the regional volcanic topographic high, indicating a preferential location near the site of the highest magma budget of the segment.

Hydrothermal deposits within ultramafic rocks along the MAR (Figures 1 and 2) are all related to low magmatic budget environments near the end of the ridge segments. In addition to hydrothermal discharge associated with the volcanic part of mid-ocean ridge spreading centers, chemical anomalies in the water column have been reported near the intersection of the ridge with fracture zones and nontransform offsets [*Bougault et al.*, 1993; *Charlou et al.*, 1991, 1997, 1998; *Gracia et al.*, 2000; *German and Parson*, 1998]. Ultramafic dome-like structures at the inside corner of ridge-transform fault intersection (Figure 2) are preferential locations for strong methane discharge [*Charlou et al.*, 1997, 1998] as well as low-temperature carbonate hydrothermal systems [*Kelley et al.*, 2001]. The methane is a by-product of active serpentinization during the Fischer Tropsch reaction [*Charlou et al.*, 1991]. Thus, hydrothermal processes associated with serpentinization are quite variable in terms of temperature and the type of deposits.

Four ultramafic hydrothermal fields (Menez Hom, Saldanha, Lost City, and 15°05′N) are located on an ultramafic dome at the inside corner of the intersection of the MAR with a transform fault or a nontransform offset. Two sites (Rainbow and Nibelungen) are located at the central part of a nontransform offset (Figure 2). Four others sites (Logatchev 1 and 2 and Ashadze 1 and 2) are controlled by deep detachment faults on the flank of the rift valley walls. The newly discovered Semyenov field [*Cherkashov*, 2008; *Murton et al.*, 2007; *Beltenev et al*., 2009], the small inactive Ashadze 4 site, and the mineralized quartz veins at 15°05′ are at the base of the detachment fault near the contact between ultramafic rocks and the basaltic coverage. All of these ultramafic sites are clearly structurally controlled. We present, hereafter, the main characteristics of typical sites for each of these types.

3.1. Ashadze Vent Fields (12°58′N)

Two active black smoker fields Ashadze 1 (4100 m) and Ashadze 2 (3260 m) are located on the western slope of the MAR rift valley [*Bel'tenev et al.*, 2003; *Cherkashov et al.*, 2008; *Sudarikov et al.*, 2001]. These sites were first visited by a submersible in 2007 during the Serpentine cruise [*Fouquet et al.*, 2008]. The Ashadze 1 and 2 sites, 5 km apart, are, respectively, 4 km and 9 km off-axis. The top of the rift

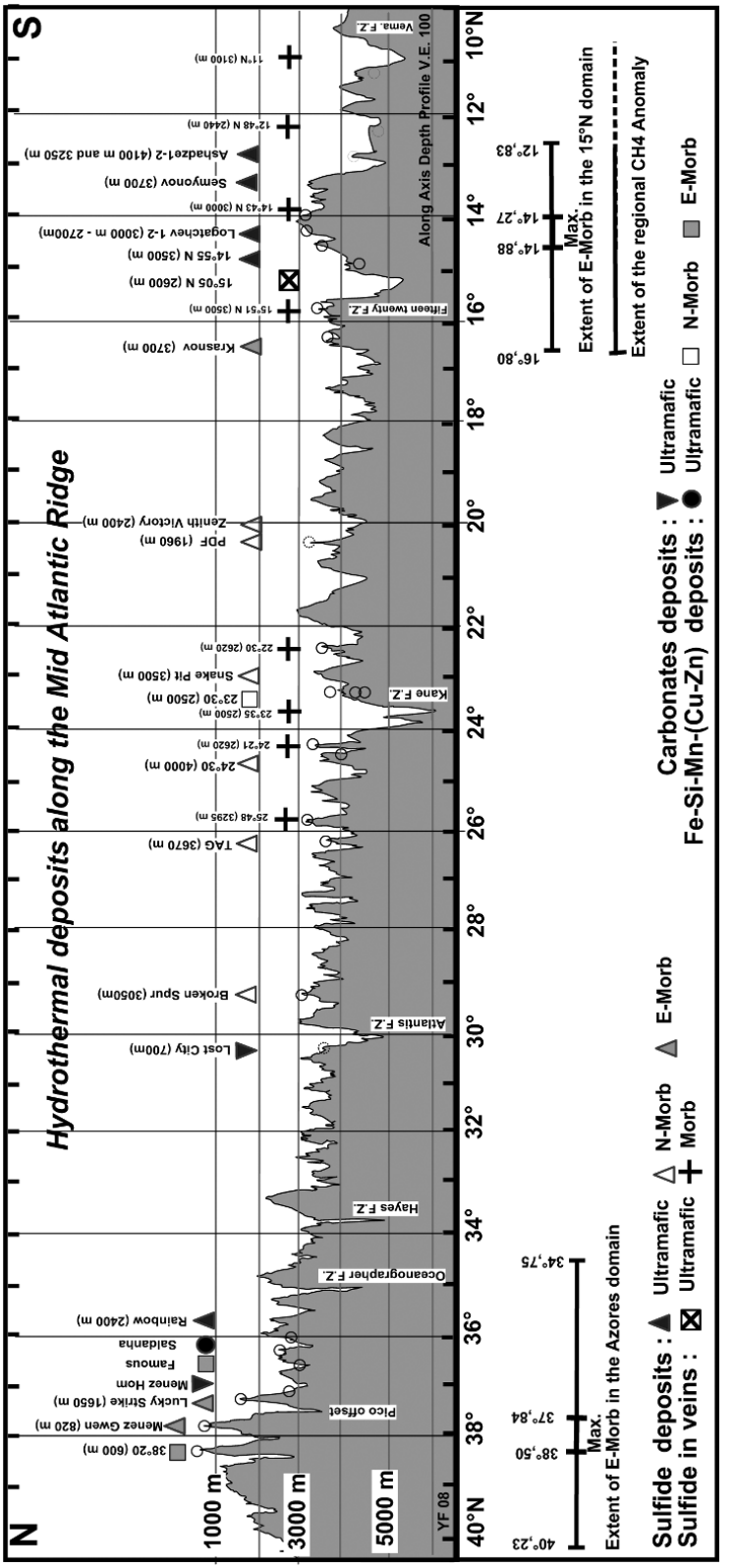

Figure 1. Along-axis bathymetric profile of the Mid-Atlantic Ridge (MAR) between 40°N and 10°N, location of the known hydrothermal fields, type of deposits, and composition of basement rocks. The extension of enriched-Mid-Ocean Ridge Basalt (E-MORB) in the Azores and 15°N domains is also shown. Note the coincidence between the northern limit of regional CH_4 anomalies and enriched domains at 15°N. In both areas, the maximum of basaltic anomaly corresponds to the regional topographic high.

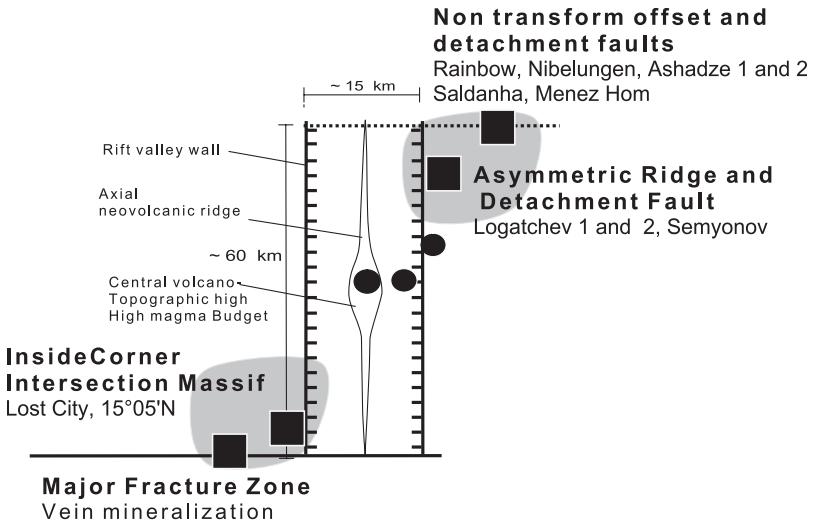

Figure 2. Geological control of hydrothermal activity along slow spreading ridges. Examples from the Mid-Atlantic Ridge (MAR) at the scale of a typical volcanic segment (modified after *Fouquet* [1997]). Solid circles indicate specific settings for basaltic-hosted deposits. Solid squares indicate specific setting for ultramafic-hosted deposits. The shaded areas correspond to ultramafic outcrops and to the asymmetric part of the ridge related to detachment faults and high permeability areas.

valley wall, at 2300 m, corresponds to the termination of a large fossil corrugated surface. The host rocks of the deposits are serpentinized peridotites with interspaced gabbroic bodies, which are very common in the rift valley slopes in this segment of the MAR. The axial valley at this latitude is strongly asymmetric, with higher relief to the west. This asymmetry is reversed immediately to the south, where the axial magnetic anomaly appears offset by a few kilometers to the west [*Cannat et al.*, 2007]. The Ashadze vents are roughly aligned to the north of an irregular, south-facing slope, which is interpreted as the surface expression of this minor axial discontinuity [*Cannat et al.*, 2007; *Fouquet et al.*, 2008]. The high-resolution bathymetric maps show a clear relationship between gravitic processes, transversal faults, and the location of the Ashadze 1 site. Extinct sulfide chimneys were also sampled near the base of the axial valley wall at 4530 m depth (Ashadze 4). Opposite to the other sites, this deepest site is basalt hosted. Active vents at Ashadze 1 are distributed over an area about 150 m long. Away from the vents, topography appears dominated by slope failure, with prominent landslides. Black smokers at Ashadze 2 lies in a narrow (about 70 m), N-S trending graben-like trough [*Ondreas et al.*, 2007] bounded to the east by a faulted gabbroic body. To the west, it is limited by a narrow N-S trending ridge, 20 to 50 m high that bears numerous extinct hydrothermal chimneys. On the Ashadze 2 site, a large group of smokers occurs, in a crater-shaped depression, about 25 m in diameter at the bottom of the graben structure. This constructional structure may indicate the sometimes-explosive nature of the hydrothermal fluid emissions [*Fouquet et al.*, 2008].

3.2. Logatchev Vent Fields (14°45′ and 14°43′N)

The hydrothermal fields are at a depth of 2970 m (Logatchev 1) and 2700 m (Logatchev 2) are on an uplifted block of serpentinized ultramafic rocks with local gabbroic intrusions on the eastern wall of the rift valley [*Krasnov et al.*, 1995; *Lein et al.*, 2003]. There are similarities between the regional context at Ashadze, and the setting of the two Logatchev vent fields. Both fields lie to the north of a small offset axial discontinuity and in an inward position relative to fossil corrugated surfaces. Logatchev sites, 5 km apart, are located 8 and 12 km off-axis and located on serpentinized mantle rocks. Logatchev 1 comprises many vents in a NW-trending elongated area about 400 m long. High-resolution mapping at 20 m (550 × 750 m) reveals the circular crater-like shape of many venting areas, 10 to15 m in diameter and a few meters deep. High-resolution map also show a complex arrays of scarps and fissures, oriented predominantly E-W, and NE-SW [*Ondreas et al.*, 2007; *Petersen et al*., 2009]. Numerous lens-shaped slump features are also revealed near the vents. The Logatchev 2 field was found to be active in 2007 [*Fouquet et al.*, 2008], its position, 12 km off-axis, moves from 8 (Logatchev 1) to 12 km the possibility to have off-axis black smokers along the MAR. The Logatchev 2 fluids (320°C) are unusual by their low salinity [*Charlou et*

al., this volume]. A low-temperature (dominantly birnessite) inactive hydrothermal field (Logatchev 5) is at the summit of the Logatchev ridge, located 1 km east of Logatchev 1 [*Fouquet et al.*, 2008]. A second inactive site, about 100 m in diameter, with unaltered sulfide chimneys, was photographed at a water depth of about 3500 m on a fault block associated with ultramafic rocks on the lower east wall of the rift valley [*Eberhart et al.*, 1989] but was never visited by a submersible.

3.3. Saldanha Field (36°33'N)

At the southern tip of the French-American Mid-Ocean Undersea Study segment, in a nontransform setting, intense CH_4 anomalies in the water column [*Charlou et al.*, 1997] indicate hydrothermal venting associated with serpentinization of an unroofed, 700 m high, serpentinite protrusion. Diving operations [*Barriga et al.*, 1998; *Fouquet et al.*, 1997, 2000] revealed intensely altered and locally silicified ultramafic and basaltic rocks at the top of the massif. Discrete low-temperature diffuse discharge (<6°C) from the sediment was observed near the top of the structure. Although no chimneys are present, the hydrothermal activity is expressed as discharge of clear fluid from several small orifices through sediment over an area of at least 50 m^2, and microchimneys with silica and sulfides were observed [*Dias et al.*, 2002; *Dias*, 2001]. Mount Saldanha, is composed, from base to top, of ultramafic rocks, metagabbro, metabasalt, indurated sediment, and sedimentary ooze, mapped on the flanks of the hill [*Barriga et al.*, 1998; *Dias et al.*, 2002]. At the top of Mount Saldanha, a mélange of all these rock types is exposed, showing varying degrees of hydrothermal alteration and silicification. The elevation of Mount Saldanha results from volume increase related to serpentinization of the ultramafic rocks. During the serpentinization of the ultramafic rock, overlying rocks were pushed upward, generating the observed mélange. Talc-rich rocks (steatite) and spilite are commonly observed [*Costa*, 2001; *Costa et al.*, 2002]. The hydrothermal alteration (chlorite, smectite, quartz, and sulfides) suggests temperatures of 200 to 300°C [*Costa*, 2001; *Costa et al.*, 2002]. Carbonate ooze covering the mound is enriched in Mg, Mn, Zn, Cu and S including locally hydrothermally produced sulfides (chalcopyrite, sphalerite) and poorly crystallized Mn oxyhydroxides [*Dias*, 2001; *Dias et al.*, 2002].

3.4. Rainbow (36°14'N)

The Rainbow field is a site of high temperature (360°C) hydrothermal activity [*Charlou et al.*, 1997; *Fouquet et al.*, 1997, 1998a; *German et al.*, 1999] located in a second-order discontinuity of the MAR south of the Azores [*Aballea et al.*, 1998; *German and Parson*, 1998; *Parson et al.*, 1997, 2000]. The high-temperature venting occurs along the shoulder of a west-facing hanging scarp of a tilted ultramafic block. The shoulder is cut by a network of intersecting N-S and NE-SW faults. Active venting and relict hydrothermal deposits exhibit tectonic control at a range of scales. Around the site and through the nontransform discontinuity, a relative chronology of normal dip-slip extensional faulting, conjugate transtensional faulting, and Riedel shears are evident. The western border of the vent field is a 25-m-high fault scarp where extensive stockwork mineralization and replacement of ultramafic rocks by sulfides are observed [*Marques et al.*, 2006, 2007]. The entire vent field is underlain by ultramafic rocks. Only a small veneer of old basalt occurs at the east-tilted summit of Rainbow ridge, 1 km east of the active vents. Since the western side of the hydrothermal field is tectonized with only low temperature diffuse discharge, and the eastern side very active with only small chimneys, it seems that the high temperature activity is propagating to the east. A second inactive site (Rainbow 2), with 2- to 3-m-high chimneys, is located near the top of Rainbow ridge. At many places, unusual lithification of the sediment around the active field and near the top of the Rainbow ridge, together with several places with dead mussels, may be related to diffuse low temperature of methane-rich fluid through the sediment. Similar processes were also proposed at Saldanha, Menez Hom, and Lost City sites where large amount of methane discharge through the sediment cover at the top of the ultramafic ridge [*Ribeiro da Costa et al.*, 2008; *Schroeder et al.*, 2002].

3.5. Lost City (30°10'N)

Lost City is an extensive hydrothermal field in ultramafic rocks at 30°N near the eastern intersection of the MAR and the Atlantis fracture zone [*Fruh Green et al.*, 2003; *Kelley et al.*, 2001]. The active vents are located on a dome-like massif at the inside corner of the intersection of the MAR and the Atlantis Transform Fault. The massif is approximately 15 km across, and the southern flanks are steep escarpments with 3800 m of relief adjacent to the transform fault. The upper surface of the dome is interpreted to be a low-angle detachment fault that has exposed variably metamorphosed peridotite and gabbro. The core complex just north of the Lost City site was drilled and revealed to be dominantly composed of gabbro with virtually no serpentinized peridotites [*Ildefonse et al.*, 2007]. Magnetic anomaly patterns show that the center of the massif, about 15 km west of the spreading axis, is about 1.5 Ma old, consistent with the local half-spreading rate of 12 mm a^{-1}. The hydrothermal deposits are dominated by steep-sided carbonate chimneys. Vent fluids are relatively cool (90°C) and alkaline (pH 9.8) [*Fruh*

Green et al., 2003; *Kelley et al.*, 2001]. Radiocarbon ages document at least 30,000 years of hydrothermal activity, which is thought to be, at least, partly driven by serpentinization reactions at Lost City [*Fruh Green et al.*, 2003].

3.5.1. Fifteen Twenty Fracture Zone site (15°05′N). Ultramafic rocks occur as domes and elongated ridges on the valley floor and on the rift wall at the intersections of the MAR with the 15°20′N Fracture Zone [*Fouquet et al.*, 1993a]. They consist of dunite, harzburgite, and gabbro. At the eastern intersection (15°N), the contact of an ultramafic dome with the neovolcanic zone of the rift valley is very sharp and controlled by a major fault parallel to the ridge system. At ultramafic outcrops, parallel to the ridge, elongated patches of white material enriched in chlorite and aragonite are interpreted to be the seafloor manifestation of water circulating along faults. Locally in these white areas, ultramafic rocks are silicified and impregnated with disseminated sulfides. The most spectacular samples are mineralized quartz veins from the major detachment fault near the contact between the ultramafic rocks and the basaltic neovolcanic ridge. The mineralized samples have been uplifted along faults and are believed to represent the deeper portions of a black smoker system, although massive sulfide mineralization has not been observed in the area. Disseminated sulfide mineralization also appears to be related to primary magmatic processes related to gabbroic dikes and is associated with serpentinization, talc-carbonate alteration, and silicification. The observed mineralization and alteration is similar to the obduction-related listwaenite mineralization known on land, such as the sulfide mineralization associated with altered ophiolitic serpentinites, particularly in carbonatized and silicified serpentinites [*Auclair et al.*, 1993; *Buisson and Leblanc*, 1985, 1986, 1987].

3.6. Menez Hom

Similar to the Saldanha, the Menez Hom ultramafic dome is situated at an inside corner position relative to the nontransform offset at the south of the Lucky Strike segment. As for the Saldanha field, one of the strongest CH_4 anomalies [*Charlou et al.*, 1997] so far known on the MAR was seen in the water column at the top of this dome. Diving operations revealed the general outcrop of ultramafic rocks at the top of the dome. No active vents were seen; however, one small carbonate chimney was sampled, and as for Saldanha and Rainbow, anomalous rapid lithification of the sediment covers was observed at the northern side of the dome, near the limit between the ultramafic rocks and the basalt coverage. This may indicate a preferential discharge of diffuse low-temperature CH_4-rich fluids at the contact between the ultramafic and the basalt cover.

4. MORPHOLOGY OF ULTRAMAFIC-HOSTED HYDROTHERMAL DEPOSITS

4.1. Mound Structures and Stockwork Mineralization

As for basaltic-hosted hydrothermal fields, the morphology of ultramafic-hosted sulfide deposits is controlled by several local factors such as depth, phase separation, hydraulic fracturing, and permeability [*Fouquet*, 1997]. In ultramafic high-temperature environments (Rainbow, Logatchev, Ashadze), the discharge is clearly less focused than at basaltic sites, with venting of a single end-member fluid occurring over most of the hydrothermal fields. This "diffuse" black smoker discharge produces relatively flat deposits without clearly organized mounds quite different from basaltic environments where a conical mound is typically formed (Figure 3). In addition, pervasive near-surface high-temperature circulation generates highly altered areas and enhance subsurface sulfide precipitation, large stockwork mineralization, and complete replacement of the ultramafic rocks by massive sulfides. Indeed, all stages of a complete replacement of serpentinites by Cu-rich massive sulfides are observed in dredged samples from Rainbow [*Fouquet et al.*, 1997; *Marques et al.*, 2006, 2007].

4.2. Hydrothermal Crater Structures and Hydraulic Fracturing

Silicification of the host rocks and precipitation of silica within the fluid channel ways commonly contribute to fluid overpressure and explosive fragmentation. This is described for many ancient deposits [*Gibson et al.*, 1999] but is not clearly demonstrated in modern deposits. An explosive episode at the active top of the Snake Pit field was observed during the Microsmoke cruise (1995), where heavy instruments for bacteria colonization, left at the base of the black smoker complex, were hurled away and broken into several pieces found several tens of meters apart on the flank of the sulfide mound. Samples collected in the small crater left at the base of the black smoker complex (water depth 3500 m) were massive pyrite with anhydrite impregnation very similar to the material cored near the surface of the TAG mound [*Humphris et al.*, 1995]. The best explanation is an explosive hydraulic fragmentation due to overpressure. This observation and the large amount of breccia within the TAG mound indicate that hydraulic fragmentation is a major process that can be observed on the seafloor in deep submarine hydrothermal systems. Silicification of the host rocks certainly favors this process. Thus, the fragmentation of the mound may not only be due to the collapse of the mound due to retrograde solubility of anhydrite, but can also be due to hydraulic fragmentation.

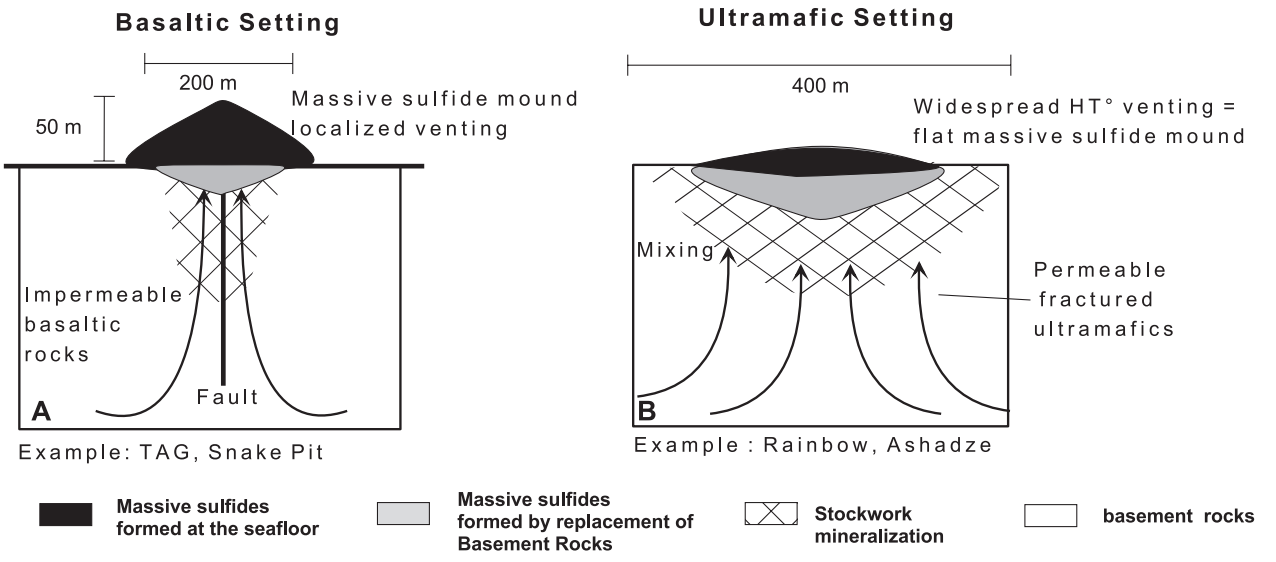

Figure 3. Differences in the morphology of deposits and type of discharge between basaltic and ultramafic hydrothermal deposits. Compared to (a) basaltic hosted fields, discharge is less focused in (b) ultramafic environments, and no real mound is formed; part of the deposit may occur as replacement of the ultramafic rocks.

In ultramafic environments, this process can also be active. The extreme diversity of mixed hydrothermally altered basaltic, gabbro and ultramafic rocks at the Saldanha site may be interpreted as the result of near-surface hydraulic fracturing. This process may be due to the silicification of altered rocks that create an impermeable lid favoring the overpressure necessary for hydraulic fracturing. At Logatchev many groups of black smokers are at the deepest part of crater-like circular structures, up to 10 m in diameter and a few meters deep. Black smokers are emitted from the very bottom of the depression where no chimneys are observed. After 10 years, they are still active but with no major chimneys in the same crater. One hypothesis to consider to create these unusual structures and for the absence of chimneys, is periodic hydraulic events similar to the one observed at Snake Pit. These events will maintain the crater structure and destroy any chimney. Similar hydrothermally very active crater-like structures were recently seen at Ashadze 2 [*Fouquet et al.*, 2008; *Ondreas et al.*, 2007] and at the Drachenschlund vent at the Nibelungen hydrothermal field vent fields, both associated with ultramafic rocks [*Koschinsky et al.*, 2006; *Melchert et al.*, 2008]. At Ashadze 2, many small active sulfide chimneys are at the deepest part of the crater structure. Similar oxided Cu-rich chimneys were sampled on the outer flank of the crater. As there is no venting at the outer part, the best explanation is that these chimneys are thrown away during an explosive event that contributes to maintain the crater shape. Thus, these crater structures seem to be a common feature in ultramafic-hosted sulfide deposits that contribute to the specific morphology of ultramafic-hosted sulfide deposits.

4.3. Zonation

As for fossil deposits, MAR basaltic-hosted deposits show a clear metal zonation; most deposits are enriched in Zn at their surface and enriched in Cu at their core. This zonation represents the successive replacement of a lower temperature pyrite-sphalerite assemblage by a higher temperature chalcopyrite-pyrite or pyrrhotite assemblage over several stages of zone-refining processes [*Sangster and Scott*, 1976] during which Zn and associated elements (Pb, As, Sb, Cd, and Ag) are progressively enriched at the surface of the deposit [*Fouquet et al.*, 1998b; *Hannington et al.*, 1998; *Humphris et al.*, 1995]. These successive dissolution, reprecipitation, or zone refining processes are clearly demonstrated by drilling the TAG mound. The thermal evolution of the sulfide lens is a function of near-surface self-sealing processes. This is important as it limits the cooling and mixing of ascending metal-rich fluids. In ultramafic environments, the vertical zonation is less clear. At Rainbow, Logatchev, and Ashadze, surface samples are enriched in copper compared to their basaltic equivalent. This is probably due to the less focused geometry of the discharge. At these fields, black smokers and high-temperature Cu-rich sulfides, are seen all over the field and not only in a small area at the top of the

mound as at TAG. Thus, more diffuse high-temperature discharge will produce Cu-rich sulfide all over the surface of the deposit and explain the spectacular Cu enrichment at the surface of high-temperature ultramafic sulfide deposits. In addition, the pervasive subsurface circulation generates an extensive Cu-rich stockwork. Thus, ultramafic-hosted massive sulfide deposits have chemical and mineralogical zonation less organized vertically and horizontally than basaltic deposits.

5. FLUID COMPOSITIONS IN ULTRAMAFIC ENVIRONMENTS

A summary of the fluid composition of active black smoker fields on the MAR is presented in Table 2 [*Campbell et al.*, 1988; *Charlou et al.*, 1996, 2000, 2002; *Douville et al.*, 2002; *Edmond et al.*, 1995; *James et al.*, 1995; *Jean Baptiste et al.*, 1991; *Lein et al.*, 2000; *Von Damm et al.*, 1998]. Details on recent sampling can also be found in the chapter by *Charlou et al.* [this volume]. Two processes play a major role in fluid compositions: phase separation and the composition of the basement rocks; magmatic fluids cannot be excluded but have not yet been demonstrated on the MAR. Except at Lucky Strike, fluids from the MAR have a single end-member composition indicating a single deep source.

High-temperature hydrothermal fluids from ultramafic environments (Logatchev and Rainbow) have significantly lower H_2S, Si, Al, and Li. Fluids from Rainbow have the highest Ca and Sr concentrations. The most metal-enriched fluids at the Rainbow site (365°C) have the lowest pH (2.8) and highest Cl (750 mM) observed on the MAR. The high salinity is commonly explained by the presence of brine formed during subcritical phase separation; however, at several sites, more complex supercritical processes have to be considered [*Charlou et al.*, this volume; *Koschinsky et al.*, 2008]. Theoretical reaction path calculations predict that peridotite-seawater interactions will generate hydrothermal fluids with higher pH, lower aqueous SiO_2, K concentrations that are highly sensitive to the water-rock ratio, and very much higher H_2 content [*Wetzel and Shock*, 2000] than in basaltic setting. Compositions of fluids at Rainbow are in agreement with these predictions, except for the very low pH. *Allen and Seyfried* [2003] have calculated a pH of 5 assuming magnetite-fluid equilibrium at temperature and pressure conditions of Rainbow and considering the measured H_2 concentration of 16 mmol [*Charlou et al.*, 2002, this volume]. They argued that the low pH and SiO_2 concentrations (~7 mmol) [*Charlou et al.*, 2002, this volume] reflect orthopyroxene dissolution. Thus, reactivity of the pyroxene strongly affects the pH decrease by providing excess silica. Excess of silica also may be due to reaction of the fluid with gabbroic intrusions. The relatively high SiO_2 content stabilizes talc and actinolite/tremolite. High metal concentrations (Fe, Ni, Cu, Zn), extracted from olivine and pyroxene, are favored by Cl complexing at low-pH and high-temperature conditions. In addition, during phase separation, both the acidity and the concentration of heavy metals increase in the chloride-rich phase [*Bischoff and Rosenbauer*, 1987].

One striking point is the high rare earth element (REE) concentration at Rainbow. Chondrite-normalized REE patterns for fluids at Rainbow show strong light REE enrichment with a positive europium anomaly indicative of basalt-seawater interaction [*Douville et al.*, 2002]. The REE pattern and concentrations seem to indicate reaction with plagioclase that is absent from ultramafic rocks. This suggests that the fluids have interacted with both gabbroic and ultramafic rocks. Barium is also much higher in fluids from Rainbow than in fluids from N-MORB environments. Because ultramafic rocks are depleted in barium, Ba enrichment in the fluid may be explained by interaction with a deep, Ba-enriched gabbroic intrusion. In addition, at Rainbow, due to the close proximity of the Azores hotspot, the enriched character of the E-MORB is also linked to Ba enrichment in the lava (and related gabbroic intrusion (see discussion on Ba in the part on hydrothermal precipitates). The high concentration of H_2 demonstrates active serpentinization in the deeper part of the hydrothermal system and indicates the extremely reducing subsurface conditions.

The concentrations of transition metals (Fe, Mn, Cu, and Zn) at Rainbow are currently the highest among the MAR fluids. The abundance of metals is favored by Cl complexing at low pH and high temperature. The best explanation for these enrichments is the fluid properties (fluid salinity, temperature, and low pH) rather than an enrichment of these elements in the source rocks. For all sites, there is a strong correlation between chlorinity and metal concentration indicating that Cl complexes dominate Rainbow fluid speciation [*Douville et al.*, 2002]. However, the high Co and Ni concentrations in both fluids and sulfide deposits are consistent with the predominant role of ultramafic source rocks at Rainbow.

Except for their low Si content, the composition of the fluids at Logatchev is similar to those at Snake Pit [*Von Damm et al.*, 1998]. The fluid chemistry indicates that Logatchev has a weaker ultramafic influence than the Rainbow field; Co and Ni are not enriched. Compared to black smoker fluids, Lost City fluids are relatively cool (40–90°C) and alkaline (pH 9.0–9.9) and are not associated with sulfide mineralization [*Kelley et al.*, 2001].

Table 2. Composition of the End-Member Hydrothermal Fluids Along the Mid-Atlantic Ridge[a]

		E-MORB			N-MORB				Ultramafic Rocks		
	Seawater	Menez Gwen[b]	Lucky Strike[c]	Lucky Strike[c]	Broken Spur[d]	TAG[e] Black Smoker	TAG[e] White Smoker	Snake Pit[f]	Rainbow[g]	Logatchev[h]	Lost City[i]
Depth (m)		850	1,700	1,700	3,200	3,670	3,670	3,460	2,300	3,000	800
T° (°C)	2	284	185	324	360	363	301	301	365	353	91
Cl (mM)	546	380	413	554	469	650	-	550	750	515	549
pH	7.8	4.4	3.4	5	-	3.1	-	3	2.8	3.3	11
Mg (mM)	53	0	0	0	0	0	-	0	0	0	19
SO_4 (mM)	28.2	0	0	0	0	0	-	0	0	0	-
Br (µM)	838	666	735	924	749	1,045	-	847	1,178	818	-
Si (mM)	0.178	8.2	8.2	16.3	-	20	19.1	20	6.9	8.2	-
Li (µM)	26	270	265	365	1,030	430	-	835	340	245	
Na (mM)	464	313	344	444	420	550	-	515	553	438	485
K (mM)	10.2	23	21	31	19	18	17.1	23	20	22	
Ca (mM)	10.2	32	31	42	12	28	27	11	67	28	23.3
Rb (µM)	1.3	30	23	48	13	9.5	9.4	12	37	28	-
Sr (µM)	87	110	80	130	45	103	91	54	200	138	-
Ag (nM)	0.023	4.3	4.7	25	-	51	-	31	47	11	-
Al (µM)	<0.1	-	4	11	-	10	-	12	2	4	-
As (nM)	23	247	-	199	-	<11	-	115	-	49.5	-
Ba (µM)	0.14	>12	>6	>80	>21	>19	-	>4.3	>67	>4.5	-
Cd (nM)	0.7	<9	18	79	-	66	-	440	130	63	-
Co (µM)	0.03	<2	<2	<2	-	<2	-	<2	13	<2	-
Cs (nM)	2	330	200	330	144	110	113	170	333	385	-
Cu (µM)	0.0033	<2	<2	30	43	130	3	35	140	27	-
Fe (µM)	<0.001	<2	70	920	1,970	5,170	3,830	2,400	24,000	2,500	-
In (nM)	0.0009	<1	<1	<1	-	2.2	-	<1	3.2	<1	-
Mn (µM)	<0.001	59	77	450	254	710	750	400	2,250	330	-
Mo (nM)	104	11	2.7	84	-	5	-	3	2	1	-
Ni (µM)	<2	<2	<2	<2	-	<2	-	<2	3	<2	-
Pb (nM)	0.013	21	35	130	-	110	-	265	148	86	-
Sb (nM)	1.2	3	<3	6.3	-	3.9	-	11	3.1	<3	-
Tl (nM)	0.069	12	7.1	16	-	13	-	25	9	7	-
Zn (µM)	0.028	<2	<2	40	72	83	350	53	160	29	-
Y (pM)	146	300	320	3,300	-	6,800	-	3,400	19,100	5,600	-
REE (pM)	10	160	190	2,550	900	1,800	-	4,300	16,800	3,600	-
H_2S (mM)	0	<1.5	0.6	3.4	11	6.7	0.5	5.9	1.2	0.8	0.064
CO_2 (mM)	2.3	17	13	28	7.1	3.4	-	6.7	16	10.1	-
CH_4 (mM)	0.0003	1.35	0.5	0.97	0.13	0.147	-	0.062	2.5	2.1	0.28
H_2 (mM)	0.0004	0.024	0.02	0.73	1.03	0.37	-	0.48	16	12	0.43–15

[a]REE is rare earth element.
[b]*Charlou et al.* [2000, 2002].
[c]*Charlou et al.* [2000], *Douville et al.* [2002], and *Von Damm et al.* [1998].
[d]*James et al.* [1995] and *Lein et al.* [2000].
[e]*Campbell et al.* [1988], *Charlou et al.* [1996], and *Edmond et al.* [1995].
[f]*Campbell et al.* [1988] and *Jean Baptiste et al.* [1991].
[g]*Charlou et al.* [2002] and *Douville et al.* [2002].
[h]*Charlou et al.* [2002] and *Douville et al.* [1997].
[i]*Kelley et al.* [2001] and *Kelley et al.* [2005].

Table 3. Mineralogical Composition of Hydrothermal Deposits Along the Mid-Atlantic Ridge[a]

				E-MORB[c]			
	T[b] (deg)	Chemical Formula	Mineral	1	2	3	4
Fe	HT	FeS_2	Pyrite	+++		++	+++
		FeS	Troilite				
		$Fe_{1-x}S$	Pyrrhotite				
	LT	FeS_2	Marcasite	++		++	++
		FeS_2	Melnikovite				
		$FeFe_2S_4$	Gregeite				
Zn	MT	(Zn,Fe)S	Sphalerite	++		++	+++
		(Zn,Fe)S	Wurtzite				
Cu	HT	$CuFeS_2$	Chalcopyrite			++	+++
		$CuFe_2S_3$	Isocubanite	×			
		$CuFe_2S_3$	Cubanite				
		$CuFe_3S_4$	"ISS"				
		$Cu_2Fe_3S_5$	Phase Y				
		Cu_5FeS_4	Bornite	×			
	LT	Cu_2S	Chalcocite				
		Cu_9S_5	Digenite				×
		CuS	Covellite	×		×	×
		$Cu_{1.1}S$	Jarrowite				
		Cu_9S_5	Roxbyite				
		Cu_5FeS_6	Idaite				
		$CuSO_4$ $5H_20$	Chalcantite				
		$Cu_{31}S_{16}$	Djurleite				
		Cu_7S_4	Anilite				
		Cu_8S_5	Geerite				
		$Cu_{1.4}S$	Spionkopite				
		Cu_9S_8	Yarrowite				
		Cu_2O	Cuprite				
Pb	MT	PbS	Galena			++	×
		$Pb_{14}As_6S_{23}$	Jordanite				
As, Sb, Ag		$(Cu,Fe)_{12}Sb_4S_{13}$	Tetraedrite				
		$(Cu,Fe)_{12}As_4S_{13}$	Tennantite			×	×
		Ag_2S	Acanthite				
		Cu_3AsS_4	Luzonite				
		$AgFe_2S_3$	Argentopyrite				
		Ag_2S	Argentite				
		CoAsS	Cobaltite				
		(Co,Fe) As_2	Loellingite-safflorite				
Ni-Co	HT	$(Fe,Ni)_9S_8$	Pentlandite				
		$(Fe,Co,Ni)_9S_8$	Co-Pentlandite				
		$(Fe,Ni,Co)S_2$	Bravoite				
	MT	NiS	Millérite				
		$(Fe,Ni)S_{0.9}$	Mackinawite				
		$CoCo_2S_4$	Linnaeite				
		Ni_2FeS_4	Violarite				

N-MORB[c]														Harzburgite[c]								
Massive Sulfides						Veins								Veins	Massive Sulfides					Carbonates		
5	6	7	8	9	10	11	12	13	14	15	16	17	18	19	20	21	22	23	24	25	26	27
+++	+++	+++	+++	+++	+++	+++	++	+++	+++	+++		+++	+++	×	×	++	×	++	×			×
															×			×				
++			++										+++	++	++	×		++	×			
++	++	++	++	++	++										×	++	×	×				
			++																			
																		×				
++	++	+++	++	×	×									×	++	++	+++	+++	++			×
	×		×												++			×				
++	++	+++	++	++	×		++	++		+++	×		+++	+++	+++	+++	+++	+++	+++			×
++	×		+++											×	+++	++	++	+++	++			×
														++								
			×													×						
															×	×	×	×				
	×		×												++	++	++	×	×			
			×												++	×	×	×				
×		×	×												×	×		×				
×	×	×	×											×	×	++	×	×	×			
															×	×	×					
															×	×		×				
			×												×	×						
															×	×						
															×	++		×				
																×		×				
															×	×		×				
															×	×	×	×				
																×						
															×							
×			×											×	×		×	×				
×			×																			
																	×					
			×												×		×	×				
																	×	×				
																	×					
																	×		×			
																	×		×			
																	×			×		
																	×					
														++	×							
															×	++		×				
														×								
														×	×							
														×								
															×							
														×								

Table 3. (continued)

	T[b] (deg)	Chemical Formula	Mineral	E-MORB[c] 1	2	3	4
Mo	MT	MoS_2	Molybdenite				
Te-Bi	HT	HgTe	Coloradoite				
		$NiTe_2$	Bi-Melonite				
Native	LT	Cu	Copper				
	MT	Au	Gold				
		(Au,Ag)	Electrum				
		Cd	Cadmium				
		Ag	Silver				
		As	Arsenic				
		Pt(Fe,Cu)	Platinum				
		S	Sulfur				
Sulfates	HT	$CaSO_4$	Anhydrite			+++	+++
		$CaSO_4 2H_2O$	Gypsum	×		×	×
	MT	$BaSO_4$	Barite	×		+++	+++
	LT	$KFe_3SO_4\ 2(OH)_6$	Jarosite				×
Oxydes	HT	Fe_2O_3	Hematite				
		Fe_3O_4	Magnetite				
	MT	SnO_2	Cassiterite				
	LT	FeO(OH)	Goethite				
		FeO(OH)	Lepidocrocite				
		$Fe_2O_3\ 0.5H_2O$	Ferrihydrite				
		$Mg(OH)_2$	Brucite				
Si	LT	SiO_2	Opal			+++	+++
		SiO_2	Chalcedony				
	HT	SiO_2	Quartz	++			×
Carbonates	LT	$FeCO_3$	Siderite				
		$CaCO_3$	Aragonite	++			
		$CaCO_3$	Calcite				
		$(Mg,Fe)CO_3$	Magnesite				
Chloride	LT	$Cu_2Cl(OH)_3$	Atacamite, Paratacamite				×
Mn	LT	$(Na,Ca,K)Mn_2O_4\ 1.5(H_2O)$	Birnessite		+++		
		$(Na,Ca,K)_2Mn_6O_{12}\ 3(H_2O)$	Todorokite		+++		
U	LT	UO_2	Uraninite				

[a]Reference numbers indicate the following: 1, Kolbeinsey [*Stefansson*, 1983; *Olafsson et al*., 1990]; 2, S. Iceland [*German et al*., 1994]; 3, Menez Gwen [*Fouquet et al*., 1994, 1997, this study]; 4, Lucky Strike (Fouquet et al., this study); 5, Broken Spur [*Duckworth et al.*, 1995]; 6, TAG [*Thompson et al*., 1985, 1988; *Fouquet et al*., 1998b; *Knott et al*., 1998]; 7, TAG (Mir) [*Rona et al*., 1993; *Lisitsyn et al*., 1989; *Tivey et al*., 1995]; 8, Snake Pit [*Thompson et al.*, 1988; *Honnorez et al*., 1990; *Fouquet et al*., 1993c]; 9, PDF (Fouquet et al., this study); 10, Krasnov [*Cherkashov*, 2008; Fouquet et al., this study]; 11, 25°48′N [*Rona*, 1984]; 12, 24°21′N [*Rona*, 1984]; 13, Kane [*Delaney et al*., 1987]; 14, 22°30′N [*Rona*, 1984]; 15, 15°51′N [*Akimtsev et al*., 1991]; 16, 14°43′N [*Akimtsev et al*., 1991]; 17, 12°48′N [*Rona* 1984]; 18, 11°N [*Bonatti et al*., 1976a]; 19, 15°05′N [*Fouquet et al*., 1993a]; 20, Rainbow [*Fouquet*, 1997; *Fouquet et al*., 1998a, unpublished data, 1997; *Lein et al*., 2003]; 21, Logatchev 1 [*Krasnov et al*., 1995; *Mozgova et al*., 1996, 1999; *Fouquet et al*., 1996; *Gablina et al*., 2000]; 22, Logatchev 2 [*Torokhov et al*., 2002; *Lein et al*., 2003]; 23, Ashadze 1 [*Beltenev et al*., 2003; *Mozgova et al*., 2008]; 24, Ashadze 2 (Fouquet et al., this study); 25, Lost City [*Kelley et al*., 2001]; 26, Menez Hom (Fouquet et al., this study); 27, Saldanha [*Barriga et al*., 1998; *Costa et al*., 2002; *Dias and Barriga*, 2006].

[b]HT is high temperature; LT is low temperature.

[c]Here +++ indicates dominant mineral >50%; ++ indicates abundant mineral 10–50%; and × indicates rare or trace mineral (<10%).

N-MORB[c]														Harzburgite[c]								
Massive Sulfides						Veins								Veins	Massive Sulfides					Carbonates		
5	6	7	8	9	10	11	12	13	14	15	16	17	18	19	20	21	22	23	24	25	26	27
															×							
															×							
															×							
	×														×	×						
	×		×											×	×	×	×	×				
																	×	×				
															×							
																×						
															×		×					
			×												×			×				
+++	++		×												×	×	×	×	×			
	×																					
×															×			×				
	×		×																			
×	++		×							+++				×	×	×		×				
×															×			×				
																		×				
	×		×										++		×		×	×				
			×													×		×	×			
															×	×	×	×	×			
																				++		×
++	×		++												×		×	×		×		++
	++																					
	++			++	++	++	+++	+++	+++					++								
															×							
	×														×			×	+++	+++	+++	×
×	×														×			×		+++		
																		×		+++		
	×		×												×	×	×	×	×			
		++																				×
		++													×	×						×
															×							

6. MINERALOGY OF ULTRAMAFIC-HOSTED HYDROTHERMAL DEPOSITS

The mineralogy of hydrothermal deposits along the MAR shows distinct differences directly related to basement rock composition. A clear distinction can be made between hydrothermal deposits hosted in E-MORB, N-MORB, and ultramafic environments. Although basement rock composition plays an important role, fluid chemistry and complexation will also impact mineralogy of vent deposits. Detailed mineral compositions of major deposits along the MAR are summarized in Table 3 where, based on the most important chemical element, minerals are presented in several groups. Hereafter, we focus on the mineralogy of ultramafic-hosted hydrothermal deposits.

6.1. Massive Sulfide Mounds

6.1.1. Major sulfide minerals. Due to the strongly reducing nature of the end-member fluids, pyrrhotite and isocubanite are the dominant iron sulfide and copper sulfide minerals at Rainbow, Logatchev 1, and Ashadze (Table 3). Chalcopyrite is present in most samples. Unlike basaltic environments, samples from the surface of the mounds contain abundant sphalerite and isocubanite compared to pyrite and marcasite. The Logatchev 2 deposit is dominated by chalcopyrite, sphalerite, and wurtzite, pyrite is rare, and pyrrhotite is absent. This probably indicates a more oxidizing fluid than at Rainbow, Logatchev 1, and Ashadze.

6.1.2. Minor sulfide minerals. In general, the diversity of minor minerals is much greater in ultramafic-hosted deposits. Marcasite (FeS_2), common in basaltic-hosted deposits, is relatively rare in ultramafic settings. Both at Rainbow and Ashadze 1, some grains of troilite (FeS) are observed. Other rare iron minerals are melnikovite (FeS_2) and greigite ($FeFe_2S_4$). A unique characteristic of ultramafic environments is the occurrence of several cobalt minerals that are not found in basaltic environments. The most common Co-Ni-mineral is Co pentlandite $(Fe,Co,Ni)_9S_8$ which occurs within the isocubanite-chalcopyrite assemblage at the core of the black smoker chimneys. This mineral, first seen at Logatchev 1 [*Mozgova et al.*, 1996, 1999], is also common at Rainbow and Ashadze. Millerite (NiS) and linnaeite (Co_2S_4) occur as late minerals associated with bornite near the external border of the copper sulfide conduit of chimneys at the Rainbow hydrothermal field. In the primary, high-temperature assemblages, an unusual trace mineral, Bi-rich melonite ($NiTe_2$), is observed at Rainbow where it is typically precipitated in contact with primary native gold at the core of active Cu-rich black smoker chimneys. Other Te minerals such as coloradoite (HgTe) are also mentioned at Rainbow [*Lein et al.*, 2003]. Surprisingly, galena, generally occurring as a rare mineral in basaltic environments, is relatively common, particularly at the inactive Rainbow 2 site. Tetraedrite and tennantite ($(Cu,Fe)_{12}(Sb,As)_4S_{13}$) also may be associated with galena-rich samples. Local enrichment in As is also seen as cobaltite (CoAsS), Luzonite (Cu_3AsS_4), and Loellingite $(Co,Fe)As_2$ [*Lein et al.*, 2003; *Mozgova et al.*, 2008]. Silver occurs in some specific trace minerals as acanthite (Ag_2S), argentopyrite ($AgFe_2S_3$), and argentite (Ag_2S). Molybdenite was observed at Rainbow [*Lein et al.*, 2003].

6.1.3. Fe and Mn oxide minerals. The most common occurrence of oxides is secondary Fe oxyhydroxide minerals after oxidation of sulfides. Goethite and sometimes ferrihydrite are the most common secondary iron oxides. Lepidocrocite is typically formed after pyrrhotite. In some cases, hematite and magnetite are common within Cu-Fe-rich chimneys and appear to be high-temperature minerals of primary origin. The low H_2S concentrations in the fluid, together with the extreme reducing conditions, make it possible to precipitate magnetite in equilibrium, although some magnetite or hematite may be formed by high-temperature oxidation of Cu-Fe sulfides. Near the seafloor, magnetic surveys above the vent field show a strong central magnetic anomaly primarily due to magnetite [*Dyment et al.*, 2005]. Some cassiterite (SnO_2) rite grains were also observed associated with sphalerite at Ashadze 1.

Mn oxides occur commonly as low-temperature distal deposits at the periphery of the black smoker field (Rainbow) or as fields or chimneys away from the high-temperature field (Logatchev, Saldanha). The main minerals are todorokite, birnessite, and δMnO_2. Hydrothermal Mn oxides also can be found cementing basaltic and ultramafic breccia (Saldanha). Similar mineralization occurs within ultramafic rocks off-axis at 23°N (H. Dick, personal communication, 2005).

6.1.4. Native elements. Due to the abundance of copper, native copper is common in weathered sulfide at the Logatchev and Rainbow sites. Sulfur, commonly associated with lepidocrocite, also is a common product of pyrrhotite oxidation. Native cadmium is mentioned at Rainbow [*Lein et al.*, 2003]. Gold is the most common native element. It is observed in a variety of mineral assemblages corresponding to different temperatures of formation. High-temperature primary gold grains are observed at the core of Cu-rich active black smokers at Rainbow. At Logatchev 1, gold is observed both in high-temperature copper sulfides and associated with lower-temperature Zn-rich sulfides. At Logatchev 2, many

secondary gold grains are observed in silica. Silver and arsenic grains are mentioned at Logatchev. Some platinum grains were identified at Rainbow [*Lein et al.*, 2003].

6.1.5. Gangue minerals. Anhydrite is the most common gangue mineral occurring in samples from active or recent chimneys. Barite is rarely observed at Rainbow, Logatchev, and Ashadze. The only place where abundant barite is seen is at the Rainbow 2 inactive site. Amorphous silica is relatively rare in ultramafic environments compared to the common occurrence of silica-rich samples in basaltic environments. However, quartz is the major gangue mineral in veins within the ultramafic rocks at 14°45′N. Silica also is locally enriched in the silicified ultramafic rocks at Saldanha. Carbonate, dominant at the Lost City site, is not common in the high-temperature vent fields. However, several chimneys with dominant carbonates (siderite, aragonite, and calcite) were sampled at Rainbow and at Ashadze 2.

6.1.6. Other secondary minerals. At most sites, secondary copper sulfides are common (bornite, chalcocite, digenite, covellite, and idaite) (Table 3). At Logatchev, several unusual secondary copper minerals such as chalchantite, djurleite, anilite, geerite, spionkopite, and yarrowite have been described [*Gablina et al.*, 2000] (Table 3). The uranium mineral uraninite is also described at Logatchev [*Torokhov et al.*, 2002]. Atacamite and paratacamite are the common secondary copper chloride minerals and are locally abundant as green patches in the sediments.

6.2. Carbonate Mounds

Carbonate mounds at Lost City have a very simple mineralogy where calcite, aragonite, and brucite are the only phases [*Kelley et al.*, 2001]. No sulfides or metal enrichments are associated with these low-temperature systems. The chimney from the Menez Hom site has a similar mineral composition with dominant calcite and traces of quartz.

6.3. Veins in Serpentinites

The disseminated mineralization at 15°05′N is associated with multiple stages of serpentinization, talc-carbonate alteration, carbonate veining, and silicification [*Fouquet et al.*, 1993a]. Sulfides also occur in altered gabbroic dikes and associated zones of metasomatism. Although it is likely that seawater was the dominant source of fluids for hydrothermal circulation and mineralization at 15°05′N, it appears that magmatic fluids also played a significant role. In some samples, quartz veins with sulfides are connected to small gabbroic veins. The mineralization has similarities with the listwaenite-style gold and Ni-Co mineralization usually associated with hydrothermal processes during ophiolite obduction [*Buisson and Leblanc*, 1985, 1987].

Disseminated sulfides in gabbroic rocks and in quartz veins in serpentinite at 15°05′N have specific mineralogical compositions. Field observations and mineralogical studies allow the discrimination of several types of sulfide mineralization corresponding to different ages and different depths of formation. The most primary and probably deepest mineralization is related to gabbroic intrusion and occurs as sulfide in gabbroic veins or disseminated in gabbro. Some sulfides are later related to serpentinization. The latest sulfide minerals occur as stockwork mineralization and in silicified areas along shear zones. These different styles of mineralization appear to link the gabbroic intrusion at depth to sulfide mounds at the surface.

The dominant sulfides vary from sample to sample but are generally chalcopyrite, cubanite and isocubanite, pyrrhotite, pentlandite, galena, sphalerite, pyrite, bravoite, and millerite. The earliest stages of mineralization, prior to serpentinization, are characterized by a pyrrhotite-pentlandite association. Chalcopyrite-pentlandite-(pyrrhotite) assemblages are related to gabbroic dikelets. The pyrrhotite-pentlandite association is not seen in basaltic seafloor sulfide deposits but is common in the high-temperature mineral assemblages at Logatchev and Rainbow. The early formed sulfide assemblage contains also millerite, mackinawite, and violarite indicating Ni enrichment at depth. Ni also occurs as a trace element in sulfides, particularly in samples from early/deep veins. Large grains (~50 μm) of Cu-rich native gold have been observed in one sample associated with small gabbroic veins in the ultramafic host rocks. Pyrite occurs only in stockwork mineralization and as a replacement of pyrrhotite. The hydrothermal assemblage (pyrite-chalcopyrite-cubanite-sphalerite-galena) is significant in later and shallower-level stockwork veins and silicified shear zones in the serpentinite.

7. CHEMICAL COMPOSITION OF DEPOSITS

Average chemical compositions of hydrothermal samples from selected major hydrothermal fields hosted by ultramafic rocks along the MAR are presented in Table 4. References used for the table are from the works of *Bogdanov et al.* [1995], *Fouquet et al.* [1993c, 1998b], *Hannington et al.* [1991], *Honnorez et al.* [1990], *Kase et al.* [1990], *Knott* [1995], *Krasnov et al.* [1995], *Mozgova et al.* [1999], *Rona et al.* [1993], *Thompson et al.* [1988]. Data from other volcanic-hosted sites are presented for comparison. The data show a correlation between the chemical compositions of the deposits and the compositions of the host rocks. We can, thus, consider after the first level of classification based on the geological control of the discharge, a second level of classification based on the composition of basement rocks.

Table 4. Average Composition of Hydrothermal Sulfide Deposits Along the Mid-Atlantic Ridge[a]

Site/Basement Rock	*n*	Depth (m)	Elements in Weight Percent							Elements in Parts per Million				
			Cu	Fe	Zn	S	SiO_2	Ba	Ca	Pb	Cd	Ag	As	Sb
E-MORB														
Menez Gwen	26	840	1.75	7.12	1.66	14.25	25.99	20.77	4.68	452	100	27	114	30
Lucky Strike	154	1650	5.37	21.05	4.16	30.97	12.38	10.85	2.70	530	195	74	334	28
N-MORB														
Broken Spur	8	3050	4.74	24.81	3.09	-	-	0.01	5.12	244	90	24	195	10
Broken Spur	70	3050	4.82	35.10	6.02	-	-	0.03	-	468	-	-	-	-
TAG (Mir Zone)	15	3500	12.46	29.99	5.19	34.44	7.52	0.01	0.10	74	199	74	129	19
TAG (active mound)	35	3670	5.50	25.30	11.25	33.93	4.66	0.01	6.17	405	350	78	80	18
TAG (active mound)	31	3670	11.54	24.94	3.54	18.23	13.66	0.01	4.98	450	37	85	119	12
TAG (active mound)	34	3670	7.77	24.89	13.38	35.21	12.83	0.47	5.38	214	549	114	62	229
MAR 24°30′N	?	4000	16.20	17.60	4.06	-	-	0.05	-	262	-	-	62	-
Snake Pit	16	3500	1.86	34.02	6.34	35.93	2.91	0.01	1.53	934	176	119	328	32
Snake Pit	32	3500	5.41	35.73	4.09	35.51	5.69	-	-	249	180	48	410	38
Snake Pit	31	3500	8.26	36.95	6.10	36.03	3.00	-	0.58	525	242	80	312	27
PDF (TAMAR)	8	1960	6.08	20.40	0.38	27.77	44.53	0.10	-	261	14	63	223	9
Krasnov	16	3700	2.21	38.96	0.14	42.90	11.21	0.27	1.61	70	19	18	66	20
TAG (ODP)	71	3670	2.65	35.15	0.65	44.13	12.75	0.20	2.56	62	19	15	41	10
Snake Pit (ODP)	8	3500	10.15	36.87	4.33	36.01	6.27	0.02	0.06	163	190	15	100	18
Ultramafic Rocks														
Rainbow 1	116	2400	12.43	28.56	14.99	32.75	0.71	0.29	2.69	342	391	188	214	34
Rainbow 2	3	2200	0.08	32.10	0.34	31.27	0.43	16.20	0.22	20,987	6	34	22	12
Logatchev 1	40	3000	25.47	24.40	2.55	26.36	4.44	0.06	2.86	209	51	35	62	21
Logatchev 1	7	3000	18.96	22.26	1.51	-	-	-	-	400	27	70	-	-
Logatchev 1	8	3000	23.10	28.60	7.85	-	-	0.16	-	220	-	-	389	-
Logatchev 2	5	2700	14.72	17.55	25.40	20.90	9.73	0.01	0.37	700	700	92	522	-
Logatchev 2	8	2700	20.05	19.68	22.78	33.24	3.23	0.05	1.27	435	356	79	289	74
Ashadze 1	49	4100	14.21	32.81	14.11	31.74	1.30	0.05	1.13	350	251	79	231	29
Ashadze 2	6	3260	14.14	21.36	7.66	12.47	10.74	0.05	8.03	215	57	59	110	32

[a]Here *n* is number of analyses used to calculate the average compositions. Different lines for one site correspond to different cruises.

Ni	Co	Se	Mo	In	Sn	Mn	Sr	U	Ge	Bi	Hg	Tl	Te	Ga	Au	References
22	18	63	55	-	-	125	4810	8	5	<10	-	-	-	-	0.1	Fouquet et al. (this study)
10	89	110	79	1	1	275	2208	<5	17	<10	-	-	-	-	0.3	Fouquet et al. (this study)
5	184	357	32	-	-	210	650	<0.5		10	7	-	-	-	1.5	*Knott* [1995]
18	200	-	-	-	-	223	-	-	-	-	-	-	-	-	-	*Bogdanov et al.* [1995]
16	112	20	118	-	-	630	-	-	-	-	-	-	-	-	6.1	*Rona et al.* [1993]
84	137	51	64	-	1	554	1226	1	20	0.05	25	33	0.02	190	2.2	*Hannington et al.* [1991]
50	46	6	105	-	4	122	652	5	13	0.05	0.15	1	0.01	23	0.4	*Thompson et al.* [1988]
22	643	159	144	<10	<20	<500	412	9	22	0.82	-	3	-	116	1.4	Fouquet et al. (this study)
45	16	-	-	-	-	260	-	-	-	-	-	-	-	-	-	*Bogdanov et al.* [1995]
49	48	88	25	-	14	263	165	1	34	5	3	21	4	10	2.2	*Hannington et al.* [1991]
-	220	-	28	-	20	116	-	-	-	3	-	-	-	-	1.6	*Krasnov et al.* [1995]
20	135	135	60	4	25	168	106	-	-	-	-	-	-	-	1.8	*Fouquet et al.* [1993c]
20	294	85	66	<10	<10	32	>20	<5	2	<10	-	-	-	-	-	Fouquet et al. (this study)
15	628	23	88	10	23	654	602	11	<5	<10	-	-	-	21	1.1	Fouquet et al. (this study)
20	327	28	78	5	11	51	189	-	6	-	-	-	-	-	-	*Fouquet et al.* [1998b], *Humphris et al.* [1995]
92	665	220	17	-	-	3313	25	<1	-	-	-	-	-	-	0.5	*Honnorez et al.* [1990], *Kase et al.* [1990]
490	5086	186	29	10	138	453	665	11	12	5	-	-	-	-	5.1	Fouquet et al. (this study)
177	42	10	159	5	79	2407	3020	-	-	-	-	-	-	-	1.0	Fouquet et al. (this study)
92	500	625	51	8	225	602	293	14	12	12	-	-	-	23	8.4	Fouquet et al. (this study)
-	329	-	-	-	-	-	-	-	-	-	-	-	-	-	9.6	*Krasnov et al.* [1995], *Mozgova et al.* [1999]
20	778	-	-	-	-	179	-	-	-	-	-	-	-	-	-	*Bogdanov et al.* [1995]
20	500	-	-	-	>50	100	-	-	50	27	-	-	-	43	23.8	*Bogdanov et al.* [1995]
31	49	1314	49	10	1107	508	154	6	19	13	-	-	-	32	25.9	Fouquet et al. (this study)
973	2882	200	31	11	347	1175	31	7	10	11	-	-	-	32	6.3	Fouquet et al. (this study)
42	566	334	73	14	371	723	2171	40	25	11	-	-	-	32	9.1	Fouquet et al. (this study)

Except for core samples from the mound interior at TAG and Snake Pit, most samples are from mound surfaces. A few samples were collected from the cores of the deposits that were exposed along faults. Thus, analyses presented here are not representative of the whole mound. For some sites, the number of samples is not high enough for meaningful comparisons; however, values are interesting to show specific metal concentrations. To discuss the specificity of ultramafic massive sulfide mineralization, we have performed principal component analysis (PCA) statistical analyses. Samples from four deposits, one N-MORB, one E-MORB, and two ultramafic deposits were numerous enough for statistical analysis, and the samples were analyzed using the same technique and the same sampling protocol. Results of factor analyses on these samples reveal three major groups for all four sites (Figure 6): the Cu-rich high-temperature group, the Zn-rich intermediate-temperature group, and the oxide/sulfate group. For some trace elements, some clear differences exist between basaltic and ultramafic environments.

7.1. Major Elements

7.1.1. Copper and zinc. Individual compositions of the sulfides depend on the type of mineralogical assemblage and temperature of formation. The triangular diagram in Figure 4 shows the contrast between Fe-dominant deposits associated with basalt and Cu-Zn-rich deposits associated with ultramafic rocks. This is also shown in Figure 5 for average compositions for each site. Menez Gwen is particular because of its high Ca and Si content (>45%). Samples collected by submersible at the surface of the TAG mound have a high Cu + Zn content close to 15%, while samples collected from the internal part during drilling operations have a Cu + Zn concentration lower than 4%. The Cu + Zn content in ultramafic-hosted deposits is 20 to 30 wt %, whereas in MORB environments, the Cu + Zn content is 5 to 20 wt % (Figure 5). The extreme Cu-Zn enrichment in ultramafic deposits is difficult to explain by an enrichment in the primary upper mantle rocks, which are depleted in Cu (31 ppm) with respect to MORB (77 ppm) (see Table 5) [*Anderson*, 1989; *Taylor and McLennan*, 1985; *Wolf and Anders*, 1980]. However, serpentinite samples from the Rainbow ridge collected away from the hydrothermal field display a significant enrichment in Cu (248 ppm) and Zn (273 ppm) that may constitute a primary enriched source for these elements (Table 5). Another explanation for the high Cu concentration is the occurrence of high-temperature venting all over the hydrothermal field (see paragraph on mound zonation above).

7.1.2. Silica. The lowest Si concentration in modern submarine hydrothermal deposits is found in ultramafic deposits (Table 4). SiO_2 concentrations in the hydrothermal deposits are less than 1 wt % at Rainbow and less than 6 wt % at Logatchev. Both sites have Si concentrations in fluids [*Charlou et al.*, 2002, this volume] that, unlike basaltic fluids, are undersaturated with respect to quartz and opal [*Fournier et al.*, 1982]. Menez Gwen also has a low Si concentration; however, due to the shallow depth and the low temperature, silica concentration is close to the quartz equilibrium curve. Lucky Strike fluids are more complex, but the highest concentration, is on the quartz saturation curve. Fluids with lower concentrations at Lucky Strike may have lost silica due to near-surface conductive cooling and amorphous silica precipitates, which are abundant at Lucky Strike. Thus, at most basaltic sites, the end-member fluids are close to be in equilibrium with quartz and are rapidly saturated with respect to amorphous silica when a slight conductive cooling occurs [*Fournier et al.*, 1982; *Hannington et al.*, 1995]. However, silica seems to play an important role in subsurface hydrothermal processes occurring in ultramafic rocks. Subsurface conductive cooling of the fluid may explain the relatively high Si content in deposits from Logatchev 2 and Ashadze 2, and pervasive silicification of both mafic and ultramafic rocks is seen at Saldanha and in meter-thick mineralized quartz veins observed within the ultramafic rocks at 15°05′N.

7.1.3. Barium. Sulfide deposits in an E-MORB environments are characterized by high Ba concentrations (see extension of the Ba-rich E-MORB in Figure 1). In N-MORB hosted sites, Ba is nearly absent (Table 4). At Rainbow, there is a slight Ba enrichment particularly seen at Rainbow 2 where barite chimneys were collected. The best explanation of Ba enrichment is the Ba concentration in the basement rocks. In the southern Azores area, barium concentrations in the basaltic rocks increase approaching the hot spot. At the scale of each segment, average Ba concentration in the basalt is 40 ppm at Rainbow, 70 ppm at Lucky Strike, 120 ppm at Menez Gwen, and 175 ppm at 38°20′N. In addition, on all segments, there is a spatial relation between the location of vents and the highest Ba concentration in basalts. For example, Ba concentration in basalts from or near the hydrothermal field were measured for this study; concentrations are 61 ppm at Rainbow, 283 ppm at Lucky Strike, 232 ppm at Menez Gwen and 219 ppm at 38°20′N. Thus, there is a direct explanation for Ba concentration in deposits. In N-MORB, the Ba concentration is generally lower than 10 ppm [*Anderson*, 1989]. Comparatively, ultramafic rocks have extremely low Ba concentrations, around 3 ppm (Table 5) [*Anderson*, 1989]. Thus, as discussed for fluids, the Ba enrichment in ultramafic-hosted mineral deposits such as at Rainbow and Logatchev 1 may be due to inter-

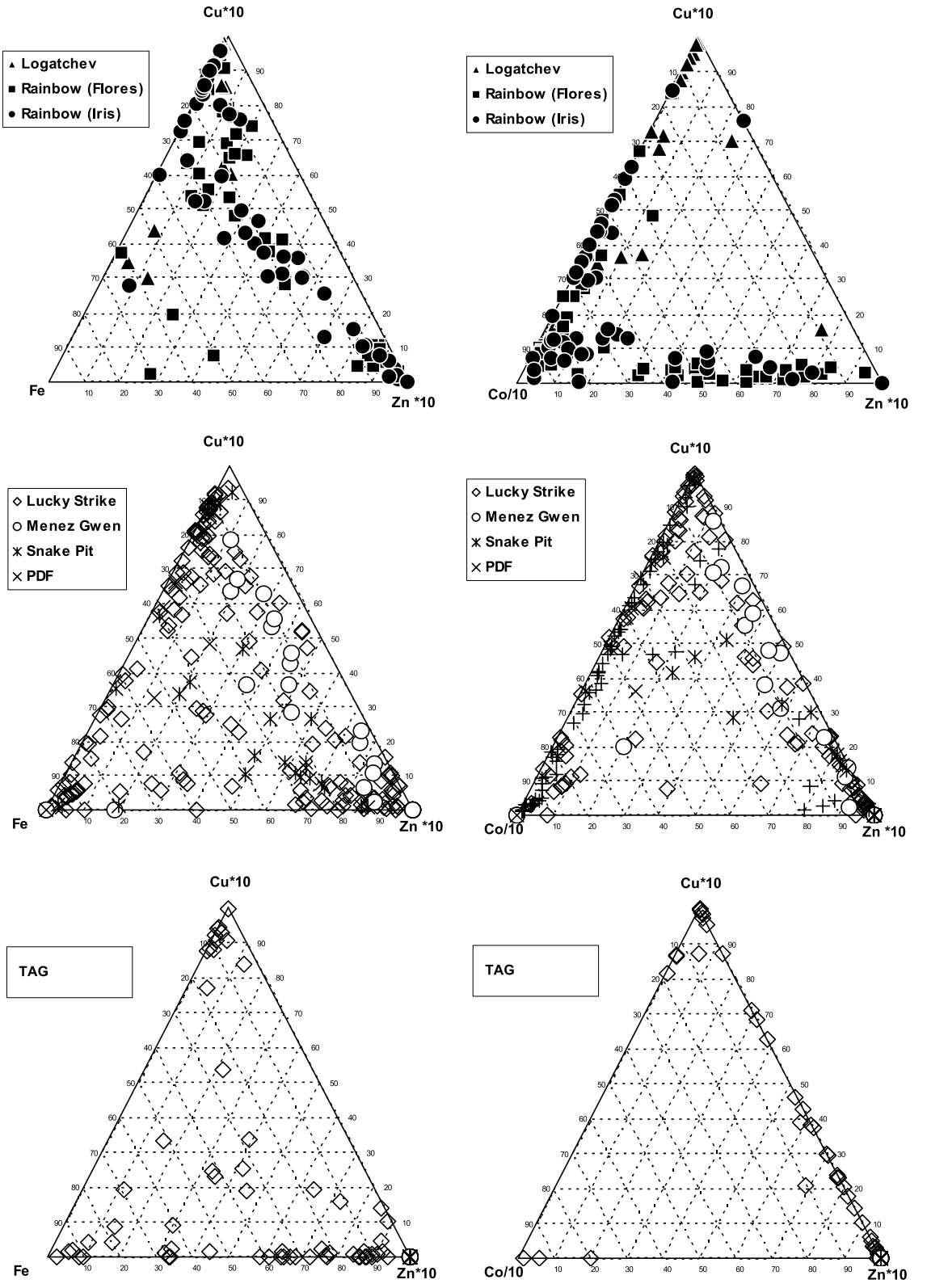

Figure 4. Comparison of major elements in hydrothermal deposits from the MAR. Open symbols are for basaltic environments, solid symbols are for ultramafic environments.

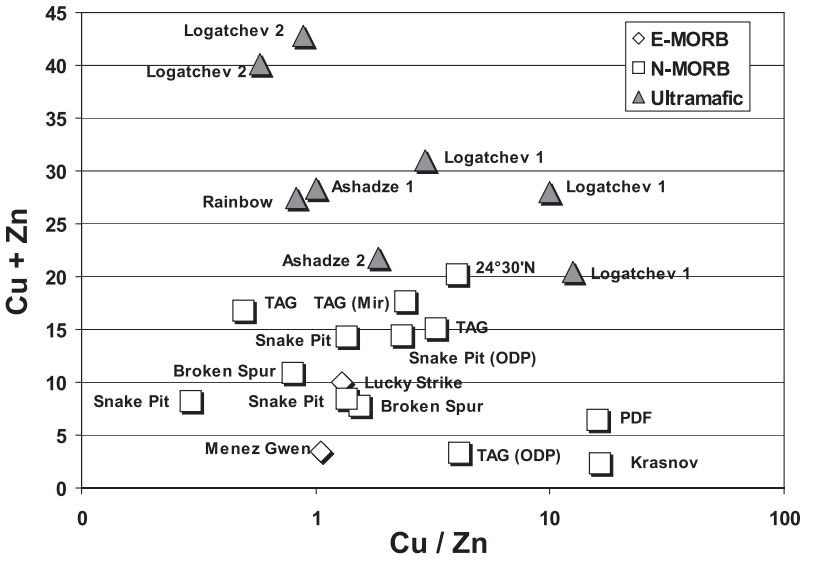

Figure 5. Average copper and zinc concentration in massive sulfides from the MAR in relation to their Cu/Zn ratio. Different values for a single site are average compositions from different cruises.

action with deep Ba-enriched gabbroic intrusions. At both sites, particularly at Logatchev, gabbros have been collected within the ultramafic rocks; thus, there is evidence for interaction with basaltic/gabbroic rocks. Similar observations were already made on Explorer Ridge west of Canada [*Scott*, 1987].

7.1.4. Calcium. Ca as carbonate chimneys is common at low-temperature fields like Lost City and Menez Hom. Calcium carbonate chimneys, carbonates within sediments, and low-temperature carbonatization (aragonite) of ultramafic rocks are also observed at Rainbow and Saldanha [*Ribeiro da Costa et al.*, 2008]. This is related to high Ca concentration in fluids due to the release of Ca during serpentinization when silicates such as clinopyroxene react with heated seawater.

7.2. High-Temperature Trace Elements Associated With Copper

Minor elements do not generally have specific visible minerals. They occur as substitution elements in the lattice of major minerals [*Huston et al.*, 1995]. Several geochemical groups can be distinguished depending on the minerals into which the elements substitute: sulfates, oxides, high-temperature Cu-rich, and medium-temperature Zn-rich. The affinity of trace elements for these different groups is best demonstrated using PCA presented in Figure 6. Elements having a strong correlation with Zn are Ag, Au, Ge, Cd, Pb, Sb, and As. Ba and Sr are close to this group in a separate group due to their occurrence as sulfates. The high-temperature Cu-rich group is characterized by In, Mo, and Se. For most elements, the same groups are seen for basaltic and ultramafic environments. However, some differences exist for Co, Mn, Sr, Sn, and Au. These differences are discussed in the following paragraphs. To facilitate the comparison, in many cases, we have used the ratio between a trace element and the major elements of his group.

7.2.1. Cobalt and nickel. One of the noteworthy characteristics of the ultramafic rock-hosted deposits is their high cobalt concentration. At Rainbow, the average Co concentration is 0.5% with maximum values as high as 4.3 wt %. At Ashadze, the average Co concentration is close to 0.3%. Logatchev is slightly enriched in Co with mean values close to 400 ppm and maximum concentrations up to 1018 ppm. In basaltic environments, samples enriched in Co are from the core of the mineral deposit, samples collected during drilling operations at TAG, for example, or from mature massive sulfides collected from off axial sulfide mounds on the EPR [*Fouquet et al.*, 1996]. Because of easy substitution to Fe, present both in high- and low-temperature minerals, cobalt has generally an intermediate position on the PCA diagrams (Figure 6). This also indicates that Co has no strong dependence to temperature. This is explained by a common occurrence of high Co concentrations in mature,

Table 5. Metal and Elemental Concentrations in MORB and Mantle Rocks Compared to Average Composition of MAR Serpentinized Harzburgite and E-MORB[a]

	N-MORB	Upper Mantle	Ultramafic Rocks	Serpentinized Harzburgite (Rainbow) This Study	E-Morb (Azores) This Study
			Values Given in Weight Percent		
Na	1.59	0.6	0.2	0.07	1.58
Mg	5.89	18.67	23.10	21.12	4.62
Al	8.48	3.65	2.00	0.4	8.69
Si	23.20	22.20	21.80	17.32	23.19
Ca	8.48	3.89	2.40	2.53	9.16
Fe	6.52	6.18	6.08	5.96	6.81
			Values Given in Parts per Million		
P	390	170	61	300	600
S	600	158	8	2149	
K	660	475	35	300	2700
Sc	37.3	22	17	7	42
Ti	5500	2159	1000	120	7290
V	210	110	77	32	263
Cr	441	1969	2500	2097	193
Mn	1080	1029	1010	618	1200
Co	53	91	105	117	40
Ni	152	1610	2110	2002	72
Cu	77	31	15	248	90
Zn	74	63	60	273	77
Ga	18	7	4	-	-
Ge	1.5	1.20	1.1	-	-
As	1	0.1	-	9	<2
Se	181	0.06	0.02	-	-
Rb	0.36	1.19	0.12	-	8
Sr	110	42.3	8.9	480	191
Y	23	9.28	4.6	3	21
Zr	70	27	11	-	80
Nb	3.3	2.03	0.9	-	17
Mo	0.31		0.063	-	-
Ag	0.019	0.01	0.0025	-	-
Cd	0.129	0.05	0.0255	-	-
In	0.072	0.02	0.002	-	-
Sn	1.36	0.79	0.52	-	-
Sb	0.01		0.005	-	-
Cs	0.007	0.05	0.006	-	-
Ba	5	13	3	<20	145
Pb	0.49	0.33	0.2	4	1.69
Bi	0.007	0.009	0.005	-	-
Th	0.035	0.224	0.094	-	-
U	0.014	0.057	0.026	-	-
Ta	0.1	0.11	0.03	-	-
			Values Given in Parts per Billion		
Re	1.1	0.45	0.23	-	-
Os	0.04	2.43	3.1	-	-
Ir	0.0011	2.43	3.2	-	-
Au	0.34	0.53	0.49	-	-
Tl	0.01	0.02	0.02	-	-

[a]All data are from *Anderson* [1989] except As, Sb, and Mo from *Taylor and McLennan* [1985] and *Wolf et al.* [1980].

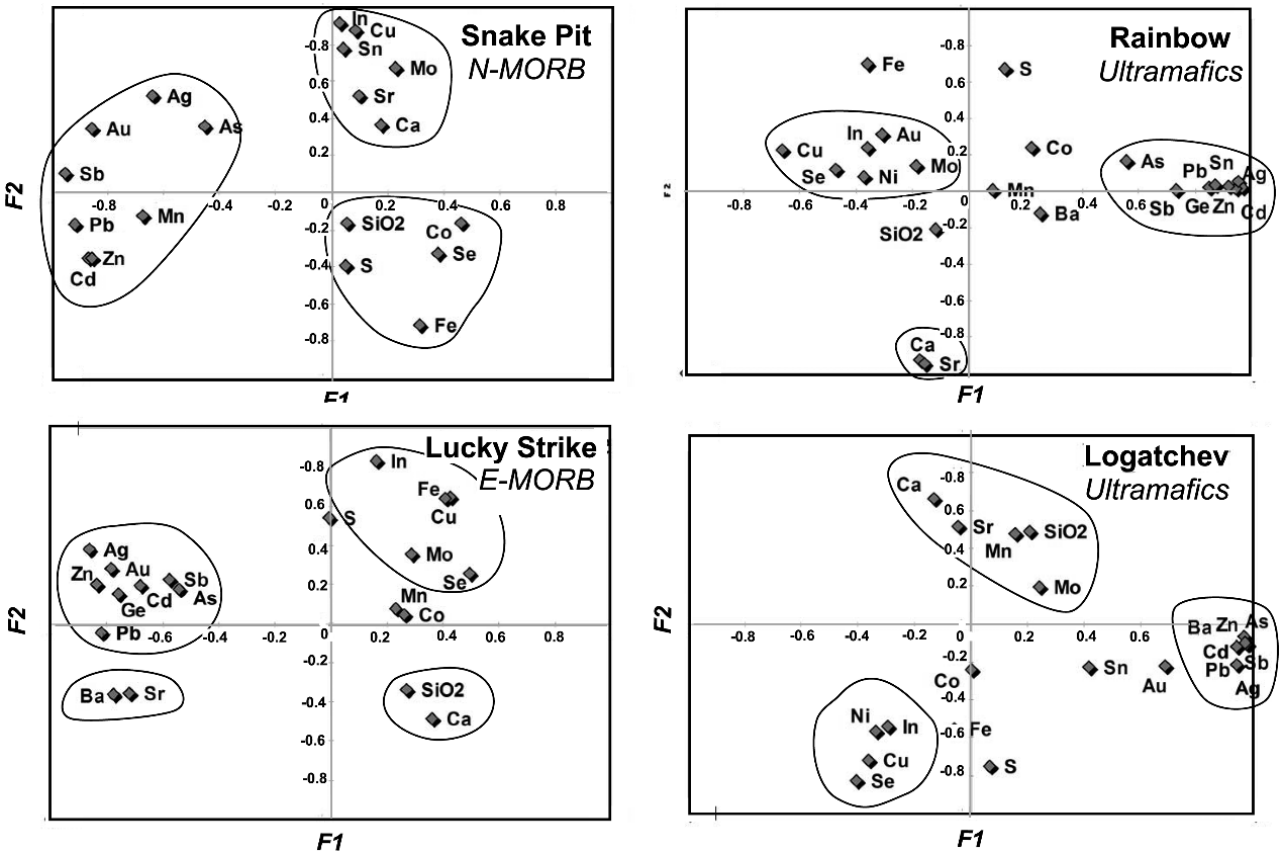

Figure 6. Principal component analysis (PCA) for typical MAR deposits. Calculated values for Factor 1 (F1) and Factor 2 (F2) are the following for Rainbow: eigenvalues, F1 = 7.30, F2 = 3.09; contribution to the variance (%), F1 = 33.17, F2 = 14.06; for Snake Pit: eigenvalues, F1 = 6.17, F2 = 4.73; contribution to the variance (%), F1 = 30.83, F2 = 23.63; for Lucky Strike: eigenvalue F1 = 6.62, F2 = 3.05; contribution to the variance (%), F1 = 33.02, F2 = 15.21; for Logatchev: eigenvalue F1 = 7.80, F2 = 4.16; contribution to the variance (%), F1 = 31.76, F2 = 19.81.

pyrite-dominant, massive sulfides. At the ultramafic-hosted Rainbow site (Figure 6), high Co concentrations are seen both in the Cu- and the Zn-rich geochemical groups. The highest concentration (4.3 wt %) is from a Zn-rich chimney. This Co enrichment in ultramafic deposits may be explained by higher concentrations of Co in the upper mantle rocks (91 ppm) when compared to MORB (53 ppm) [*Anderson*, 1989] (Table 5). However, this difference cannot explain the extreme enrichment found at Rainbow and Ashadze. A local Co enrichment in serpentinized rocks, similar to that discussed for Cu and Zn, is not seen at the Rainbow site (Table 5) where Co in serpentinized rocks averages 117 ppm, close to the Co concentration in upper mantle rocks (91 ppm) (Table 5). We may thus consider that specific fluid composition and extreme reducing conditions in ultramafic environments are more efficient systems to extract and transport Co, or that there is an intermediate enriched source of cobalt in the hydrothermal system. This source could be old stockwork mineralization or magmatic sulfides related to a deep gabbroic intrusion and similar to those seen at 15°05′N. The nickel content varies considerably among N-MORB (152 ppm) [*Anderson*, 1989], ultramafic rocks (1610 ppm), and serpentinized ultramafic rocks (2002 ppm at Rainbow) (Table 5). Nickel can thus potentially discriminate the importance of ultramafic source rocks. The highest nickel enrichments are in ultramafic-hosted vent deposits. The average Ni concentration is 973 at Ashadze, 490 ppm at Rainbow, and 93 at Logatchev. Ni is concentrated at the core of high-temperature chimneys with a maximum of 6900 ppm at Rainbow and 445 ppm at Logatchev. Specific Ni sulfides minerals (Table 3) also indicate that Ni is concentrated in the deep magmatic and stockwork mineralization from 15°05′N. At Rainbow, Co/Ni ratio was also used to discriminate between massive sulfide formed by chimney accumulations and deep min-

eralization formed by replacement of the ultramafic rocks [*Marques et al.*, 2006]. The deepest replacement mineralization have a Co/Ni ratio <1. Thus, Ni in the deep mineralization is more likely inherited from the basement rocks during replacement processes. At all basaltic sites, Ni concentration is lower than 100 ppm. All these observations indicate that Ni is not extremely mobile at temperatures lower than 350°C typical of ocean ridges, its transport being restricted to temperature and chemical conditions close to the end-member fluids. At highest temperature (i.e., >400°C), Ni is probably more mobile, Ni minerals are common in the deep mineralization at 15°05′N, and Ni is also found to be common in vapor bubbles associated with magmatic fluids [*Yang and Scott*, 1996].

7.2.2. Selenium. *Selenium* is typical of high-temperature assemblages and a substitute for sulfur in high temperature sulfides (Figure 6) [*Auclair et al.*, 1987; *Layton-Matthews et al*., 2008]. Compared to N-MORB (70 ppm), the upper mantle (0.06 ppm) [*Anderson*, 1989] is highly depleted in Se. We may thus expect a clear difference for sulfide deposits from the two types of basement rocks, but, in fact, there is no significant evidence for variation in the concentration of Se. However, PCA analyses show a strong Cu-Se correlation only for ultramafic environments. Thus, we may consider that this difference has perhaps more to be related to the mobility of Se in fluids rather than to its concentration in the source rock. *Tin* is enriched in sulfide deposits from mantle environments (between 80 and 1100 ppm), even though tin is not enriched in mantle rocks (0.79 ppm) compared to N-MORB (1.36 ppm), MORB related sites have average Sn concentrations between 1 and 25 ppm. On the PCA diagram (Figure 6), at Rainbow, Sn is associated with the Zn geochemical group. At Snake Pit, Sn is in the Cu-rich high-temperature geochemical group indicating a different precipitating process. *Wilson and Eugster* [1985] have demonstrated that $SnCl_2$ is a dominant species in aqueous chloride solution in equilibrium with the nickel-nickel oxide redox buffer at 1.5 kbar and over a temperature range from 400 to 700°C. Thus, the systematic Sn enrichment in all ultramafic sulfide deposits may be related to the high Ni content in ultramafic rocks. In most samples, *indium* concentration is lower than 10 ppm in primary mineral assemblages. However, indium may be enriched during low-temperature alteration of sulfides. Maximum concentrations reach 37 ppm at Snake Pit, 30 ppm at Rainbow, and 23 ppm at Lucky Strike. Two processes may be considered first, indium precipitates with high temperature Cu-rich sulfides creating a primary concentration. This was clearly established, for example, in the Lau basin back-arc deposit [*Fouquet et al.*, 1993b]. Then, a secondary and higher concentration is produced during the oxidation of the copper sulfides during which In seems not to be mobile and to concentrate in the secondary copper sulfides. This was demonstrated for secondary Cu-rich sulfides at Snake Pit [*Fouquet et al.*, 1993c].

7.3. Low-Temperature Trace Elements Associated With Zinc

Most elements from this group have a strong positive correlation with Zn as seen in Figure 6 where Zn, Cd, Pb, As, Sb, Ag, Ge, and Sn form a narrow group because *cadmium* substitutes into sphalerite Cd has the highest correlation with Zn in all sites. However, Cd/Zn ratios are the lowest in ultramafic hydrothermal deposits (Figure 7) (47 to 60 × 10^3 in shallow E-MORB, 28 to 44 × 10^3 in N-MORB, and 10 to 32 × 10^3 in ultramafic environments). The relative low Cd concentration in ultramafic-hosted deposits may be explained by the difference in Cd concentration between MORB (0.129 ppm) and ultramafic rocks (0.026 ppm), while the Zn concentration is similar (74 ppm in NMORB and 60 in ultramafic rocks) (Table 5) [*Anderson*, 1989]. *Lead* shows low concentrations at most sites along the MAR. Surprisingly, the highest concentration (2 wt %) is from the small inactive ultramafic-hosted vent field (Rainbow 2), 1 km east of the active Rainbow field. The common occurrence of galena in ultramafic-hosted mineralization is not easily explained, since there is no major difference in Pb concentration between the upper mantle (0.33 ppm) and N-MORB (0.49 ppm) [*Anderson*, 1989]. The relative enrichment in lead at Rainbow 2 may be related to a high concentration of lead in the serpentinite (4 ppm) (Table 5). Mobility and concentration of lead deeper in the system in mantle-dominated hydrothermal systems is also indicated by the abundance of galena in the silicified ultramafic rocks at 15°05′N (see mineralogical section). *Antimony* and *arsenic* are generally highly correlated with each other and with Zn. Despite a relative enrichment in Sb and As in the oceanic crust (1 ppm) compared to the upper mantle (0.1 ppm) (Table 5), there are no real differences between ultramafic and basaltic environments. However, many As minerals are found at ultramafic sites. *Uranium* was not analyzed at all sites. Except for the old Krasnov site, (11 ppm) U concentration is lower than 5 ppm at basaltic sites. In ultramafic environments, some U enrichment (maximum 40 ppm at Ashadze 2) is observed in the vent deposits. At Rainbow, 38 ppm U was measured in a Cu-Zn-rich chimney and 27 ppm in a massive Fe-rich sulfide. Some uranium minerals [*Torokhov et al.*, 2002] have been described at Logatchev 2. Compared to N-MORB (0.014 ppm), U is slightly enriched in ultramafic rocks (0.057 ppm). However, most studies indicate that U is preferentially scavenged from seawater into iron oxides rather than related to the hydrothermal fluid. The highest *silver* concentration in hydrothermal deposits is at Rainbow (188 ppm);

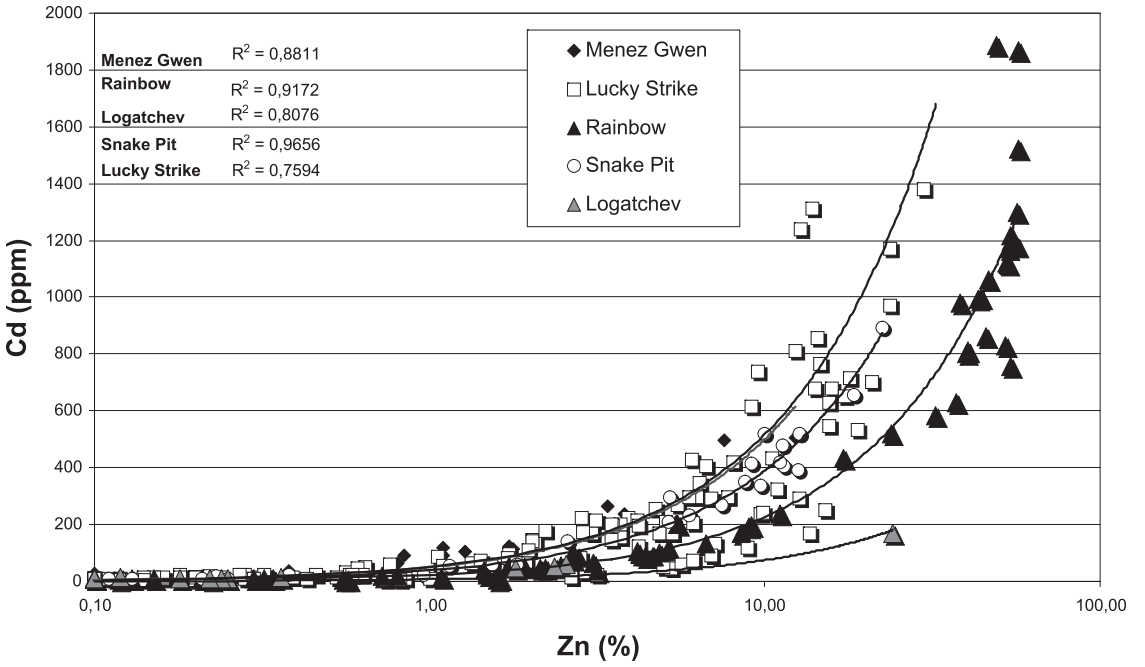

Figure 7. Correlation between Cd and Zn in massive sulfide from mafic and ultramafic environments along the MAR.

however, there is no major difference in Ag concentration between basaltic and ultramafic environments. This is probably explained by similar concentrations of Ag in N-MORB (0.02 ppm) and ultramafics (0.01 ppm) [*Anderson*, 1989]. At the scale of a vent field, due to zone refining processes, there is considerable variation in the silver content (Figure 8). Silver is preferentially precipitated at medium to low temperature. However, there is a clear Ag difference for Cu/Zn ratios. For ratios lower than 1, most Ag concentrations range from 100 and 900 ppm in ultramafic sulfide deposits, whereas Ag is between 0 and 100 ppm in N-MORB and between 0 and 300 ppm in E-MORB sulfide deposits (Figure 8).

7.4. Gold

For basaltic environments, most Au-rich samples are in the Zn-rich geochemical group (Cu/Zn < 1) (Figure 8). This correlation between Zn and Au is clearly seen on the PCA diagrams showing a Zn-Au affinity for Lucky Strike, Snake Pit, and Logatchev (Figure 6). The strongest Au-Zn correlation is found at Lucky Strike (R^2 Zn-Au = 0.76). At Snake Pit, the correlation is weaker (R^2 Zn-Au = 0.65), but Au is still in the Zn group (Figures 7, 9, and 10). This is explained by Au enrichment in some Cu-rich mature samples from the mound [*Fouquet et al.*, 1993c]. For ultramafic-hosted systems, there is a bimodal distribution for gold. At Logatchev, Au is close to the Zn geochemical group (R^2 Zn-Au = 0.62) [*Murphy and Meyer*, 1998]. At Rainbow, PCA shows a clear correlation between gold and the Cu-rich high-temperature group (Figures 7 and 9). The highest concentrations are observed in the Cu-rich mineral assemblages, where gold concentrations are much higher than in most samples from basaltic hydrothermal deposits. For that reason, Au is correlated with the Cu-rich high-temperature chemical group at Rainbow (R^2 Zn-Au = −0.22) (Figure 6). This relation is confirmed by the presence of numerous gold grains within copper sulfides at the core of active black smokers. This implies precipitation of gold at temperatures close to the end-member fluid (360°C). These gold grains are commonly associated with Te and Bi minerals (melonite). Thus, it seems that in deposits having a marked influence of an ultramafic source rock, a specific behavior for gold must be considered in terms of fluid chemistry and complexation.

7.5. Minor Element in Oxides and Sulfates

In surface samples, *strontium* is highly correlated to Ca, at Ba-free sites. As for Ca, the concentration depends on the amount of anhydrite. At these sites, Sr/Ca ratios vary between 130 and 180, and the correlation between Ca and Sr is high (R^2 between 0.9 and 0.99). For Ba-rich deposits, strontium is highly correlated with Ba (R^2 > 0.90) due to the

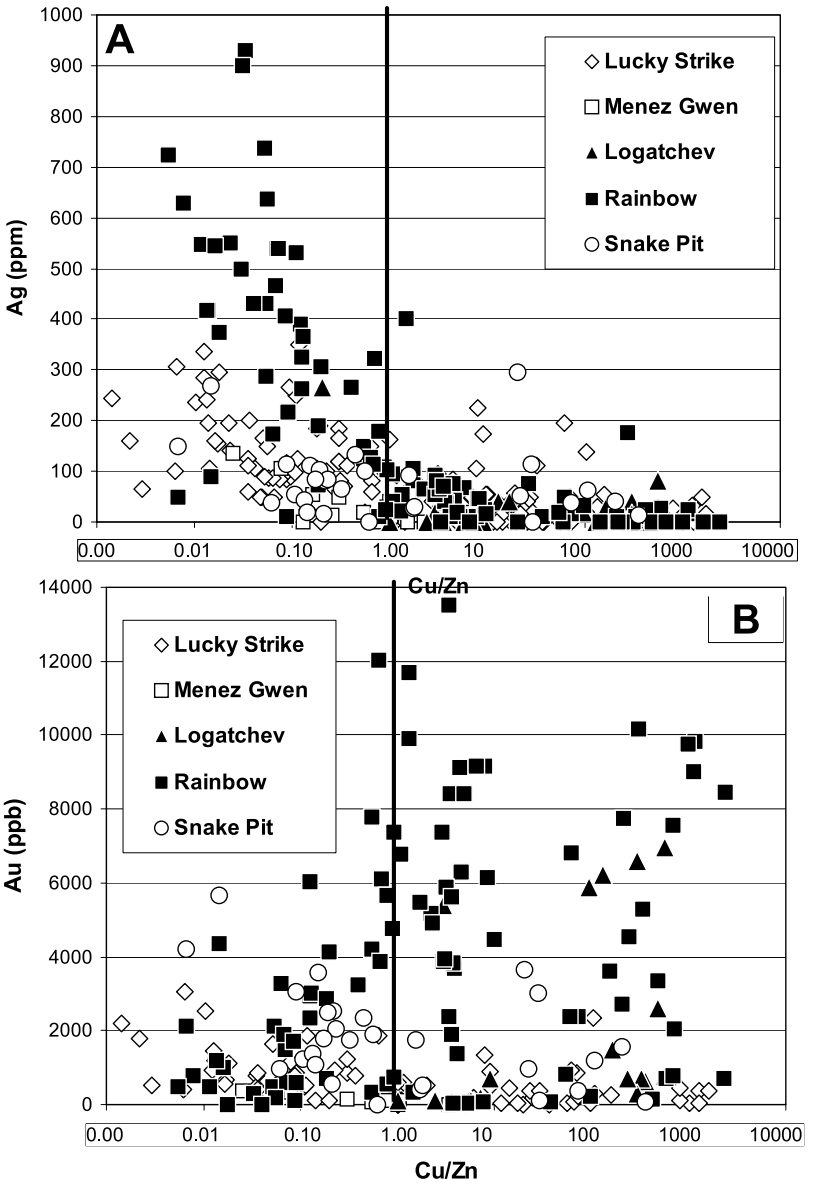

Figure 8. Comparison between high-temperature Cu-rich (Cu/Zn > 1) and medium- to low-temperature Zn-rich (Cu/Zn < 1) mineralization along the MAR. Solid symbols are for ultramafic environments; open symbols are for basaltic environments. Note the difference in high Au concentration between ultramafic (Au in Cu-rich samples) and basaltic environments (Au in Zn-rich samples). Ag is at high concentration in both types of environments, but a clear difference exists with ultramafic deposits being enriched in Ag compared to basalt-hosted deposits.

incorporation of Sr in barite (Sr/Ba ratios between 200 and 230). *Manganese* has no clear correlation with any of the different geochemical groups because there is no primary Mn sulfide or Mn sulfates. The manganese oxides occur commonly as a late precipitate from seawater at the outer surface of the chimneys and in alteration products. *Molybdenum* has two types of occurrences. It is typically associated with copper in the high-temperature geochemical group (Figure 6). However, Mo concentration in seawater is higher than the Mn concentration (Table 2), and Mo is scavenged from seawater during the formation of low-temperature manganese oxides.

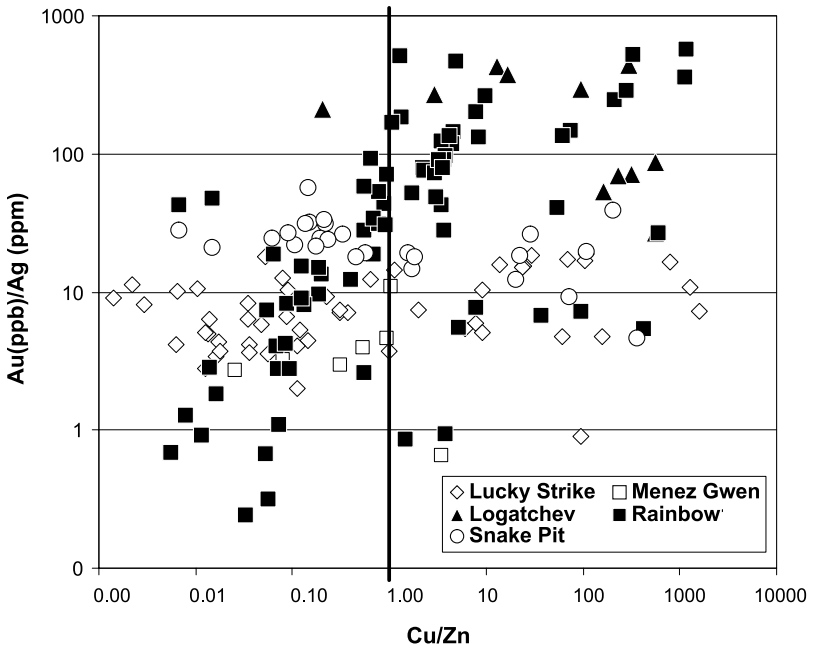

Figure 9. Comparison of Au/Ag ratios between high-temperature Cu-rich (Cu/Zn > 1) and medium- to low-temperature Zn-rich (Cu/Zn < 1) mineralization along the MAR. Solid symbols are for ultramafic environments; open symbols are for basaltic environments.

8. DISCUSSION

8.1. Driving Force of the Ultramafic Hydrothermal Systems

Hydrothermalism in ultramafic systems may be driven by the heat of exothermic serpentinization reactions between seawater and mantle rocks [*German and Lin*, 2004; *Lowell and Rona*, 2002], by the regional thermal gradient of the ridge, or by a high-temperature shallow magmatic intrusion. Heat balance models predict that heat released upon serpentinization of peridotites can result in a wide range of hydrothermal venting temperatures up to 50°C [*Allen and Seyfried*, 2003]. Hydrothermal venting driven by high rates of serpentinization may occur episodically as new reaction surfaces are made available by tectonic activity or crack propagation [*Allen and Seyfried*, 2004; *Fruh Green et al.*, 2003]. Even the low-temperature Lost City site is probably not only driven by exothermic heat produced during serpentinization. It is more likely that tectonic processes associated permit access of seawater to relatively deep and still hot lithospheric units and/or near-axis magmatic heat sources, before venting [*Allen and Seyfried*, 2004]. At Rainbow, elevated REE concentration (the highest on the MAR) in the fluids may be due to a higher extraction efficiency favored by high temperature, low pH, redox state and high chloride content [*Douville et al.*, 2002] (Table 2). However, to explain REE pattern and high REE concentrations, reaction between the hydrothermal fluid and plagioclase from a deep gabbroic intrusion and related dykes has to be considered [*Douville et al.*, 2002] (Plate 2). Silica concentrations (6.9 mmol/kg) are too high when compared with the theoretical prediction (0,5 mmol/kg) of the composition of fluids coexisting with ultramafic assemblages [*Wetzel and Shock*, 2000]. Thus, hydrothermal alteration of gabbroic intrusions in the ultramafic rock may also explain the excess of SiO_2 in the end-member fluid and favor the hypothesis of a deep intrusion driving the hydrothermal system. In addition, the high Ba concentration in fluid, the occurrence of barite at Rainbow, and the relative Ba enrichment in sulfides also suggest a deep Ba-enriched source. As ultramafic rocks are depleted in Ba (<5 ppm), the best candidate to explain Ba enrichment is a gabbroic intrusion where, due to the influence of hotspots (Azores and 14°50′N), Ba concentration in excess of 100 ppm are seen in the basalts from these areas. Contrary to the more diffuse and regional heat release due to the regional heat flow and serpentinization, we consider that a deep hot magmatic intrusion is necessary to organize the convective cells and to focus the high-temperature hydrothermal discharge. Thus, fluid and sulfide compositions indicate a variable contribution of deep gabbroic intrusions in ultramafic hydrothermal systems.

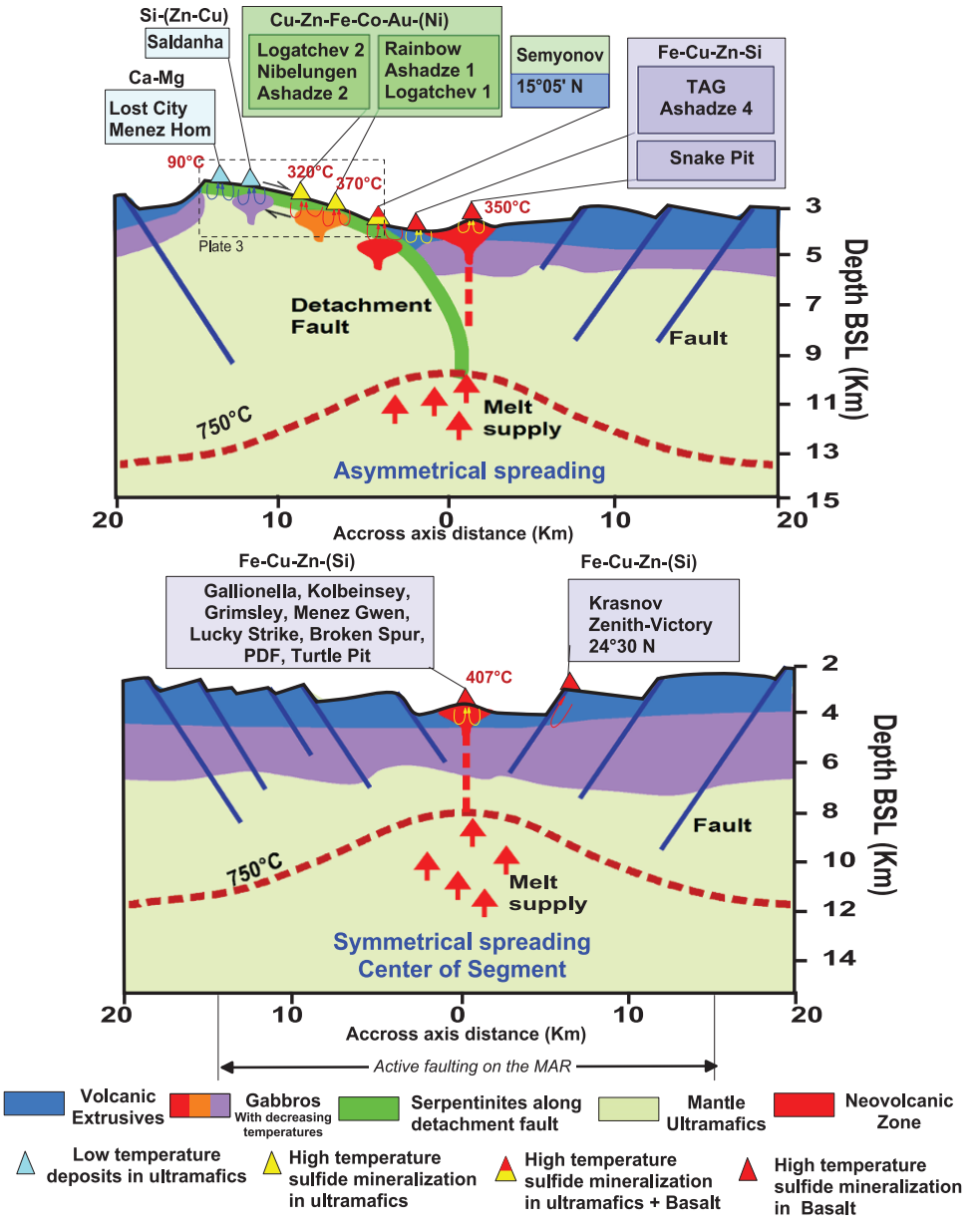

Plate 2. Schematic model for the location and composition of major hydrothermal deposits along the MAR. The structure of the ridge is modified after the works of *McCaig et al.* [2007] and *Escartín et al.* [2008]. Positions of vents are at the scale of their distance from the axis (Lost City, 15 km; Saldanha, 12 km; Logatchev 2, 12 km; Ashadze 2, 9 km; Nibelungen, 9 km; Logatchev 1, 8 km, Rainbow, 6 km; Ashadze 1, 4 km; Semionov, ~2 km; 15°05′N, ~2 km; Krasnov, 7 km; Zenith-Victory, 9 km (see also Table 1). Note that black smokers with a temperature of 320°C are seen as far as 12 km off-axis at Logatchev 2. Many sites associated with detachment faults are also controlled by nontransform discontinuities.

We propose that at ultramafic sites, vigorous high-temperature hydrothermal systems are enhanced by a combination of three factors: (1) extraction of regional heat by deep and pervasive fracturing of rocks associated with high permeability along detachment faults and in nontransform tectonic offsets; (2) small cooling gabbroic intrusions that provide the significant heat necessary to drive and focus high-temperature convective cells; these intrusions, cooler as the distance to the axis increases, are still hot enough to drive high temperature (320°C) venting 12 km off-axis; and (3) additional exothermic heat, due to

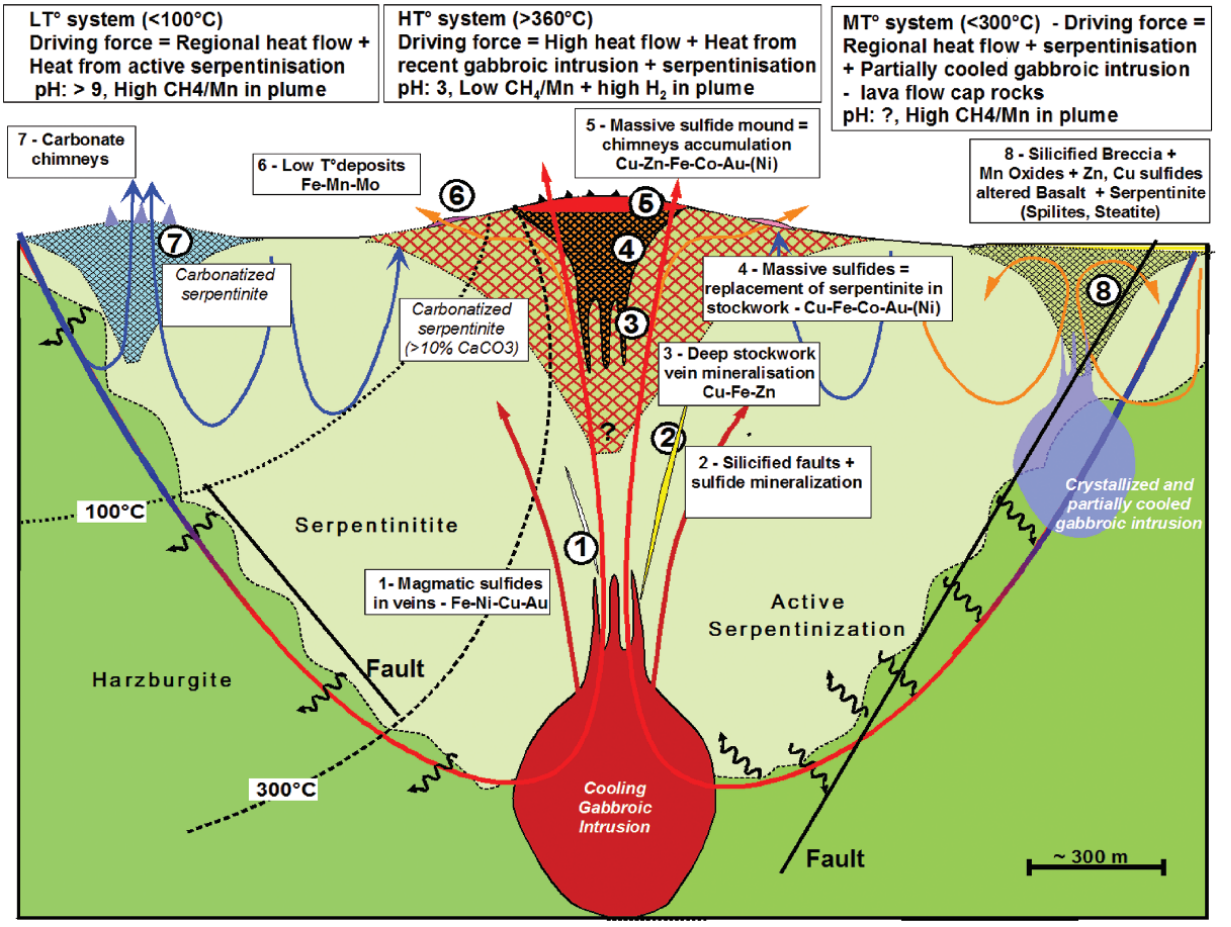

Plate 3. Genetic model and diversity of mineralization in ultramafic environments along slow spreading ridges. Type definitions are 1, 2, and 3, 15°05′N; 4, Rainbow; 5, Rainbow, Logatchev, and Ashadze; 6, Rainbow and Logatchev; 7, Lost City and Menez Hom; and 8, Saldanha.

serpentinization, contributes to support temperatures exceeding 360°C.

8.2. Geological Control of the Hydrothermal Fields

At the scale of the MAR (Figure 1), it seems that the density of vent fields is greater in the E-MORB domains centered at 38°N for the Azores area and at 14°06′N for the 15°N area [*Dosso et al.*, 1991, 1993, 1999]. Both places show very strong regional CH_4 anomalies in the water column [*Charlou et al.*, 1991, 1997]. In addition, the northern limit (at 16°50′N) of E-MORB in the 15°N hot spot also corresponds to the northern limit of the regional CH_4 anomaly that is seen all over the hot spot domain (Figure 1). These two places correspond to the topographic minimum of the area and to places where outcrops of serpentinized ultramafic are common. Unlike the bidimensional hydrothermal systems along the EPR, many deposits along the MAR are related to three-dimensional convective systems focused around local magmatic intrusions. The temporal stability of these systems [*Lalou et al.*, 1986, 1993] over several thousands of years allows for the accumulation of large quantities of sulfides in many of the fields along the MAR.

Data presented here show some specific characteristics of modern sulfide deposits associated with ultramafic rocks along slow spreading ridges. Ultramafic-hosted deposits occur at the amagmatic part of the ridges and show a strong tectonic control of mineralization, by ridge-transform intersections, nontransform offsets, or the deep rift valley faults near the end of the volcanic segments. Along these faults, hydrothermal fields may be located at the base or near the top of the faults. In fact, all ultramafic sites are off-axis sites (Plate 2), and active black smokers (320°C) are known as far as 12 km off-axis at Logatchev 2 [*Fouquet et al.*, 2007,

2008; *Ondreas et al.*, 2007]. The Lost City site (<100°C) is 15 km off-axis [*Kelley et al.*, 2001]. All these settings greatly expand the potential places where hydrothermal activity can be found on slow spreading ridges. Recent studies by *deMartin et al.* [2007] and *McCaig et al.* [2007] also reveal the importance of detachment faults to focus high-temperature hydrothermal discharge. According to the tectonic setting of deposits, it is clear that both serpentinization and hydrothermal activity are enhanced by tectonic activity along detachment faults in areas including the local intrusion of mafic dikes and plutonic rocks. These results indicate that a much larger portion of the oceanic crust may support high-temperature hydrothermal activity than previously thought. The off-axis location of vents is also in agreement with the estimated width of active faulting (15 km) [*Smith et al.*, 2002] and progressive cooling of gabbroic intrusions as they move away from the ridge axis (Plate 2).

8.3. Gold Enrichment in Ultramafic Deposits

In contrast with basaltic environments, ultramafic environments are quite enriched in gold. In high-temperature Cu-Au systems, gold transport is controlled mainly by chloride complexing and is favored by acid oxidized fluids and/or by the presence of high-salinity brines [*Hannington et al.*, 1999; *Huston and Large*, 1989]. At lower temperatures, gold is transported mainly as an aqueous sulfur complex and tends to be concentrated in Zn-rich sulfides. The quantitative precipitation of gold from either of these complexes requires a change in temperature, pH, and oxidation state, which may involve conductive cooling, mixing, and phase separation. In most known oceanic sites, the chemical behavior of gold is well documented as being related to low-temperature deposits associated in the Zn-rich geochemical group [*Hannington and Scott*, 1988, 1989; *Hannington et al.*, 1999]. The maximum concentration of gold in vent deposits along the MAR is found in ultramafic environments where the average Au concentration ranges from 1 to 26 ppm. Ultramafic-hosted deposits yield some of the highest gold values (maximum 63 ppm at Logatchev and 51 ppm at Rainbow) reported from marine hydrothermal deposits. This demonstrates that gold-rich deposits are not specific to felsic environments in island arc settings and early stage back-arc systems.

The bimodal occurrence of gold in ultramafic-hosted deposits (Figure 8) may indicate that both mechanisms may be involved. The problem is that in fossil Cu-Au deposits, gold is precipitated from chloride complexes at relatively high temperatures [*Hannington et al.*, 1999] under relatively oxidizing conditions. This is not the case at Rainbow where fluids are extremely reducing compared to basaltic environments. Pyrrhotite and isocubanite are the stable Fe and Cu minerals under these reducing conditions. Thus, complexes other than the classical $Au(HS)^{2-}$, $Au(HS)^{0}$ and $Au(Cl)^{2-}$ may have to be considered. *Seward and Barnes* [1997] have discussed the importance of organic complexes in transporting metals. The Rainbow fluids are extremely enriched in abiotic organic compounds generated during serpentinization [*Charlou et al.*, 2002; *Holm and Charlou*, 2001]. Another possibility is gold scavenging by bismuth melts. This hypothesis was discussed recently for hydrothermal fluids [*Ciobanu et al.*, 2006; *Tooth et al.*, 2008]. The occurrence of gold grains directly joined to Bi-Melonite grains at the core of the copper chimneys at Rainbow may attest for a possible role of Bi in the transports and precipitation of gold. In fossil volcanogenic massive sulfide (VMS) deposits, similar to MAR ultramafic sulfide deposits, Cu-Au deposits have a high Au/Ag ratio and posses notable Cu-Au-Bi-Se-Te association [*Hannington et al.*, 1999]. In this type of deposit, gold is present as a native metal and as Au tellurides. Another possibility to explain higher Au concentrations in ultramafic-hosted deposits is the concentration of Au in the source rocks. The Au concentration is nearly twice as high in the upper mantle (0.54 ppm) than in the N-MORB (0.34 ppm) (Table 5), but this enrichment does not seem to explain the observed differences.

8.4. Where Are Similar Cu-Zn-Co-Au Deposits on Land?

Ultramafic-hosted massive sulfides are particularly rare on land. The best examples are probably the Outokumpu deposits in Finland and the small St Veran Massive sulfide in the French Alps ophiolites. Other examples are the Cu-Co-Zn Dur'ngoi sulfide deposit in China [*Yang et al.*, 1997, 2004]; the Eastern Metal Ni-Cu-Zn sulfide deposit in Quebec [*Auclair et al.*, 1993], the Sykesville Fe-Cu-Co-Zn-Ni deposit in the Appalachian mountains in the United States of America [*Candela et al.*, 1989]; the Ivanovka and Ishkinino Fe-Cu-Ni-Co sulfide deposits in Ural [*Nimis et al.*, 2008]; the Limassol forest Cu-Ni-CO-As-Au deposits in the Cyprus ophiolite [*Panayiotou*, 1986; *Thalhammer et al.*, 1986], and the Bou Azzer Co-As-Au deposit in Morocco [*Leblanc and Billaud*, 1982; *Leblanc and Fischer*, 1990].

8.4.1. Outokumpu. The Precambrian Outokumpu [*Gaal and Parkkinen*, 1993; *Peltonen et al.*, 2008] deposits in Finland occur in a dismembered ophiolite, where mafic volcanic are scarce, and no sheeted dike complex is observed. The model of formation assumes that serpentinite was exposed on the seafloor when the ore deposits formed [*Gaal and Parkkinen*, 1993]. Eleven Cu-Zn-Co-Au massive sulfide deposits totaling 50 MT were mined in this area. The grade for the largest (28 MT) Keretti deposit was 3.8% Cu, 1% Zn, 0.2%

Co, 0.1% Ni, and 0.8 ppm Au [*Gaal and Parkkinen*, 1993]. The ore is hosted in quartzite and calc silicates associated with serpentinite and dolomite. The chemistry of this deposit is characterized by the predominance of Cu over Zn and is anomalously high in Ni and Cr when compared to most other VMS deposits. The Outokumpu deposits formed during rifting of the crust 1.95 Ga ago, in connection with the continental breakup. Oceanic crust with associated hydrothermal systems formed along a linear basin. Polymetallic sulfides, silica, and carbonates related to seafloor venting were precipitated along the central axis of the rifted basin. The ore is commonly associated with black sediments and was later covered by carbonaceous mud and turbidites. Due to the lack of mafic volcanic rocks and the composition of ore mineralization, the classification as a Cyprus type is not evident for this deposit. The unique features of the Outokumpu deposits can be explained by the ultramafic composition of the oceanic crust. Geological setting in a low-magmatic rifted basin, the high Cu/Zn ratio, together with Co, Ni, and Au enrichment, indicate processes similar to those of ultramafic-hosted massive sulfide in the modern ocean.

8.4.2. Limassol Forest, Cyprus. Hydrothermal sulfides associated with ultramafic rocks occur in the Cyprus ophiolite at the Limassol Forest area [*Panayiotou*, 1986; *Thalhammer et al.*, 1986]. The dominant rock type is highly serpentinized and tectonized residual harzburgite. These mantle rocks are intersected by mafic dykes and plutonic rocks, mostly wherlite and gabbro. The Limassol Forest site is considered to represent a fossil transform fault [*Simonian and Gass*, 1978]. Mineralization occurs within the serpentinite as lenticular bodies, veins, and disseminated sulfides, with arsenides [*Panayiotou*, 1980]. The mineral association shows an evolutionary trend, which is closely linked to serpentinization. The first high-temperature stage at about 400–500°C is dominated by pyrrhotite, pentlandite, and cobalt-nickel arsenides. This stage is followed by deposition of copper sulfides at about 250°C, and finally, valleriite and bravoite are deposited at temperatures ranging from 100 to 200°C [*Thalhammer et al.*, 1986]. The high As (up to 2.7 wt %) and Ni (up to 4.8 %) content of this deposit is not seen in modern ultramafic deposits. However, the highest As concentration along the MAR are in ultramafic-hosted vent deposits. Similar to Rainbow and Ashadze, Co (up to 0.36 wt %) and Au (average 6.2 ppm) are also enriched in these deposits [*Panayiotou*, 1980, 1986].

8.4.3. St Veran massive sulfide, French Alps. In the French Alps, sulfides from the St Veran VMS deposit were mined very early in history up until the last century. The St Veran deposit is genetically related to an ophiolite section [*Bouvier et al.*, 1990]. Basement rocks are serpentinites and peridotites from the upper mantle. Mafic rocks are gabbroic intrusions into the ultramafic sequence and tholeitic pillow lava flows. Lava flows are absent near the massive sulfide that are directly covered with silicic sediment and then carbonaceous sediments of Cretaceous age. This geological setting is very close to the modern setting of high-temperature ultramafic sulfide deposits. In addition, as early as 1987, it was proposed that a major, oblique, normal detachment fault that cuts across the lithosphere, explains some asymmetrical features on both sides of the preoceanic continental rift. An increase of the offset of the detachment fault leads to the tectonic denudation of the upper mantle and thus gives birth to an ultramafic ocean floor [*Lemoine et al.*, 1987]. Several similarities exist between modern deposits and the mineralogy of the St Veran deposit. Major minerals are pyrite, chalcopyrite, sphalerite, bornite, chalcocite, hematite, and magnetite. Minor minerals include digenite, covellite, idaite, cobalt-pentlandite, carollite, clausthalite, native copper, native silver, and uraninite. Gold is not mentioned, but clausthalite contains up to 1% of gold. Several Te minerals, altaite, hessite, coloradoite are also described [*Bouvier et al.*, 1990].

8.4.4. Ivanovka deposit, Ural. At the Ivanovka massive sulfide deposit, a mixed mafic-ultramafic sequence hosts the sulfide mineralization and lies on a serpentinite unit [*Nimis et al.*, 2004]. The sulfide mineralization comprises massive, disseminated, and stockwork ore consisting of lamellar pyrrhotite, with pyrite, chalcopyrite, and cubanite similar to those found in the modern ocean. Accessory minerals are cobaltite, sphalerite, Co-rich pyrite, Co-rich pentlandite, Ni-rich glaucodot, and trace of native gold, native bismuth, and pilsenite (Bi tellurite). The sulfide includes abundant relict chromite. Gangue minerals are Mg-rich chlorite, talc, saponite, quartz (Ca, Mg, and Fe) carbonates and dolomite. The metal grades and the abundance of accessory sulfides appear to be controlled by the composition of the host rock. Ni content may be up to 0.2%. Significant Au content (up to 5.4 ppm) is found near the top of the ore-bearing sequence within pyrite, chalcopyrite, and pyrrhotite assemblages. The deposit is characterized by very low Zn and As-Ni-Bi-Au assemblages. The upper part of the deposit probably formed at the seafloor; however, the widespread occurrence of sulfides, with altered minerals and the relict of chromite as well as replacement of alteration phyllosilicates by sulfide, indicates that the Ivanovka ores dominantly formed in the subsurface by cementation, replacement, and veining. All these textural, mineralogical, and geochemical characteristics are very close to those of the Rainbow, Logatchev, and Ashadze sulfide deposits discussed in this chapter. However, the most probable setting for this deposit is an early arc or a fore-arc. This opens the possibility to discover ultramafic-hosted mas-

sive sulfide in arc, back-arc, and fore-arc systems in the modern ocean.

8.4.5. "Listwaenite" mineralization. Sulfide mineralization of a hydrothermal origin is reported in a wide variety of altered ophiolitic serpentinites, particularly in carbonatized and silicified serpentinites [*Auclair et al.*, 1993; *Buisson and Leblanc*, 1985, 1987]. This style of mineralization is frequently referred to as listwaenite. *Halls and Zhao* [1995] points out that the term listwaenite should be applied only to the product of potassium carbonate metasomatism of serpentinites. Nevertheless, there is a clear association of sulfide mineralization, as well as gold enrichment, associated with carbonatized and silicified serpentinites at the 15°05′N subsurface mineralization site. *Auclair et al.* [1993] describe a sequence of alteration in the Eastern Metals deposit from serpentinites to a talc-carbonate assemblage, then to a dominantly quartz-carbonate rock ("listwaenite"), and finally to an almost completely silicified rock ("birbirite"). Mineralization is associated with the last two stages of alteration. This alteration is hydrothermal in origin and fault controlled. The extreme silicification seen in samples from the 15°05′N fracture zone appears to be analogous to the "birbirite," which is the final alteration product in some ancient listwaenite occurrences [*Auclair et al.*, 1993].

The occurrence of this sample type on a major fault zone at the limit between the inner valley floor and the rift valley wall indicates that the fault acted as a channel for the large amounts of fluid required to achieve such an alteration. The talc-carbonate alteration is observed only to a relatively minor degree, and truly carbonatized samples have not been collected. However, the presence of veins and patches of carbonate in many samples indicates the presence of a late-stage carbonate-bearing fluid. Such carbonate veins are also described in ultramafic rocks that outcrop elsewhere on the seafloor [*Bideau et al.*, 1991], and carbonatized ultramafic rocks are seen at Rainbow and carbonate chimneys at Lost City. In ultramafic rocks from the Garret transform fault, the carbonate veins postdate serpentinization, and $\delta^{18}O$ values suggest low temperatures (<100°C) [*Bideau et al.*, 1991]. Late carbonates in ultramafic rocks from Rainbow also indicate a low-temperature process [*Ribeiro da Costa et al.*, 2008]. This suggests that a carbonate source from sediments is unlikely, [*Bideau et al.*, 1991] points out that Ca^{2+} alteration is also seen in the form of roddingitization of mafic rocks.

8.5. Specificity of Ultramafic Mineralization in the Modern Ocean

The proportion of hydrothermal sulfide deposits in ultramafic rocks along the MAR is much greater than on land. About one third of the known hydrothermal fields are related to ultramafic rocks. This proportion is probably higher because, for a long time, exploration was focused near the axis on the magmatic portion of the ridge. This observation raises the question as to why these types of deposits are so scarce in the geological record. One possible explanation is that, during obduction, back-arcs, together with arc, are preferentially incorporated into the continent as ophiolite complexes. We may thus consider that large, mature slow spreading mid-ocean ridges, such as the MAR, are particular locations for the formation of specific oceanic mineralization, which are not easily incorporated into the continent. We propose that ultramafic Cu-Zn-Co-Au deposits are a specific oceanic type of deposit that is probably common on amagmatic portions of slow spreading ridges.

9. SUMMARY AND CONCLUSIONS

At the regional scale, hydrothermal fields on the MAR are found on axial and in off-axis regions. Both volcanic and tectonic controls of the hydrothermal processes exist. The occurrence of active hydrothermal systems in these two distinctly different environments considerably enlarges the areas where potential hydrothermal sulfide deposits can be found on slow spreading ridges. The different regional settings and geological controls are summarized on Plate 2. Basaltic hosted hydrothermal deposits are volcanically controlled at the central part of segments or fault controlled at the base and the top of the rift walls. In these areas, the rift valley is relatively symmetric. Mantle-hosted hydrothermal fields are, at the regional scale, tectonically controlled along detachment faults and nontransform offsets. In these areas, the ridge has a clear asymmetry. Off-axis ultramafic-hosted mineral deposits indicate that high-temperature hydrothermal convection may exist in the absence of surface volcanic activity at slow spreading ridges. Low-temperature (<100°C) hydrothermal activity is seen 15 km off-axis and black smoker activity (>300°C) can be found as far as 12 km off-axis. As exothermic heat produced during serpentinization cannot provide sufficient heat alone to drive a high-temperature hydrothermal system, we have to consider cooling gabbroic intrusions to provide the heat necessary to drive and focus high-temperature venting. In addition, regional conductive heat can be mined out from the ridge when water circulates along the detachment faults. Many sites are probably a combination of these three factors. The off-axis location of vents is also in agreement with the estimated width of active faulting (15 km) and progressive cooling of gabbroic intrusions as they move away from the ridge axis (Plate 2).

At the local scale, major types of ultramafic-hosted hydrothermal mineralization observed in the modern ocean are

summarized as a genetic model on Plate 3. The different types of high- and low-temperature mineralization are presented. At all sites, fluid compositions indicate active serpentinization; however, the depth and geometry of the serpentinization front is not known (dashed line on Plate 3 is hypothetic) and may be controlled by the detachment fault. A gabbroic intrusion drives and focuses high-temperature convective cells toward the black smoker fields at the seafloor. Hydrothermal fluids react with the gabbroic intrusion and extract some elements such as barium and REE. In this system, we consider several types of mineralization shown as numbers on Plate 3: (1) Small gabbroic dykes and magmatic fluids are injected in the serpentinite. Fe-Ni-Cu-Au mineralization is observed in these veins. (2) Along major faults, hydrothermal fluids are channeled, and thick quartz veins are formed. These veins contain Cu-Fe-Ni-Pb mineralization. (3) Closer to the surface, stockwork formations are characterized by Cu-Fe-Zn mineralization. (4) Under major black smoker fields, extensive replacement of the ultramafic rocks with massive sulfide is seen. Such a replacement process seems to be a common characteristic of many fossil ultramafic VMS deposits on land. This mineralization is enriched in copper. (5) Massive sulfides are formed at the seafloor by chimney accumulation, diagenesis, and zone-refining processes. Unlike in basaltic environments, there is no conical mound, and the zonation is poorly organized. Due to more diffuse black smoker venting all over the field, surface samples are Cu-rich or Cu-Zn-rich. (6) Away from the high temperature areas, diffuse low-temperature discharge may produce extensive Fe-Mn deposits at the surface. Serpentinite rocks are commonly carbonatized and sediments lithified in these areas. Some (Fe, Mg, Ca) carbonates chimneys are also observed. (7) Away from volcanic intrusions or when the gabbroic intrusion has cooled, vigorous hydrothermal convection is driven both by regional heat flow and exothermic heat released during active serpentinization. Temperature is lower than 100°C, and the alkaline fluids do not transport metals. No sulfides are present, and the discharge mainly produces carbonate chimneys. (8) More complex hydrothermal systems are also related to low-temperature discharge through volcanic and serpentinite breccia. This breccia at the top of a dome structure may be produced by unroofing of lava flows due to diapiric uplift during serpentinization. Lava flows may act as a lid on the system. In areas of intense alteration in both basalt and serpentinite, hydrothermal precipitates occur as silicification, Mn oxides, and locally disseminated sulfides.

Sulfide mineralization at basaltic environments is primarily composed of pyrite, chalcopyrite, sphalerite, and amorphous silica and has low Cu + Zn concentrations (2 to 20%). E-MORB-hosted deposits are enriched in Ba and Si. Opposite to basaltic-hosted deposits, ultramafic sulfide deposits are primarily composed of chalcopyrite, isocubanite, sphalerite, and pyrrhotite and correspond to more reducing conditions. They differ from MORB-hosted mineralization by their high Cu + Zn content (20 to 40%) and their Co, Ni, and Au enrichment. The influence of the ultramafic basement is clearly marked in some specific minor minerals such as pentlandite, millerite, and melonite. Ultramafic-hosted sulfide deposits are significantly enriched in Au. Se and Ni are also enriched in Cu-rich high-temperature chimneys. In addition, in ultramafic environments, Au has a bimodal occurrence and may be concentrated both in low- and high-temperature mineral assemblages. Basement rocks are one parameter that controls the composition of deposits, although the solubility and complexation of metals in the fluid is likely to be very important.

The frequency of ultramafic ore deposits along slow mid-ocean ridges is higher than expected. In addition, this type of deposit is not common on land and seems to be more common in the modern ocean than in fossil deposits on land where many VMS deposits are more typical of back-arc environments. Because the preservation in ophiolites is higher for back-arc environments, it must be considered that ultramafic-hosted VMS deposits are a specific oceanic type of mineralization that is not common on the continent.

Acknowledgments. Much of the chapter is based on data and samples obtained during several diving cruises organized along the Mid-Atlantic Ridge through the French American FARA program and two EEC-funded programs south of the Azores (Marflux: contract Mast2-CT93-0070 and Amores: contract Mast3-CT95-0040). Work south of the Azores was also done trough bilateral French-Portuguese cooperation. Between 13°N and 23°N, data were obtained through French-Russian and French-American cooperation. At TAG, samples were obtained during the international drilling operation Leg 158. We acknowledge financial support from Ifremer, for the ship time and submersible operations. This publication was much improved by constructive, pertinent, and thorough reviews by S. Humphris and S. D. Scott, they both are strongly acknowledged.

REFERENCES

Aballea, M., K. J. Radford, P. Appriou, H. Bougault, J. L. Charlou, J. P. Donval, J. Etoubleau, Y. Fouquet, C. R. German, and M. Miranda (1998), Manganese distribution in the water column near the Azores triple junction along the Mid-Atlantic Ridge and the Azores domain, *Deep Sea Res., Part I*, *45*(8), 1319–1338.

Akimtsev, V. A., V. N. Sharapov, V. Y. Kolobov, V. S. Nagrebetskii, N. M. Podgornykh, V. A. Simonov, and G. A. Tretiakov (1991), Hydrothermal mineralization of Mid-Atlantic Ridge in the zone of its joining with the Cape Verde transform fault, *Sov. Geol. Geophys., Engl. Transl.*, *32*(8), 20–24.

Allen, D. E., and W. E. Seyfried (2003), Compositional controls on vent fluids from ultramatic-hosted hydrothermal systems at mid-ocean ridges: An experimental study at 400°C, 500 bars, *Geochim. Cosmochim. Acta*, *67*(8), 1531–1542.

Allen, D. E., and W. E. Seyfried Jr. (2004), Serpentinization and heat generation; constraints from Lost City and Rainbow hydrothermal systems, *Geochim. Cosmochim. Acta*, *68*(6), 1347–1354.

Allen, R. L., et al. (2002), Global comparisons of volcanic-associated massive sulphide districts, in *The Timing and Location of Major ore Deposits in an Evolving Orogen*, edited by J. Blundell Derek et al., *Geol. Soc. Spec. Publ.*, *204*, 13–37.

Ames, D. E., J. M. Franklin, and M. D. Hannington (1993), Mineralogy and geochemistry of active and inactive chimneys and massive sulfide, Middle Valley, northern Juan de Fuca Ridge; an evolving hydrothermal system, *Can. Mineral.*, *31*(4), 997–1024.

Anderson, D. L. (1989), Composition of the Earth, *Science*, *243*(4889), 367–370.

Auclair, G., Y. Fouquet, and M. Bohn (1987), Distribution of selenium in high-temperature hydrothermal sulfide deposits at 13° North, East Pacific Rise, *Can. Mineral.*, *25*(4), 577–587.

Auclair, M., M. Gauthier, J. Trottier, M. Jebrak, and F. Chartrand (1993), Mineralogy, geochemistry, and paragenesis of the Eastern Metals serpentinite-associated Ni-Cu-Zn deposit, Quebec Appalachians, *Econ. Geol.*, *88*, 123–138.

Bach, W., N. R. Banerjee, H. J. B. Dick, and E. T. Baker (2002), Discovery of ancient and active hydrothermal systems along the ultraslow spreading Southwest Indian Ridge 10°–16° E, *Geochem. Geophys. Geosyst.*, *3*(7), 1044, doi:10.1029/2001GC000279.

Baker, E. T., H. N. Edmonds, P. J. Michael, W. Bach, H. J. B. Dick, J. E. Snow, S. L. Walker, N. R. Banerjee, and C. H. Langmuir (2004), Hydrothermal venting in magma deserts: The ultraslow-spreading Gakkel and Southwest Indian Ridges, *Geochem. Geophys. Geosyst.*, *5*, Q08002, doi:10.1029/2004GC000712.

Barriga, F., et al. (1998), Discovery of the Saldanha hydrothermal field on the Famous segment of the MAR (36°30′N), *Eos Trans. AGU*, *79*(45), Fall Meet. Suppl., F67.

Bel'tenev, V., et al. (2003), New discoveries at 12°58′N, 44°52′W, MAR: Professor Logatchev-22 cruise, initial results, *InteRidge News*, *12*(1), 13–14.

Bel'tenev, V., A. Shagin, V. Markov, I. Rozhdestvenskaya, T. Stepanova, G. Cherkashev, I. Fedorov, A. Rumyantsev, and I. Poroshina (2004), A new hydrothermal field at 16°–38.4′N, 46° 28.5′W on the Mid-Atlantic Ridge, *InterRidge News*, *13*, 5–6.

Beltenev, V., et al. (2009), New data about hydrothermal fields on the Mid-Atlantic Ridge between 11°–14°N: 32nd cruise of R/V *Professor Logatchev*, *InterRidge News*, *18*, 13–17.

Bideau, D., R. Hebert, R. Hekinian, and M. Cannat (1991), Metamorphism of deep-seated rocks from the Garrett ultrafast transform (East Pacific Rise near 13° 25′S), *J. Geophys. Res.*, *96*(B6), 10,079–10,099.

Binns, R. A., and S. D. Scott (1993), Actively forming polymetallic sulfide deposits associated with felsic volcanic rocks in the eastern Manus back-arc basin, Papua New Guinea, *Econ. Geol.*, *88*(8), 2226–2236.

Binns, R. A., et al. (1993), Hydrothermal oxide and gold-rich sulfate deposits of Franklin Seamount, western Woodlark Basin, Papua New Guinea, *Econ. Geol.*, *88*(8), 2122–2153.

Bischoff, J. L., and R. J. Rosenbauer (1987), Phase separation in seafloor geothermal systems; an experimental study of the effects on metal transport, *Am. J. Sci.*, *287*(10), 953–978.

Bogdanov, Y., A. Sagalevitch, E. Chernyaev, A. Ashadze, E. Gurvich, V. Lukashin, G. Ivanov, and V. Peresypkin (1995), A study of the hydrothermal field at 14°45′N on the Mid Atlantic Ridge using the MIR submersibles, *Bridge Newsl.*, 9–13.

Bonatti, E., B. M. Guerstein-Honnorez, and J. Honnorez (1976a), Copper-iron sulfide mineralizations from the equatorial Mid-Atlantic Ridge, *Econ. Geol.*, *71*(8), 1515–1525.

Bonatti, E., B. M. Guerstein-Honnorez, J. Honnorez, and C. Stern (1976b), Hydrothermal pyrite concretions from the Romanche fracture zones, *Earth Planet. Sci. Lett.*, *32*, 1–10.

Bougault, H., J. L. Charlou, Y. Fouquet, H. D. Needham, N. Vaslet, P. Appriou, P. J. Baptiste, P. A. Rona, L. Dmitriev, and S. Silantiev (1993), Fast and slow spreading ridges: Structure and hydrothermal activity, ultramafic topographic highs, and CH_4 output, *J. Geophys. Res.*, *98*(B6), 9643–9651.

Bougault, H., M. Aballea, J. RadfordKnoery, J. L. Charlou, P. J. Baptiste, P. Appriou, H. D. Needham, C. German, and M. Miranda (1998), FAMOUS and AMAR segments on the Mid-Atlantic Ridge: Ubiquitous hydrothermal Mn, CH_4, delta He-3 signals along the rift valley walls and rift offsets, *Earth Planet. Sci. Lett.*, *161*(1–4), 1–17.

Bouvier, J., H. Dabrowski, F. Jaffe, and M. Vuagnat (1990), The copper-deposit of Saint-Veran, *Arch. Sci.*, *43*(2), 273–294.

Buisson, G., and M. Leblanc (1985), Gold in carbonatized ultramafic rocks from ophiolite complexes, *Econ. Geol.*, *80*(7), 2028–2029.

Buisson, G., and M. Leblanc (1986), Gold-bearing listwaenites (carbonatized ultramafic rocks) from ophiolite complexes, in *Metallogeny of Basic and Ultrabasic Rocks*, edited by M. J. Gallagher et al., pp. 121–131, Inst. Min. and Metall., London.

Buisson, G., and M. Leblanc (1987), Gold in mantle peridotites from upper proterozoic ophiolites in Arabia, Mali, and Morocco, *Econ. Geol.*, *82*(8), 2091–2097.

Campbell, A. C., et al. (1988), Chemistry of hot springs on the Mid-Atlantic Ridge, *Nature*, *335*(6190), 514–519.

Candela, P. A., A. G. Wylie, and T. M. Burke (1989), Genesis of the ultramafic rock-associated Fe-Cu-Co-Zn-Ni deposits of the Sykesville District, Maryland Piedmont, *Econ. Geol.*, *84*(3), 663–675.

Cann, J. R., D. K. Blackman, D. K. Smith, E. McAllister, B. Janssen, S. Mello, E. Avgerinos, A. R. Pascoe, and J. Escartin (1997), Corrugated slip surfaces formed at ridge–transform intersections on the Mid-Atlantic Ridge, *Nature*, *385*(6614), 329–332.

Cannat, M. (1993), Emplacement of mantle rocks in the seafloor at mid-ocean ridges, *J. Geophys. Res.*, *98*(B3), 4163–4172.

Cannat, M., and J. F. Casey (1995), An ultramafic lift at the Mid-Atlantic Ridge: Successive stages of magmatism in serpentinized peridotites from the 15°N region, in *Mantle and Lower Crust Exposed in Oceanic Ridges and in Ophiolites*, edited by R. L. M. Vissers and A. Nicolas, pp. 5–34, Springer, Dordrecht, Netherlands.

Cannat, M., Y. Lagabrielle, H. Bougault, J. Casey, N. de Coutures, L. Dmitriev, and Y. Fouquet (1997), Ultramafic and gabbroic exposures at the Mid-Atlantic Ridge; geological mapping in the 15° N region, in *The Adolphe Nicolas Volume*, edited by D. Mainprice et al., pp. 193–213, Elsevier, Amsterdam.

Cannat, M., H. Ondreas, Y. Fouquet, S. Silantiev, E. Hoise, F. Fontaine, and Scientific Party of the Serpentine Cruise (2007), Geological context of ultramafic-hosted hydrothermal vent fields in the 13–15° N region of the Mid-Atlantic Ridge; preliminary results of the Serpentine cruise, *Eos Trans., AGU*, *88*(52), Fall Meet. Suppl., Abstract T51F-02.

Cannat, M., F. Fontaine, and J. Escartín (2010), Serpentinization and associated hydrogen and methane fluxes at slow spreading ridges, in *Diversity of Hydrothermal Systems on Slow Spreading Ocean Ridges*, *Geophys. Monogr. Ser*., doi:10.1029/2008GM000760, this volume.

Charlou, J. L., H. Bougault, P. Appriou, T. Nelsen, and P. Rona (1991), Different TDM/CH_4 hydrothermal plume signatures; TAG site at 26° N and serpentinized ultrabasic diapir at 15° 05′N on the Mid-Atlantic Ridge, *Geochim. Cosmochim. Acta*, *55*(11), 3209–3222.

Charlou, J. L., J. P. Donval, P. Jean-Baptiste, A. Dapoigny, and P. A. Rona (1996), Gases and helium isotopes in high temperature solutions sampled before and after ODP Leg 158 drilling at TAG hydrothermal field (26°N, MAR), *Geophys. Res. Lett.*, *23*(23), 3491–3494.

Charlou, J. L., J. P. Donval, E. Douville, J. Knoery, Y. Fouquet, H. Bougault, B. P. Jean, M. Stievenard, and C. R. German (1997), High methane flux between 15° N and the Azores triple junction, Mid-Atlantic Ridge; hydrothermal and serpentinization processes, *Eos Trans. AGU*, *78*(46), Fall Meet. Suppl., F831.

Charlou, J. L., Y. Fouquet, H. Bougault, J. P. Donval, J. Etoubleau, B. P. Jean, A. Dapoigny, P. Appriou, and P. A. Rona (1998), Intense CH 4 plumes generated by serpentinization of ultramafic rocks at the intersection of the 15° 20′N fracture zone and the Mid-Atlantic Ridge, *Geochim. Cosmochim. Acta*, *62*(13), 2323–2333.

Charlou, J. L., J. P. Donval, E. Douville, B. P. Jean, K. J. Radford, Y. Fouquet, A. Dapoigny, and M. Stievenard (2000), Compared geochemical signatures and the evolution of Menez Gwen (37° 50′N) and Lucky Strike (37° 17′N) hydrothermal fluids, south of the Azores triple junction on the Mid-Atlantic Ridge, *Chem. Geol.*, *171*(1-2), 49–75.

Charlou, J. L., J. P. Donval, Y. Fouquet, P. Jean Baptiste, and N. Holm (2002), Geochemistry of high H-2 and CH_4 vent fluids issuing from ultramafic rocks at the Rainbow hydrothermal field (36° 14′N, MAR), *Chem. Geol.*, *191*(4), 345–359.

Charlou, J. L., J. P. Donval, C. Konn, H. Ondréas, Y. Fouquet, P. Jean-Baptiste, and E. Fourré (2010), High production and fluxes of H_2 and CH_4 and evidence of abiotic hydrocarbon synthesis by serpentinization in ultramafic-hosted hydrothermal systems on the Mid-Atlantic Ridge, in *Diversity of Hydrothermal Systems on Slow Spreading Ocean Ridges*, *Geophys. Monogr. Ser*., doi:10.1029/2008GM000752, this volume.

Cherkashov, G. (2008), Seafloor massive sulfides studies at the Mid Atlantic Ridge geological and technological aspects: Russia's efforts to develop deep sea marine mineral resources, in *Conference on Marine Mineral Resources of the South and Equatorial Atlantic Ocean*, Minist. of Mine and Energy, Rio de Janeiro.

Cherkashov, G., V. Bel'tenev, V. Ivanov, L. Lazareva, M. Samovarov, V. Shilov, T. Stepanova, G. P. Glasby, and V. Kuznetsov (2008), Two new hydrothermal fields at the Mid-Atlantic Ridge, *Mar. Georesour. Geotechnol.*, *26*(4), 308–316.

Ciobanu, C. L., N. J. Cook, F. Damian, and G. Damian (2006), Gold scavenged by bismuth melts: An example from Alpine shear-remobilizates in the Highis massif, Romania, *Mineral. Petrol.*, *87*(3-4), 351–384.

Corliss, J., et al. (1979), Submarine thermal springs on the Galapagos Rift, *Science*, *203*, 1073–1083.

Costa, R. L. P. (2001), Estudo mineralogico e geoquimico da alteracao hidrothermal das rochas vulcanicas e ultramaficas serpentinizadas do monte Saldanha (RMA, Segmento Famous/Amar), Dissertaçao de Mestrado thesis, 143 pp., Univ. de Lisboa, Lisbon.

Costa, R. L. P., F. J. A. S. Barriga, and Y. Fouquet (2002), Evidence for a late steatization process at the Saldanha massif (MAR 36°33′50″N–36°26′W), paper presented at Thermal Regime of Ocean Ridges and Dynamics of Hydrothermal Circulation Exploratory Workshop, Eur. Sci. Found., Pavia/Sestri Levante, Italy.

Cyamex (1978), Découverte par submersible de sulfures polymétalliques massifs sur la dorsale du Pacifique oriental, par 21°N (projet "Rita"), *C. R. Acad. Sci.*, *287*, 1365–1368.

Dekov, V. M., Z. K. Damyanov, G. D. Kamenov, I. K. Bonev, and K. B. Bogdanov (1999), Native copper and alpha -copper-zinc in sediments from the TAG hydrothermal field (Mid-Atlantic Ridge, 26° N); nature and origin, *Mar. Geol.*, *161*(2-4), 231–247.

Delaney, J. R., D. W. Mogk, and M. J. Mottl (1987), Quartz-cemented breccias from the Mid-Atlantic Ridge: Samples of a high-salinity hydrothermal upflow zone, *J. Geophys. Res.*, *92*(B9), 9175–9192.

deMartin, B. J., R. A. R. Canales, J. P. Canales, and S. E. Humphris (2007), Kinematics and geometry of active detachment faulting beneath the Trans-Atlantic Geotraverse (TAG) hydrothermal field on the Mid-Atlantic Ridge, *Geology*, *35*(8), 711–714.

de Ronde, C. E. J., et al. (2005), Evolution of a submarine magmatic-hydrothermal system; Brothers Volcano, southern Kermadec Arc, New Zealand, *Econ. Geol.*, *100*(6), 1097–1133.

Devey, C. W., K. S. Lackschewitz, and E. Baker (2005), Hydrothermal and volcanic activity found on the southern Mid-Atlantic Ridge, *Eos Trans. AGU*, *86*(22), 209, doi:10.1029/2005EO220001.

Dias, A. S., and F. J. A. S. Barriga (2006), Mineralogy and geochemistry of hydrothermal sediments from the serpentinite-hosted Saldanha hydrothermal field (36°34′N; 33°26′W) at MAR, *Mar. Geol., 225*, 157–175.

Dias, A. S. C. M. A. (2001), Sedimentos hidrothermais do Monte Saldanha (crista Médio-Atlantica, Famous/Amar), Dissertaçao de Mestrado thesis, 115 pp., Univ. de Lisboa, Lisbon.

Dias, A. S. C. M. A., F. J. A. S. Barriga, and Y. Fouquet (2002), Hydrothermal sediments from Saldanha Mount (MAR-Famous-Amar), paper presented at Thermal Regime of Ocean Ridges and Dynamics of Hydrothermal Circulation Exploratory Workshop, Eur. Sci. Found., Pavia/Sestri Levante, Italy.

Dick, H. J. B. (1989), Abyssal peridotites, very slow spreading ridges and ocean ridge magmatism, in *Magmatism in the Ocean Basins*, edited by A. D. Saunders and M. J. Norry, *Geol. Soc. Spec. Publ., 115*, 71–105.

Dick, H. J. B., J. Lin, and H. Schouten (2003), An ultraslow-spreading class of ocean ridge, *Nature*, *426*(6965), 405–412.

Diehl, P. (1987), Geostatistical reserve modeling and mining simulation of the Atlantis II Deep's metalliferous sediments, in *Marine Minerals; Advances in Research and Resource Assessment*, edited by G. Teleki Paul et al., pp. 541–558, Springer, Dordrecht, Netherlands.

Dosso, L., B. B. Hanan, H. Bougault, J. G. Schilling, and J. L. Joron (1991), Sr-Nd-Pb geochemical morphology between 10° and 17° N on the Mid-Atlantic Ridge; a new MORB isotope signature, *Earth Planet. Sci. Lett.*, *106*(1-4), 29–43.

Dosso, L., H. Bougault, and J. L. Joron (1993), Geochemical morphology of the North Mid-Atlantic Ridge, 10°–24° N; trace element-isotope complementarity, *Earth Planet. Sci. Lett.*, *120*(3-4), 443–462.

Dosso, L., H. Bougault, C. Langmuir, C. Bollinger, O. Bonnier, and J. Etoubleau (1999), The age and distribution of mantle heterogeneity along the Mid-Atlantic Ridge (31–41° N), *Earth Planet. Sci. Lett.*, *170*(3), 269–286.

Douville, E., J. L. Charlou, J. P. Donval, J. Knoery, Y. Fouquet, P. Bienvenu, P. Appriou, and I. Flores Scientific Party (1997), Trace elements in fluids from the new Rainbow hydrothermal field (36° 14 N, MAR); a comparison with other Mid-Atlantic Ridge fluids, *Eos Trans. AGU, 78*(46), Fall Meet. Suppl., F832.

Douville, E., J. L. Charlou, E. H. Oelkers, P. Bienvenu, C. C. F. Jove, J. P. Donval, Y. Fouquet, D. Prieur, and P. Appriou (2002), The Rainbow Vent fluids (36° 14′N, MAR); the influence of ultramafic rocks and phase separation on trace metal content in Mid-Atlantic Ridge hydrothermal fluids, *Chem. Geol.*, *184*(1-2), 37–48.

Duckworth, R. C., R. Knott, A. E. Fallick, D. Rickard, B. J. Murton, and C. Van Dover (1995), Mineralogy and sulfur isotope geochemistry of the Broken Spur sulphides, 29°N, Mid-Atlantic Ridge, in *Hydrothermal Vents and Processes*, edited by L. M. Parson et al., pp. 175–189, Geol. Soc., London.

Dyment, J., K. Tamaki, H. Horen, Y. Fouquet, K. Nakase, M. Yamamoto, M. Ravilly, M. Kitazawa (2005), A positive magnetic anomaly at Rainbow hydrothermal site in ultramafic environment, *Eos Trans. AGU*, *86*(52), Fall Meet. Suppl., Abstract OS21C-08.

Eberhart, G. L., P. A. Rona, and J. Honnorez (1989), Geologic controls of hydrothermal activity in the Mid-Atlantic Ridge rift valley; tectonics and volcanics, *Mar. Geophys. Res.*, *10*(3-4), 233–259.

Edmond, J. M., A. C. Campbell, M. R. Palmer, G. P. Klinkhammer, C. R. German, H. N. Edmonds, H. Elderfield, G. Thompson, and P. Rona (1995), Time series studies of vent fluids from the TAG and MARK sites (1986, 1990) Mid-Atlantic Ridge: a new solution chemistry model and a mechanism for Cu/Zn zonation in massive sulphide orebodies, in *Hydrothemal Vents and Processes*, edited by L. M. Parson et al., pp. 77–86, Geol. Soc., London.

Edmonds, H. N., P. J. Michael, E. T. Baker, D. P. Connelly, J. E. Snow, C. H. Langmuir, H. J. B. Dick, R. Muhe, C. R. German, and D. W. Graham (2003), Discovery of abundant hydrothermal venting on the ultraslow-spreading Gakkel ridge in the Arctic, *Nature*, *421*(6920), 252–256.

Elderfield, H., et al. (1993), Preliminary geochemical results from the Broken Spur hydrothermal field, 29° N, Mid-Atlantic Ridge, *Eos Trans. AGU*, *74*(43), Fall Meet. Suppl., 99.

Escartín, J., and M. Cannat (1999), Ultramafic exposures and the gravity signature of the lithosphere near the Fifteen-Twenty fracture zone (Mid-Atlantic Ridge, 14°–16.5° N), *Earth Planet. Sci. Lett.*, *171*(3), 411–424.

Escartín, J., and J. Lin (1998), Tectonic modification of axial crustal structure; evidence from spectral analyses of residual gravity and bathymetry of the Mid-Atlantic Ridge flanks, *Earth Planet. Sci. Lett.*, *154*(1-4), 279–293.

Escartín, J., D. K. Smith, J. Cann, H. Schouten, C. H. Langmuir, and S. Escrig (2008), Central role of detachment faults in accretion of slow-spreading oceanic lithosphere, *Nature*, *455*(7214), 790–794.

Fouquet, Y. (1997), Where are the large hydrothermal sulphide deposits in the oceans?, *Philos. Trans. R. Soc. London, Ser. A*, *355*(1723), 427–440.

Fouquet, Y., et al. (1993a), Sulfide mineralizations associated with ultramafic rocks on the MAR near 15° 20′N, *Terra Nova Abstr., 5*, suppl. 1, 444–445.

Fouquet, Y., U. von Stackelberg, J. L. Charlou, J. Erzinger, P. M. Herzig, R. Muehe, and M. Wiedicke (1993b), Metallogenesis in back-arc environments; the Lau Basin example, *Econ. Geol.*, *88*(8), 2150–2177.

Fouquet, Y., A. Wafik, P. Cambon, C. Mevel, G. Meyer, and P. Gente (1993c), Tectonic setting and mineralogical and geochemical zonation in the Snake Pit sulfide deposit (Mid-Atlantic Ridge at 23° N), *Econ. Geol.*, *88*(8), 2014–2032.

Fouquet, Y., J. L. Charlou, I. Costa, J. P. Donval, J. Radford-Knoery, H. Pellé, H. Ondréas, N. Lourenço, M. Ségonsac, and M. Kingston-Tivey (1994), A detailed study of the Lucky Strike hydrothermal site and discovery of a new hydrothermal site: Menez Gwen. Preliminary results of the DIVA1 cruise (5–29 May, 1994), *InterRidge News*, *3*(2), 14–18.

Fouquet, Y., H. Ondréas, J. L. Charlou, J. P. Donval, J. Radford-Knoery, I. Costa, N. Lourenço, and M. K. Tivey (1995), Atlantic lava lakes and hot vents, *Nature*, *377*, 201.

Fouquet, Y., R. Knott, P. Cambon, A. Fallick, D. Rickard, and D. Desbruyeres (1996), Formation of large sulfide mineral deposits along fast spreading ridges; example from off-axial deposits at 12° 43′N on the East Pacific Rise, *Earth Planet. Sci. Lett.*, *144*(1-2), 147–162.

Fouquet, Y., et al. (1997), Discovery and first submersible investigations on the Rainbow Hydrothermal Field on the MAR (36°14N), *Eos Trans. AGU*, *78*(46), Fall Meet. Suppl., F832.

Fouquet, Y., et al. (1998a), FLORES diving cruise with the Nautile near the Azores. First dives on the Rainbow field: Hydrothermal seawater/mantle interaction, *InterRidge News*, *7*(1), 24–28.

Fouquet, Y., K. Henry, R. Knott, and P. Cambon (1998b), Geochemical section of the TAG hydrothermal mound, in *TAG: Drilling an Active Hydrothermal System on a Sediment-Free*

Slow-Spreading Ridge, edited by P. M. Herzig et al., *Proc. Ocean Drill. Program Sci. Results*, *158*, 363–388.

Fouquet, Y., et al. (2000), Hydrothermal processes in oceanic ultramafic environments; the Rainbow hydrothermal sulfide deposit, paper presented at 31st International Geological Congress, Int. Union of Geol. Sci., Rio de Janeiro, Brazil.

Fouquet, Y., G. Cherkashov, J. L. Charlou, H. Ondréas, M. Cannat, N. Bortnikov, S. Silantyev, J. Etoubleau, and P. Serpentine (2007), Diversity of ultramafic hosted hydrothermal deposits on the Mid Atlantic Ridge; first submersible studies on Ashadze, Logatchev 2 and Krasnov vent fields during the Serpentine cruise, *Eos Trans. AGU*, *88*(52), Fall Meet. Suppl., Abstract T51F-03.

Fouquet, Y., et al. (2008), Serpentine cruise–ultramafic hosted hydrothermal deposits on the Mid Atlantic Ridge: First submersible studies on Ashadze 1 and 2, Logatchev 2 and Krasnov vent fields, *InterRidge News*, *18*, 15–19.

Fournier, R. O., R. J. Rosenbauer, and J. L. Bischoff (1982), The Solubility of quartz in aqueous sodium chloride solution, *Geochim. Cosmochim. Acta*, *46*, 1975–1978.

Francheteau, J., et al. (1979), Massive deep-sea sulfide ore deposits discovered on the East Pacific Rise, *Nature*, *277*, 523–528.

Fruh Green, G. L., D. S. Kelley, S. M. Bernasconi, J. A. Karson, K. A. Ludwig, D. A. Butterfield, C. Boschi, and G. Proskurowski (2003), 30,000 years of hydrothermal activity at the Lost City vent field, *Science*, *301*(5632), 495–498.

Gaal, G., and J. Parkkinen (1993), Early Proterozoic ophiolite-hosted copper-zinc-cobalt deposits of the Outokumpu type, in *Mineral Deposit Modeling*, edited by R. V. Kirkham et al., pp. 335–341, Geol. Assoc. of Canada, Toronto, Ont., Canada.

Gablina, I. F., N. N. Mozgova, Y. S. Borodaev, T. V. Stepanova, G. A. Cherkashev, and M. I. Il'in (2000), Copper sulfide associations in recent oceanic ores of the Logatchev hydrothermal field (Mid-Atlantic Ridge, 14° 45′ N), *Geol. Ore Deposits*, *42*(4), 296–316.

Gallant, R. M., and K. L. Von Damm (2006), Geochemcial controls on hydrothermal fluids from the Kairei and Edmond vent fields, 23°–25° S, Central Indian Ridge, *Geochem., Geophys., Geosyst.*, *7*, Q06018, doi:10.1029/2005GC001067.

German, C. R., and J. Lin (2004), The thermal structure of the oceanic crust, ridge-spreading and hydrothermal circulation: How well do we understand their inter-connections?, in *Mid-Ocean Ridges: Hydrothermal Interactions Between the Lithosphere and Oceans, Geophys. Monogr. Ser.*, vol. 148, edited by C. R. German, J. Lin, and L. M. Parson, pp. 1–18, AGU, Washington, D. C.

German, C. R., and L. M. Parson (1998), Distributions of hydrothermal activity along the Mid-Atlantic Ridge; interplay of magmatic and tectonic controls, *Earth Planet. Sci. Lett.*, *160*(3-4), 327–341.

German, C. R., et al. (1994), Hydrothermal activity on the Reykjanes Ridge: The Steinahóll vent-field at 63°06′N, *Earth Planet. Sci. Lett.*, *121*, 647–654.

German, C. R., et al. (1999), A segment scale study of fluxes through the Rainbow hydrothermal plume, 36°N Mid-Atlantic Ridge, *Eos Trans. AGU, 80*(46), Fall Meet. Suppl., F957–F958.

Gibson, H. L., R. L. Morton, and G. J. Hudak (1999), Submarine volcanic processes, deposits, and environments favorable for the location of volcanic-associated massive sulfide deposits, in *Volcanic-Associated Massive Sulfide Deposits; Processes and Examples in Modern and Ancient Settings*, edited by C. T. Barrie and M. D. Hannington, *Rev. Econ. Geol.*, *8*, 13–51.

Goodfellow, W. D., and J. M. Franklin (1993), Geology, mineralogy, and chemistry of sediment-hosted clastic massive sulfides in shallow cores, Middle Valley, northern Juan de Fuca Ridge, *Econ. Geol.*, *88*(8), 2037–2068.

Gracia, E., D. Bideau, R. Hekinian, Y. Lagabrielle, and L. M. Parson (1997), Along-axis magmatic oscillations and exposure of ultramafic rocks in a second-order segment of the Mid-Atlantic Ridge (33° 43′N to 34° 07′N), *Geology*, *25*(12), 1059–1062.

Gracia, E., J. L. Charlou, J. Radford Knoery, and L. M. Parson (2000), Non-transform offsets along the Mid-Atlantic Ridge south of the Azores (38° N–34° N): Ultramafic exposures and hosting of hydrothermal vents, *Earth Planet. Sci. Lett.*, *177*(1-2), 89–103.

Haase, K. M., et al. (2007), Young volcanism and related hydrothermal activity at 5° S on the slow-spreading southern Mid-Atlantic Ridge, *Geochem., Geophys., Geosyst.*, *8*, Q11002, doi:10.1029/2006GC001509.

Halbach, P., et al. (1989), Probable modern analogue of Kuroko-type massive sulphide deposits in the Okinawa Trough back-arc basin, *Nature*, *338*(6215), 496–499.

Halbach, P., B. Pracejus, and A. Maerten (1993), Geology and mineralogy of massive sulfide ores from the central Okinawa Trough, Japan, *Econ. Geol.*, *88*(8), 2210–2225.

Halls, C., and R. Zhao (1995), Listvenite and related rocks: Perspectives on terminology and mineralogy with reference to an occurrence at Cregganbaun, Co. Mayo, Republic of Ireland, *Mineral. Dep.*, *30*, 303–313.

Hannington, M., P. Herzig, S. Scott, G. Thompson, and P. Rona (1991), Comparative mineralogy and geochemistry of gold-bearing sulfide deposits on the mid-ocean ridges, *Mar. Geol.*, *101*(1-4), 217–248.

Hannington, M., et al. (2001), First observations of high-temperature submarine hydrothermal vents and massive anhydrite deposits off the north coast of Iceland, *Mar. Geol.*, *177*(3-4), 199–220.

Hannington, M. D., and S. D. Scott (1988), Gold mineralisation in volcanogenic massive sulphides; modern and ancient, in *Bicentennial Gold; 1988; Extended Abstracts; Oral Programme*, edited by A. D. T. Goode and L. I. Bosma, pp. 353–358, Geol. Soc. of Aust., Sydney, N.S.W., Australia.

Hannington, M. D., and S. D. Scott (1989), Sulfidation equilibria as guides to gold mineralization in volcanogenic massive sulfides; evidence from sulfide mineralogy and the composition of sphalerite, *Econ. Geol.*, *84*(7), 1978–1995.

Hannington, M. D., G. Thompson, P. A. Rona, and S. D. Scott (1988), Gold and native copper in supergene sulphides from the Mid-Atlantic Ridge, *Nature*, *333*(6168), 64–66.

Hannington, M. D., I. R. Jonasson, P. M. Herzig, and S. Petersen (1995), Physical and chemical processes of seafloor mineralization at mid-ocean ridges, in *Seafloor Hydrothermal Systems: Physical, Chemical, Biological, and Geological Interactions*,

Geophys. Monogr. Ser., vol. 91, edited by S. E. Humphris et al., pp. 115–157, AGU, Washington, D. C.

Hannington, M. D., A. G. Galley, P. M. Herzig, and S. Petersen (1998), Comparison of the TAG mound and stockwork complex with cyprus-type massive sulfide deposits, in *TAG: Drilling an Active Hydrothermal System on a Sediment-Free Slow-Spreading Ridge,* edited by P. M. Herzig et al., *Proc*. *Ocean Drill. Program Sci*. *Results*, *158*, 389–415.

Hannington, M. D., K. H. Poulsen, J. F. H. Thompson, and R. H. Sillitoe (1999), Volcanogenic gold in the massive sulfide environment, in *Volcanic-Associated Massive Sulfide Deposits; Processes and Examples in Modern and Ancient Settings*, edited by C. T. Barrie and M. D. Hannington, pp. 325–356, Soc. of Econ. Geol., Littleton, Colo.

Hellebrand, E., J. E. Snow, and R. Muehe (2000), Mantle melting beneath Gakkel Ridge (Arctic Ocean); abyssal peridotite spinel compositions, *Chem. Geol.*, *182*(2-4), 227–235.

Herzig, P. M., and M. D. Hannington (1995), Polymetallic massive sulfides at the modern seafloor; a review, *Ore Geol. Rev.*, *10*(2), 95–115.

Herzig, P. M., M. D. Hannington, Y. Fouquet, U. Von Stackelberg, and S. Petersen (1993), Gold-rich polymetallic sulfides from the Lau back arc and implications for the geochemistry of gold in sea-floor hydrothermal systems of the southwest Pacific, *Econ. Geol.*, *88*(8), 2182–2209.

Hoffert, M., A. Perseil, R. Hékinian, P. Choukroune, H. D. Needham, J. Francheteau, and X. Le Pichon (1978), Hydrothermal deposits sampled by diving saucer in Transform Fault "A" near 37°N on the Mid Atlantic Ridge, FAMOUS area, *Oceanol. Acta*, *1*, 73–86.

Holm, N. G., and J. L. Charlou (2001), Initial indications of abiotic formation of hydrocarbons in the Rainbow ultramafic hydrothermal system, Mid-Atlantic Ridge, *Earth Planet. Sci. Lett.*, *191*(1-2), 1–8.

Honnorez, J., et al. (1990), Mineralogy and chemistry of sulfide deposits drilled from hydrothermal mound of the Snake Pit active field, MAR, *Proc. Ocean Drill. Program Sci. Results*, *106/109*, 145–162.

Houghton, J. L., W. C. Shanks III, and W. E. Seyfried Jr. (2004), Massive sulfide deposition and trace element remobilization in the Middle Valley sediment-hosted hydrothermal system, northern Juan de Fuca Ridge [modified], *Geochim. Cosmochim. Acta*, *68*(13), 2863–2873.

Humphris, S. E., et al. (1995), The internal structure of an active sea-floor massive sulphide deposit, *Nature*, *377*(6551), 713–716.

Huston, D. L., and R. R. Large (1989), A chemical model for the concentration of gold in volcanogenic massive sulphide deposits, *Ore Geol. Rev.*, *4*(3), 171–200.

Huston, D., S. Sie, G. Suter, D. Cooke, and R. Both (1995), Trace elements in sulfide minerals from eastern Australian volcanic-hosted massive sulfide deposits. 1. Proton microprobe analyses of pyrite, chalcopyrite, and sphalerite, and 2. selenium levels in pyrite—Comparison With δS^{34} values and implications for the source of Sulfur in volcanogenic hydrothermal systems, *Econ. Geol.*, *90*(5), 1167–1171.

Ildefonse, B., D. Blackman, B. John, Y. Ohara, D. Miller, and C. MacLeod (2007), Oceanic core complexes and crustal accretion at slow-spreading ridges, *Geology*, *35*(7), 623–626.

James, R. H., H. Elderfield, and M. R. Palmer (1995), The chemistry of hydrothermal fluids from the Broken Spur site, 29° N Mid-Atlantic Ridge, *Geochim. Cosmochim. Acta*, *59*(4), 651–659.

Jean Baptiste, P., J. L. Charlou, M. Stievenard, J. P. Donval, H. Bougault, and C. Mevel (1991), Helium and methane measurements in hydrothermal fluids from the Mid-Atlantic Ridge; the Snake Pit site at 23° N, *Earth Planet. Sci. Lett.*, *106*(1-4), 17–28.

Johnson, K. T. M., and H. J. B. Dick (1992), Open system melting and temporal and spatial variation of peridotite and basalt at the Atlantis II fracture zone, *J. Geophys. Res.*, *97*(B6), 9219–9241.

Karson, J. A., and J. R. Brown (1989), Geologic setting of the Snake Pit hydrothermal site; an active vent field on the Mid-Atlantic Ridge, *Mar. Geophys. Res.*, *10*(1-2), 91–107.

Karson, J. A., and P. A. Rona (1990), Block-tilting, transfer faults, and structural control of magmatic and hydrothermal processes in the TAG area, Mid-Atlantic Ridge 26° N; with Suppl. Data 90-21, *Geol. Soc. Am. Bull.*, *102*(12), 1635–1645.

Kase, K., et al. (1990), Copper-rich sulfide deposit near 23°N, Mid-Atlantic Ridge: Chemical composition, mineral chemistry, and sulfur isotopes, *Proc. Ocean Drill. Program Sci. Results*, *106/109*, 163–177.

Kelley, D. S., and J. R. Delaney (1987), Two-phase separation and fracturing in mid-ocean ridge gabbros at temperatures greater than 700° C, *Earth Planet. Sci. Lett.*, *83*(1-4), 53–66.

Kelley, D. S., et al. (2001), An off-axis hydrothermal vent field near the Mid-Atlantic Ridge at 30° N, *Nature*, *412*(6843), 145–149.

Kelley, D. S., et al. (2005), A serpentinite-hosted ecosystem; the Lost City hydrothermal field, *Science*, *307*(5714), 1428–1434.

Kirst, P. W. (1976), Petrology of metamorphic rocks from the Mid Atlantic Ridge and fracture zones, Ph.D. thesis, Univ. of Miami, Miami, Fla.

Klinkhammer, G., P. Rona, M. Greaves, and H. Elderfield (1985), Hydrothermal manganese plumes in the Mid-Atlantic Ridge Rift valley, *Nature*, *314*(6013), 727–773.

Knott, R. (1995), Hydrothermal diagenesis, Ph.D. thesis, 313 pp., Univ. of Wales, Cardiff.

Knott, R., Y. Fouquet, J. Honnorez, S. Petersen, and M. Bohn (1998), Petrology of hydrothermal mineralization: A vertical section through the TAG mound, in *TAG: Drilling an Active Hydrothermal System on a Sediment-Free Slow-Spreading Ridge*, edited by P. M. Herzig et al., *Proc. Ocean Drill. Program Sci. Results, 158*, 5–26.

Koschinsky, A., et al. (2006), Discovery of new hydrothermal vents on the southern Mid-Atlantic Ridge (4° S–10° S) during cruise M68/1, *InterRidge News*, *15*, 9–15.

Koschinsky, A., D. Garbe-Schonberg, S. Sander, K. Schmidt, H. H. Gennerich, and H. Strauss (2008), Hydrothermal venting at pressure-temperature conditions above the critical point of seawater, 5° S on the Mid-Atlantic Ridge, *Geology*, *36*(8), 615–618.

Koski, R. A., P. F. Lonsdale, W. C. Shanks, M. E. Berndt, and S. S. Howe (1985), Mineralogy and geochemistry of a sediment-hosted hydrothermal sulfide deposit from the Southern Trough of Guaymas Basin, Gulf of California, *J. Geophys. Res.*, *90*(B8), 6695–6707.

Koski, R. A., W. C. Shanks III, W. A. Bohrson, and R. L. Oscarson (1988), The composition of massive sulfide deposits from the sediment-covered floor of Escanaba Trough, Gorda Ridge; implications for depositional processes, *Can. Mineral.*, *26*(3), 655–673.

Krasnov, S. G., I. M. Poroshina, and G. A. Cherkashev (1995), Geological setting of high-temperature hydrothermal activity and massive sulphide formation on fast- and slow-spreading ridges, in *Hydrothermal Vents and Processes*, edited by L. M. Parson et al., pp. 17–23, Geol. Soc., London.

Lagabrielle, Y., D. Bideau, M. Cannat, J. A. Karson, and C. Mével (1998), Ultramafic-mafic plutonic rock suites exposed along the Mid-Atlantic Ridge (10°N–30°N) Symmetrical-assymetrical distribution and implications for seafloor spreading processes, in *Faulting and Magmatism at Mid-Ocean Ridges*, *Geophys. Monogr. Ser.*, vol. 106, edited by W. R. Buck et al., pp. 153–176, AGU, Washington, D. C.

Lalou, C., G. Thompson, P. A. Rona, E. Brichet, and C. Jehanno (1986), Chronology of selected hydrothermal Mn oxide deposits from the Transatlantic Geotraverse "TAG'' area, Mid-Atlantic Ridge 26° N, *Geochim. Cosmochim. Acta*, *50*(8), 1737–1743.

Lalou, C., J. L. Reyss, E. Brichet, M. Arnold, G. Thompson, Y. Fouquet, and P. A. Rona (1993), New age data for Mid-Atlantic Ridge hydrothermal sites: TAG and Snakepit chronology revisited, *J. Geophys. Res.*, *98*(B6), 9705–9713.

Langmuir, C., et al. (1997), Hydrothermal vents near a mantle hot spot; the Lucky Strike vent field at 37° N on the Mid-Atlantic Ridge, *Earth Planet. Sci. Lett.*, *148*(1-2), 69–91.

Lavier, L. L., W. R. Buck, and A. N. B. Poliakov (1999), Self-consistent rolling-hinge model for the evolution of large-offset low-angle normal faults, *Geology*, *27*(12), 1127–1130.

Layton-Matthews, D., J. M. Peter, S. D. Scott, M. I. Leybourne, S. J. Piercey, and J. K. Mortensen (2008), Distribution, mineralogy, and geochemistry of selenium in felsic volcanic-hosted massive sulfide deposits of the Finlayson Lake District, Yukon Territory, Canada, *Econ. Geol.*, *103*, 61–88.

Leblanc, M., and P. Billaud (1982), Cobalt arsenide orebodies related to an upper Proterozoic ophiolite; Bou Azzer (Morocco), *Econ. Geol.*, *77*(1), 162–175.

Leblanc, M., and W. Fischer (1990), Gold and platinum group elements in cobalt-arsenide ores; hydrothermal concentration from a serpentinite source-rock (Bou Azzer, Morocco), in *Mineralogy and Petrology*, edited by E. F. Stumpfl and H. Papunen, pp. 197–209, Springer, Vienna.

Lein, A. Y., D. V. Grichuk, E. G. Gurvich, and Y. A. Bogdanov (2000), A new type of hydrogen- and methane-rich hydrothermal solutions in the rift zone of the Mid-Atlantic Ridge, *Dokl. Earth Sci.*, *375A*(9), 1391–1394.

Lein, A. Y., G. A. Cherkashev, A. A. Ul' yanov, N. V. Ul' yanova, T. V. Stepanova, A. M. Sagalevich, Y. A. Bogdanov, E. G. Gurvich, and A. P. Torokhov (2003), Mineralogy and geochemistry of sulfide ores from the Logatchev-2 and Rainbow fields: Similar and distinctive features, *Geochem. Int.*, *41*(3), 271–294.

Lemoine, M., P. Tricart, and G. Boillot (1987), Ultramafic and gabbroic ocean floor of the Ligurian Tethys (Alps, Corsica, Apennines): In search of a genetic imodel, *Geology*, *15*(7), 622–625.

Lentz, D. R. (1998), Petrogenetic evolution of felsic volcanic sequences associated with Phanerozoic volcanic-hosted massive sulphide systems; the role of extensional geodynamics, *Ore Geol. Rev.*, *12*(5), 289–327.

Lisitsyn, A. P., Y. A. Bogdanov, L. P. Zonenshayn, M. I. Kuz'min, and A. M. Sagalevich (1989), Hydrothermal phenomena in the Mid-Atlantic Ridge at lat.26° N (TAG hydrothermal field), *Int. Geol. Rev.*, *31*, 1183–1189.

Lowell, R. P., and P. A. Rona (2002), Seafloor hydrothermal systems driven by the serpentinization of peridotite, *Geophys. Res. Lett.*, *29*(11), 1531, doi:10.1029/2001GL014411.

Macdonald, K. C. (1984), A geophysical comparison between fast and slow-spreading centers; constraints on magma chamber formation and hydrothermal activity, in *Hydrothermal Processes at Seafloor Spreading Centers*, edited by P. Rona et al., pp. 27–51, Springer, New York.

Marques, A. F. A., F. Barriga, V. Chavagnac, and Y. Fouquet (2006), Mineralogy, geochemistry, and Nd isotope composition of the Rainbow hydrothermal field, Mid-Atlantic Ridge, *Miner. Deposita*, *41*(1), 52–67.

Marques, A. F. A., F. Barriga, and S. D. Scott (2007), Sulfide mineralization in an ultramafic-rock hosted seafloor hydrothermal system: From serpentinization to the formation of Cu-Zn-(Co)-rich massive sulfides, *Mar. Geol.*, *245*, 20–39.

McCaig, A. M., R. A. Cliff, J. Escartin, A. E. Fallick, and C. J. MacLeod (2007), Oceanic detachment faults focus very large volumes of black smoker fluids, *Geology*, *35*(10), 935–938.

Melchert, B., et al. (2008), First evidence for high-temperature off-axis venting of deep crustal/mantle heat; the Nibelungen hydrothermal field, southern Mid-Atlantic Ridge, *Earth Planet. Sci. Lett.*, *275*(1-2), 61–69.

Michael, P. J., et al. (2003), Magmatic and amagmatic seafloor generation at the ultraslow-spreading Gakkel Ridge, Arctic Ocean, *Nature*, *423*(6943), 956–961.

Mozgova, N. N., S. G. Krasnov, B. N. Batuyev, Y. S. Borodaev, A. Efimov, V. F. Markov, and T. V. Stepanova (1996), The first report of cobalt pentlandite from a Mid-Atlantic Ridge hydrothermal deposit, *Can. Mineral.*, *34*, 23–28.

Mozgova, N. N., A. Efimov, Y. S. Borodaev, S. G. Krasnov, G. A. Cherkashov, T. V. Stepanova, and A. M. Ashadze (1999), Mineralogy and chemistry of massive sulfides from the Logatchev hydrothermal field (14° 45′N Mid-Atlantic Ridge), in *Ancient and Modern Seafloor Volcanogenic Massive Sulfide Deposits*, edited by P. A. Rona and Z. Hou, pp. 379–395, Can. Inst. of Min., Metal. and Pet., Montreal, Que., Canada.

Mozgova, N. N., N. V. Trubkin, Y. S. Borodaev, G. A. Cherkashev, T. V. Stepanova, T. A. Semkova, and T. Y. Uspenskaya (2008), Mineralogy of massive sulfides from the Ashadze hydrothermal field, 13° N, Mid-Atlantic Ridge, *Can. Mineral.*, *46*, 545–567.

Murphy, P. J., and G. Meyer (1998), A gold-copper association in ultramafic-hosted hydrothermal sulfides from the Mid-Atlantic Ridge, *Econ. Geol.*, *93*(7), 1076–1083.

Murton, B., S. Unsworth, M. Harris, C. MacLeod, R. Searle, J. Casey, K. Achenbach, and C. Mallows (2007), Fluid flow at active oceanic core complexes, 13° N Mid-Atlantic Ridge, *Eos Trans. AGU*, *88*(52), Fall Meet. Suppl., Abstract T53B-1309.

Murton, B. J., et al. (1994), Direct evidence for the distribution and occurrence of hydrothermal activity between 27° N–30° N on the Mid-Atlantic Ridge, *Earth Planet. Sci. Lett.*, *125*(1-4), 119–128.

Murton, B. J., C. Van Dover, and E. Southward (1995), Geological setting and ecology of the Broken Spur hydrothermal vent field: 29°10′N on the Mid Atlantic Ridge, *Geol. Soc. Spec. Publ.*, *87*, 33–42.

Nakamura, K., T. Morishita, K. Takai, K. Hara, and H. Kumagai (2008), Serpentinized olivine-rich gabbros near the Kairei Hydrothermal Field, Central Indian Ridge; a key to understanding the unique chemistry of the vent fluid, *Geochim. Cosmochim. Acta*, *72*(12), 670.

Nimis, P., S. G. Tesalina, P. Omenetto, P. Tartarotti, and C. Lerouge (2004), Phyllosilicate minerals in the hydrothermal mafic-ultramafic-hosted massive-sulfide deposit of Ivanovka (southern Urals): Comparison with modern ocean seafloor analogues, *Contrib. Mineral. Petrol.*, *147*, 363–383.

Nimis, P., V. V. Zaykov, P. Omenetto, I. Y. Melekestseva, S. G. Tesalina, and J. J. Orgeval (2008), Peculiarities of some mafic-ultramafic- and ultramafic-hosted massive sulfide deposits from the Main Uralian fault zone, Southern Urals, *Ore Geol. Rev.*, *33*(1), 49–69.

Olafsson, J., K. Thors, U. Stefansson, S. P. Jakobsson, W. J. Jenkins, F. T. Manheim, R. F. Commeau, and R. R. Jones (1990), Geochemical observations from a boiling hydrothermal site on the Kolbeinsey Ridge, *Eos Trans. AGU*, *71*, 1650.

Ondreas, H., M. Cannat, G. Cherkashov, Y. Fouquet, A. Normand, and Serpentine Scientific Party (2007), High resolution mapping of the Ashadze and Logatchev hydrothermal fields, Mid Atlantic Ridge 13–15° N, *Eos Trans*. *AGU*, *88*(52), Fall Meet. Suppl., Abstract T53B-1310.

Ondréas, H., M. Cannat, Y. Fouquet, A. Normand, P. M. Sarradin, and J. Sarrazin (2009), Recent volcanic events and the distribution of hydrothermal venting at the Lucky Strike hydrothermal field, Mid-Atlantic Ridge, *Geochem. Geophys. Geosyst.*, *10*, Q02006, doi:10.1029/2008GC002171.

Palmer, M. R., E. M. Ludford, C. R. German, and M. D. Lilley (1995), Dissolved methane and hydrogen in the Steinaholl hydrothermal plume, 63°N, Reykjanes Ridge, in *Hydrothermal Vents and Processes*, pp. 111–120, edited by L. M. Parson et al., Geol. Soc., London.

Panayiotou, A. (1980), Cu-Ni-Co-Fe sulphide mineralization, Limassol Forest, Cyprus, in *Ophiolites; Proceedings, International Ophiolite Symposium*, edited by A. Panayiotou, pp. 102–116, Cyprus, Minist. Agric. Nat. Resour., Geol. Surv. Dep., Nicosia, Cyprus.

Panayiotou, A. (1986), Sulfide and arsenide mineralization associated with the basic and ultrabasic plutonic rocks of the Trodoos ophiolite, Cyprus, in *Metallogeny of Basic and Ultrabasic Rocks*, pp. 417–447, Theophrastus Publ. S.A., Athens.

Parson, L., E. Gracia, E. Coller, C. German, and D. Needham (2000), Second order segmentation—The relationship between volcanism and tectonism at the MAR, 38°N-35°40′N, *Earth Planet. Sci. Lett.*, *178*(3-4), 231–251.

Parson, L. M., Y. Fouquet, H. Ondreas, F. J. A. S. Barriga, J. M. R. S. Relvas, A. Ribeiro, J. L. Charlou, C. R. German, and I. Flores Scientific Party (1997), Non-transform discontinuity settings for contrasting hydrothermal systems on the MAR: Rainbow and FAMOUS at 36° 14′ and 36° 34′N, *Eos Trans. AGU*, *78*(46), Fall Meet. Suppl., F832.

Pedersen, R. B., et al. (2001), Crustal accretion, hydrothermal activity and microbial colonization along the Mohns and the Knipovich ridges; preliminary results from the SUBMAR-2000 and 2001 cruises, *InterRidge News*, *10*(2), 54–56.

Pedersen, R. B., I. H. Thorseth, B. Hellevang, A. Schultz, P. Taylor, H. P. Knudsen, and B. O. Steinsbu (2005), Two vent fields discovered at the ultraslow spreading Arctic Ridge system, *Eos Trans. AGU*, *86*(52), Fall Meet. Suppl., Abstract OS21C-01C.

Peltonen, P., A. Kontinen, H. Huhma, and U. Kuronen (2008), Outokumpu revisited: New mineral deposit model for the mantle peridotite-associated Cu-Co-Zn-Ni-Ag-Au sulphide deposits, *Ore Geol. Rev.*, *33*(3–4), 559–617.

Peter, J. M., and S. D. Scott (1988), Mineralogy, composition, and fluid inclusion microthermometry of sea-floor hydrothermal deposits in the southern trough of Guaymas Basin, Gulf of California, *Can. Mineral.*, *26*(3), 567–587.

Petersen, S., P. M. Herzig, M. D. Hannington, I. R. Jonasson, and A. Arribas Jr. (2003), Submarine gold mineralization near Lihir Island, New Ireland fore-arc, Papua New Guinea, *Econ. Geol.*, *97*(8), 1795–1813.

Petersen, S., P. M. Herzig, U. Schwarz-Schampera, M. D. Hannington, and I. R. Jonasson (2004), Hydrothermal precipitates associated with bimodal volcanism in the central Bransfield Strait, Antarctica, *Miner. Deposita*, *39*(3), 358–379.

Petersen, S., T. Kuhn, P. M. Herzig, and M. D. Hannington (2005), Factors controlling precious and base-metal enrichments at the ultramafic-hosted Logatchev hydrothermal field, 14° 45′N on the MAR; new insights from cruise M60/3, in *Mineral Deposit Research: Meeting the Global Challenge*: *Proceedings of the 8th Biennial SGA Meeting*, edited by J. Mao and F. P. Bierlein, pp. 679–682, Springer, Berlin.

Petersen, S., K. Kuhn, T. Kuhn, N. Augustin, R. Hekinian, L. Franz, and C. Borowski (2009), The geological setting of the ultramafic-hosted Logatchev hydrothermal field (14º45′N, Mid-Atlantic Ridge) and its influence on massive sulfide formation, *Lithos*, *112*, 40–56.

Pushcharovsky, Y. M. (2003), Tectonics of the ocean floor of the central Atlantic and South Atlantic; structural, compositional and metallogenic heterogeneities; their correlation and geodynamic consequences, *InterRidge News*, *12*(1), 17.

Ribeiro da Costa, I., F. J. A. S. Barriga, and R. N. Taylor (2008), Late seafloor carbonate precipitation in serpentinites from the Rainbow and Saldanha sites (Mid-Atlantic Ridge), *Eur. J. Mineral.*, *20*(2), 173–181.

Rona, P. A. (1984), Hydrothermal mineralization at seafloor spreading centers, *Earth Sci. Rev.*, *20*(1), 1–104.

Rona, P. A. (1987), Hydrothermal mineralization at slow-spreading centers; the Atlantic model, *Mar. Min.*, *6*(1), 1–7.

Rona, P. A. (1988), Hydrothermal mineralization at oceanic ridges, *Can. Mineral.*, *26*, 431–446.

Rona, P. A., and S. D. Scott (1993), A special issue on sea-floor hydrothermal mineralization; new perspectives; preface, *Econ. Geol.*, *88*(8), 1933–1973.

Rona, P. A., K. Boström, L. Widenfalk, D. S. Cronan, W. J. Jenkins, and M. Mallette (1982), Hydrothermal mineralization of Mid-Atlantic Ridge 10–27° N, *Geol. Soc. Am. Abstr. Programs*, *14*, 602.

Rona, P. A., G. Klinkhammer, T. A. Nelsen, J. H. Trefry, and H. Elderfield (1986), Black smokers, massive sulphides and vent biota at the Mid-Atlantic Ridge, *Nature*, *321*(6065), 33–37.

Rona, P. A., L. Widenfalk, and K. Boström (1987), Serpentinized ultramafics and hydrothermal activity at the Mid-Atlantic Ridge crest near 15°N, *J. Geophys. Res.*, *92*(B2), 1417–1427.

Rona, P. A., H. Bougault, J. L. Charlou, P. Appriou, T. A. Nelsen, J. H. Trefry, G. L. Eberhart, A. Barone, and H. D. Needham (1992), Hydrothermal circulation, serpentinization, and degassing at a rift valley-fracture zone intersection; Mid-Atlantic Ridge near 15° N, 45° W, *Geology*, *20*(9), 783–786.

Rona, P. A., M. D. Hannington, C. V. Raman, G. Thompson, M. K. Tivey, S. E. Humphris, C. Lalou, and S. Petersen (1993), Active and relict sea-floor hydrothermal mineralization at the TAG hydrothermal field, Mid-Atlantic Ridge, *Econ. Geol.*, *88*(8), 1987–2013.

Sangster, D. F., and S. D. Scott (1976), Precambrian, strata-bound, massive Cu-Zn-Pb sulfide ores of North America, in *Handbook of Strata-bound and Stratiform Ore Deposits; II. Regional Studies and Specific Deposits; Cu, Zn, Pb, and Ag Deposits*, edited by K. H. Wolf, pp. 129–222, Elsevier, New York.

Sauter, D., V. Mendel, C. Rommevaux-Jestin, L. M. Parson, H. Fujimoto, C. Mével, M. Cannat, and K. Tamaki (2004), Focused magmatism versus amagmatic spreading along the ultra-slow spreading Southwest Indian Ridge: Evidence from TOBI side scan sonar imagery, *Geochem. Geophys. Geosyst.*, *5*, Q10K09, doi:10.1029/2004GC000738.

Schroeder, T., B. John, and B. R. Frost (2002), Geologic implications of seawater circulation through peridotite exposed at slow-spreading mid-ocean ridges, *Geology*, *30*(4), 367–370.

Scott, S. D. (1987), Seafloor polymetallic sulfides: Scientific curiosities or mines of the future?, *NATO Advanced Research Workshop on Marine Minerals; Resource Assessment Strategies, NATO ASI Ser.*, *Ser. C*, vol. 194, pp. 277–300, D. Reidel, Dordrecht, Netherlands.

Searle, R., C. MacLeod, B. Murton, C. Mallows, J. Casey, K. Achenbach, S. Unsworth, and M. Harris (2007), Development of oceanic core complexes on the Mid-Atlantic Ridge at 13–14°N; deep-towed geophysical measurements and detailed seafloor sampling, *Eos Trans. AGU, 88*(52), Fall Meet. Suppl., Abstract T51F-01.

Seward, T. M., and H. L. Barnes (1997), *Metal Transport by Hydrothermal Ore Fluids*, 3rd ed., pp. 435–486, John Wiley, Hoboken, N. J.

Seyler, M., M. Cannat, and C. Mével (2003), Evidence for major-element heterogeneity in the mantle source of abyssal peridotites from the Southwest Indian Ridge (52° to 68°E), *Geochem. Geophys. Geosyst.*, *4*(2), 9101, doi:10.1029/2002GC000305.

Simonian, K. O., and I. G. Gass (1978), Arakapas fault belt, Cyprus; a fossil transform fault, *Geol. Soc. Am. Bull.*, *89*(8), 1220–1230.

Smith, D. K., M. Tolstoy, C. G. Fox, D. R. Bohnenstiehl, H. Matsumoto, and M. J. Fowler (2002), Hydroacoustic monitoring of seismicity at the slow-spreading Mid-Atlantic Ridge, *Geophys. Res. Lett.*, *29*(11), 1518, doi:10.1029/2001GL013912.

Smith, D. K., J. R. Cann, and J. Escartín (2006), Widespread active detachment faulting and core complex formation near 13° N on the Mid-Atlantic Ridge, *Nature*, *442*(7101), 440–443.

Snow, J., E. Hellebrand, W. Jokat, and R. Muehe (2001), Magmatic and hydrothermal activity in Lena Trough, Arctic Ocean, *Eos Trans. AGU*, *82*(17), 193.

Spiess, F. N., et al. (1980), East Pacific Rise; hot springs and geophysical experiments, *Science*, *207*(4438), 1421–1433.

Stanton, R. L. (1994), *Ore Elements in Arc Lavas*, 391 pp., Oxford Sci., Oxford, U. K.

Stefansson, V. (1983), Physical environment of hydrothermal systems in Iceland and on submerged oceanic ridges, in *Hydrothermal Processes at Seafloor Spreading Centers*, *NATO Conf. Ser. IV*, vol. 12, edited by P. Rona, K. Boström, and L. Laubier, pp. 321–360, Springer, New York.

Sudarikov, S. M., M. P. Davydov, G. A. Cherkashev, V. V. Gubenkov, O. A. Pivovarchuk, V. F. Kazechenkok, and A. L. Mikhailov (2001), A new area of hydrothermal activity in the rift zone of the Mid-Atlantic Ridge, 13° N, *Dokl. Earth Sci.*, *381A*(9), 1099–1102.

Tanahashi, M., S. Shiokawa, N. Murayama, and R. Takatori (2006), A large hydrothermal sulfide deposit discovered in the Bayonnaise Knoll, Izu-Bonin back-arc rift, *Shigen Chishitsu*, *56*(2), 185–196.

Taylor, S. R., and S. M. McLennan (1985), *The Continental Crust: Its Composition and Evolution*, 312 pp., Blackwell Sci., Oxford, U. K.

Thalhammer, O., E. F. Stumpfl, and A. Panayiotou (1986), Post-magmatic, hydrothermal origin of sulfide and arsenide mineralizations at Limassol Forest, Cyprus, *Miner. Deposita*, *21*(2), 95–105.

Thompson, G., M. J. Mottl, and P. A. Rona (1985), Morphology, mineralogy and chemistry of hydrothermal deposits from the TAG area, 26° N, Mid-Atlantic Ridge, *Chem. Geol.*, *49*(1–3), 243–257.

Thompson, G., S. E. Humphris, B. Schroeder, M. Sulanowska, and P. A. Rona (1988), Active vents and massive sulfides at 26°N (TAG) and 23°N (Snake Pit) on the Mid-Atlantic Ridge, *Can. Mineral.*, *26*, 697–711.

Tivey, M. K., S. E. Humphris, G. Thompson, M. D. Hannington, and P. A. Rona, (1995), Deducing patterns of fluid flow and mixing within the TAG active hydrothermal mound using mineralogical and geochemical data, *J. Geophys. Res.*, *100*(B7), 12,527–12,555.

Tooth, B., J. Brugger, C. Ciobanu, and W. Liu (2008), Modeling of gold scavenging by bismuth melts coexisting with hydrothermal fluids, *Geology*, *36*(10), 815–818.

Torokhov, M. P., G. A. Cherkashev, T. V. Stepanova, and E. A. Zhirnov (2002), Uranium, its minerals and parageneses in massif sulphides of the Logatchev-2, MAR ore field, *InterRidge News*, *11*(2), 32–33.

Tucholke, B. E., J. Lin, and M. C. Kleinrock (1998), Megamullions and mullion structure defining oceanic metamorphic core complexes on the Mid-Atlantic Ridge, *J. Geophys. Res.*, *103*(B5), 9857–9866.

Tufar, W. (1989), Modern hydrothermal activity, formation of complex massive sulfide deposits and associated vent communities in the Manus back-arc basin (Bismarck Sea, Papua New Guinea), *Mitt. Osterr. Geol. Ges.*, *82*, 183–210.

Von Damm, K. L., A. M. Bray, L. G. Buttermore, and S. E. Oosting (1998), The geochemical controls on vent fluids from the Lucky Strike vent field, Mid-Atlantic Ridge, *Earth Planet. Sci. Lett.*, *160*(3-4), 521–536.

Wetzel, L. R., and E. L. Shock (2000), Distinguishing ultramafic-from basalt-hosted submarine hydrothermal systems by comparing calculated vent fluid compositions, *J. Geophys. Res.*, *105*(B4), 8319–8340.

Wilson, G. A., and H. P. Eugster (1985), Metal-chloride speciation from supercritical solubility experiments, *Geol. Soc. Am. Abstr. Programs, 17*, 751.

Wolf, R., and E. Anders (1980), Moon and Earth; compositional differences inferred from siderophiles, volatiles, and alkalis in basalts, *Geochim. Cosmochim. Acta*, *44*(12), 2111–2124.

Wolf, R., G. R. Richter, A. B. Woodrow, and E. Anders (1980), Chemical fractionations in meteorites; XI, C2 chondrites, *Geochim. Cosmochim. Acta*, *44*(5), 711–718.

Yang, J., X. Zheng, W. Bai, Y. Ren, and X. Hu (1997), A preliminary study on genesis of the Dur'ngoi massive Cu-Co-Zn sulfide deposit hosted by the peridotite of A'nyemaqen Ophiolite, Kunlun Mt., China, in *Proceedings of the 30th International Geological Congress*, edited by R. Pei, pp. 381–392, VSP, Utrecht, Netherlands.

Yang, J., X. Wang, R. Shi, Z. Xu, and C. Wu (2004), The Dur'ngoi Ophiolite in east Kunlun Mountains, northern Tibetan Plateau, China; a fragment of Paleotethyan oceanic crust, *Zhongguo Dizhi, Chin. Geol.*, *31*(3), 225–239.

Yang, K., and S. D. Scott (1996), Possible contribution of a metal-rich magmatic fluid to a sea-floor hydrothermal system, *Nature*, *383*(6599), 420–423.

Zierenberg, R. A., R. A. Koski, J. L. Morton, and R. M. Bouse (1993), Genesis of massive sulfide deposits on a sediment-covered spreading center, Escanaba Trough, southern Gorda Ridge, *Econ. Geol.*, *88*(8), 2069–2098.

Zierenberg, R. A., et al. (1998), The deep structure of a sea-floor hydrothermal deposit, *Nature*, *392*(6675), 485–488.

Zonenshain, L. P., M. I. Kuzmin, A. P. Lisitsin, Y. A. Bogdanov, and B. V. Baranov (1989), Tectonics of the Mid-Atlantic rift valley between the TAG and MARK areas (26–24° N): Evidence for vertical tectonism, *Tectonophysics*, *159*(1-2), 1–23.

F. J. A. S. Barriga, GeoFCUL/Creminer, Faculdade Ciencias, Universidade Lisboa, Campo Grande, 1749-016 Lisboa, Portugal.

M. Bohn, Centre de Brest, CNRS-IFREMER, BP 70, F-29280 Plouzané, France.

P. Cambon, J. L. Charlou, J. P. Donval, J. Etoubleau, Y. Fouquet, K. Henry, P. Murphy, H. Ondréas, and O. Rouxel, Centre de Brest, IFREMER, BP 70, F-29280 Plouzané, France. (fouquet@ifremer.fr)

G. Cherkashov, I. Poroshina, and T. Semkova, Institute for Geology and Mineral Resources of the Ocean, Angliisky Avenue, St. Petersburg 190121, Russia.